ALTISSIMO CONSULTING

Road Surface Noise

Effects of Porous Asphalt Thickness, Ageing, and Epoxy, and CPX Speed and Tyre Hardness

Client: NZ Transport Agency - Waka Kotahi
Date: 8th April 2024
Ref: 23-117-R01-D

Prepared for (the Client)
NZ Transport Agency – Waka Kotahi

Prepared by the Consultant)
Altissimo Consulting Ltd

Project Road Surface Noise
Report Effects of Porous Asphalt Thickness, Ageing, and Epoxy, and CPX Speed and Tyre Hardness

Reference 23-117-R01-D

Prepared by

George Bell
Consultant

Reviewed by

Robin Wareing
Principal Acoustic Engineer

Version history:

Version	Date	Comment
A	08/01/2023	Preliminary report for client review
B	01/02/2024	Updated following client feedback.
C	05/03/2024	Updated following client feedback.
D	08/04/2024	Updated following client feedback.

Report disclaimer and limitations:

This report has been prepared in accordance with the usual care and thoroughness of the consulting profession for the use of the Client. It is based on generally accepted practices and standards at the time it was prepared. No other warranty, expressed or implied, is made as to the professional advice included in this report.

This report should be read in full. No responsibility is accepted for use of any part of this report in any other context or for any other purpose or by third parties. This report does not purport to give legal advice. Legal advice can only be given by qualified legal practitioners.

Abstract

Porous Asphalt Thickness

High-resolution laser survey data was used to analyse the variability of porous asphalt layer thickness and its relationship with tyre/road noise, focusing on nine one-kilometre sections of porous asphalt from two recent projects. Key findings included a significant variability in asphalt thickness, with the 25th percentile thicknesses in wheel paths being on average 7% below the specified values. The overall noise level and thickness were negatively correlated. A multivariate regression model between L_{CPX}, thickness, and MPD demonstrated very strong (R^2 = 0.88) agreement with the measured data. Additionally, complex relationships between thickness and noise in the 630 to 2,500 Hz bands were observed, with a local minimum noise level identified within the 25 to 60 mm thickness range. The study employed laser survey data to simulate discrete point measurements of thickness (e.g., magnetic induction), determining that the 25th percentile thickness can be accurately estimated with a longitudinal spacing of discrete points less than or equal to 50 metres. Factors contributing to thickness variability were explored, including geometric differences and construction processes, with geometric differences having the most impact.

Porous Asphalt Ageing

Changes in tyre/road noise were analysed from 2018 to 2023 measurements by the Waka Kotahi CPX system, focusing on various porous asphalt low-noise surfaces. Two methods were used - chronological and cross-sectional. The long-term stability of the measurement system was explored, and anomalous readings were excluded. Key findings included a small but steady increase of 0.2-0.4 dB per year in the overall noise levels for sections of surfaces with relatively low texture, particularly in the left lane, driven by mid to high-frequency band increases. However, surfaces with high initial noise levels and texture showed decreasing overall levels due to low-frequency band reductions. The results suggest that the increasing noise levels may be due to reduced void volume from compaction or debris accumulation. The relative effectiveness of thicker, porous asphalt layers in noise reduction remains unaltered.

Epoxy-Modified Porous Asphalt

Sample sections of epoxy-modified and conventional porous asphalt on a recent project were analysed to quantify the effect of epoxy on tyre/road noise. The epoxy-modified porous asphalt was an average of 0.8 to 1.1 dB quieter than the conventional porous asphalt for this one site. The frequency spectra showed that reductions occurred in the mid (1,000-1,600 Hz) and high (3,150-5,000 Hz) bands. It is hypothesised that the surfaces have different void characteristics.

CPX Speed and Tyre Hardness

A comprehensive measurement program was undertaken to explore the influence of CPX measurement speed and tyre hardness on CPX level, specifically the overall level and spectra. The measurements covered speeds from 40 to 90 km/h and tyre hardness levels from 67.9 to 78.1 Shore A on different surfaces, including asphaltic mix and chipseals. Speed exponents for the overall noise level were consistent with the International Standard for CPX measurements, with impervious surfaces showing higher exponents compared to porous asphalt. The speed exponent's dependence on frequency was also established. Although the range of speed exponents has minimal impact on the overall L_{CPX} correction at typical measurement speeds (80 ±3 km/h), extrapolating over wider speed ranges requires the use of a surface-specific speed exponent. There was a significant variation in the tyre hardness coefficient across surface types, with the mean value aligning with existing literature. Similar to speed, the hardness coefficient varied with frequency. The current broadband correction methods suffice for routine measurements, however more detailed investigations require surface-specific frequency-dependent corrections.

Contents

Abstract ii
Glossary v
Introduction 1

Part I Porous Asphalt Thickness 2

1 Introduction 2
2 Thickness Analysis 3
2.1 Laser Survey Data 3
2.2 Repeatability 6
2.3 MIT-SCAN Comparison 10
2.4 Thickness and L_{CPX} 12
2.5 Simulated Point Measurements 17
3 Sources of Thickness Variation 22
3.1 Geometry 23
3.2 Construction 36
4 Future Work 40
5 Conclusions 41

Part II Porous Asphalt Ageing 42

1 Introduction and Background 42
2 Measurement System 43
3 Method 45
3.1 Method One – Chronological Analysis 45
3.2 Method Two – Cross-Sectional Analysis 46
4 Results and Discussion 47
4.1 Chronological Analysis 47
4.2 Cross-Sectional Analysis 56
4.3 Summary of Chronological and Cross-Sectional Analyses 57
5 Future Work 58
6 Conclusions 59

Part III Epoxy-Modified Porous Asphalt 60

1 Introduction 60
2 Data 61
3 Results and Discussion 61
4 Future Work 66
5 Conclusions 66

Part IV CPX Speed and Tyre Hardness 67

1 Introduction 67
2 Background 67
2.1 Speed 67
2.2 Tyre Hardness 69
3 Measurements 71
4 Results and Discussion 71
4.1 Speed 72
4.2 Hardness 81
4.3 Parameter Influence by Thickness 85
4.4 Effect on CPX Results 87

5 Future Work 88
6 Conclusions 89
References 90
Appendix A – Additional Data 92
Appendix B – Road IDs and Reference Stations 96
Appendix C – Project and Trial Section Locations 97
Appendix D – Lane Numbering 98

Glossary

CAPTIF	Canterbury Accelerated Pavement Testing Indoor Facility
CNC	Christchurch Northern Corridor
CPX	Close proximity
CSM	Christchurch Southern Motorway (both stages)
CSM2	Christchurch Southern Motorway (stage 2 only)
EPA	Epoxy-modified porous asphalt
Lane 1	Closest lane to the centre of the road (see Figure 91).
Lane 2	Second-closest lane to the centre of the road (see Figure 91).
L_{CPX}	Close proximity sound pressure level
LWP	Left wheel path
MIT-SCAN	Brand of device for measuring pavement thickness using magnetic induction.
ML	Machine learning
MPD	Mean profile depth
NDI	Non-destructive inspection
NB	Northbound
NDM	Nuclear densometer
P1	Standard reference test tyre for passenger vehicles
PA	Porous asphalt
PA7 HS	Porous asphalt high strength
PP2Ō	Peka Peka to Ōtaki
RS	Reference station
RWP	Right wheel path
SB	Southbound
SLP	Stationary laser profilometer
SMA	Stone mastic asphalt
WBB	Western Belfast Bypass

Introduction

This study is a continuation of research into tyre/road noise led by Waka Kotahi (*Noise and Vibration Research | Waka Kotahi NZ Transport Agency*). The aim of this work was to extend the current understanding of tyre/road noise by examining several key factors, including the effects that surface thickness, ageing, and binder type have on porous asphalt tyre/road noise emission, and the influence of speed and tyre hardness on CPX noise measurement.

Surface thickness has been identified as the primary source of intra-surface variability in porous asphalt tyre/road noise (Bull, 2019). Newly available high-resolution thickness data from two projects has enabled an in-depth analysis of variability, an expansion of the exploration of the relationships between L_{CPX} and thickness, the evaluation and definition of on-site local verification requirements, and an analysis of several sources of variability.

Over time, surfaces undergo changes that can affect their acoustic properties. This analysis aimed to quantify how samples of New Zealand's low-noise surfaces have changed between the five years from 2018 to 2023, where repeated CPX measurement data was available.

Some low-noise surfaces employ an epoxy modification to the bituminous binder to extend the service life. This study aimed to quantify the effect that epoxy had on tyre/road noise within the CNC project.

The variables of speed and tyre hardness were examined for their effect on measured CPX level. These factors are crucial in understanding the relative performance of road surfaces under different operational conditions. It is important for applications that deviate from the standard measurement speed of 80 km/h.

There are four parts to this report:

- Part I Porous asphalt thickness: Analysis of thickness variability using high resolution data, expanded analysis of the relationship between surface thickness and tyre/road noise, simulation of point measurements, and analysis of sources of variability.
- Part II Porous asphalt ageing: Analysis of the change in tyre/road noise over time for different surfaces.
- Part III Epoxy-modified porous asphalt: Analysis of the effect of the epoxy modification on tyre/road noise.
- Part IV CPX speed and tyre hardness: Analysis of the effect of speed and tyre hardness on tyre/road noise.

Part I Porous Asphalt Thickness

1 Introduction

Surface thickness is the greatest source of variation in the tyre/road noise of low-noise asphaltic mix surfaces on New Zealand's state highway network (Bell, 2022; Bull et al., 2021; Wareing et al., 2021).

Prior to the release of the revised P11 specification (Waka Kotahi NZ Transport Agency, 2024) there were no formal requirements to demonstrate the achievement of the specified surface thickness. Thickness is typically estimated by taking the total bulk asphalt utilisation over the paved area for each shift, which only provides a coarse measure of the mean thickness across a broad area. For tyre/road noise it is critical to maintain a minimum layer thickness in the wheel paths; this can only be demonstrated by local measurements. It is imperative that measurement processes are practical for use on site during construction.

Previous investigations of thickness have used mean bulk thickness, manual surveys, and the magnetic induction methods. These methods have limited spatial resolution and therefore offered a constrained ability to explore the relationship between thickness and noise, and the causes of variation. A technique utilising a pre and post-surfacing mobile laser survey (Mobile Laser Scanning | Woods, 2023) was used on the 2022 CNC and PP2Ō projects.

Prior to 2024, there was no detailed description of the specified thickness for low-noise asphaltic mix surfaces. The specified thickness (also referred to as nominal thickness) was simultaneously interpreted as the minimum and mean. P11 (Waka Kotahi NZ Transport Agency, 2024) has resolved this ambiguity by formally defining the specified thickness as the 25th percentile. All thickness data considered in this report are from projects that were not subject to the new requirements of P11.

This analysis aimed to utilise the high-resolution data to:

- Quantify thickness variability.
- Develop a practical point measurement requirement for the on-site qualification of thickness.
- Expand the understanding of the relationship between thickness and tyre/road noise.
- Explore possible sources of variability in thickness.

This analysis of thickness data for the CNC and PP2Ō projects is for noise research purposes only and provides a level of detail beyond the current knowledge of road surfacing in New Zealand.

2 Thickness Analysis

The aim of this part of the analysis was to use the available thickness data to determine how discrete point measurements (e.g., magnetic induction) could be utilised as a verification method. The process for the determination of the verification requirements is illustrated in Figure 1.

Figure 1: Process for the determination of the thickness verification requirements.

Data: The laser survey data was explored to quantify the variation in thickness.

Repeatability: The laser survey data for the pre- and post-surfacing surveys were compared for sections that were not paved (e.g., bridge decks) to establish inter-survey repeatability.

MIT-SCAN: The laser survey and MIT-SCAN results were compared.

CPX: The relationship between L_{CPX} and thickness was analysed to confirm that the previously observed trends were present. Additional multivariate regression between LCPX, thickness, and MPD was conducted.

Simulated points: Point measurements were simulated on multiple sub-samples of the laser survey measurements.

2.1 Laser Survey Data

The purpose of this section is to explore the variation in thickness using the laser survey data. The variation for the entire lane (i.e., between the edge line and centreline) and within the wheel paths was analysed. The 2.5th, 5th, and 25th percentiles and mean thicknesses were calculated for nine one-kilometre sample sections.

Laser surveys were completed for the entirety of CNC and a one km section of PP2Ō. For CNC, the pre- and post-surfacing surveys were conducted on 15-09-2021 and 7-6-2022, respectively. Surfacing was completed from Feb-Mar 2022. For PP2Ō, the pre- and post-surfacing surveys were conducted on 19-05-2022 and 27-7-2022, respectively. Surfacing was only partially completed at the time of the post-surfacing survey, resulting in one lane of data.

The processed output of the laser surveys is a series of surfaces with 0.1 m horizontal (x and y) resolution and thickness (and elevation) on the z axis. It was assumed that the resolution is sufficient to be used for analysing the variation in thickness.

Multiple sets of data were extracted from the laser survey results: (1) sample sections for detailed thickness analysis, (2) reference surfaces, and (3) MIT-SCAN disk locations (i.e., the physical disks that were placed prior to surfacing).

Nine continuous one-kilometre lane samples were used for the analysis of variability and the simulation of point measurements. The samples and their locations are shown in Table 1.

Table 1: Samples and locations for thickness analysis.

Project	Surface	Underlying Pavement	Road ID*: Chainage	Lane(s)
CNC	PA7 (30 mm)	Foam bitumen stabilised	3844: 3086-4086	1&2
			3843: 2394-3394	
	EPA7 (50 mm)		3844: 5085-6085	
			3843: 4894 – 5894	
PP2Ō	EPA10 (25 mm)	Structural asphalt concrete	3816: 14045-15045	2

*Road ID to Reference Station mapping can be found in Table 15 in the appendix

A colour map of thickness of a one-kilometre sample from the EPA7 (50 mm) section of CNC is shown in Figure 2. The solid left edge line and centreline are at 0 and 3.5 m on the y-axis, respectively. The observed

variation in thickness is understood to be representative of typical paving practices, albeit with a greater specified thickness than most porous asphalt surfaces.

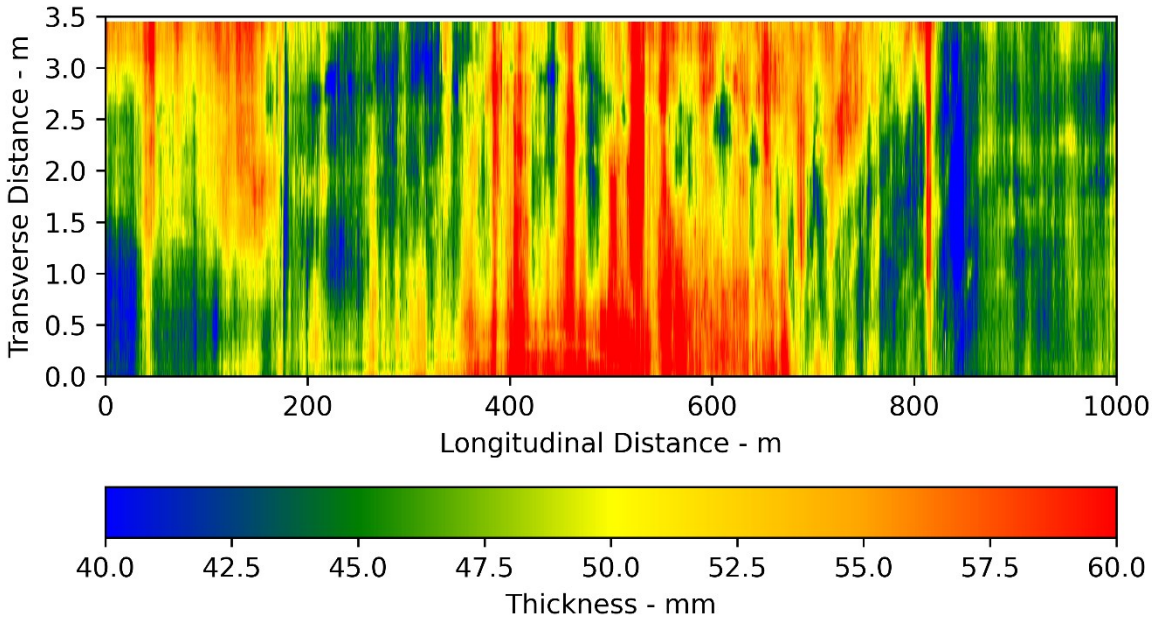

Figure 2: Colour map of thickness for EPA7 (50 mm) in lane 2, on SB carriageway on CNC.

For tyre/road noise, the primary region of influence by thickness is within the wheel paths. The thickness within the wheel path was calculated by extracting the mean value of a 0.4 m strip centred 0.95 m towards the centre of each lane from the edge and centrelines (see Figure 3). The transverse mean thickness, and lower 5% and upper 95% values are shown in Figure 3 for a one-kilometre sample.

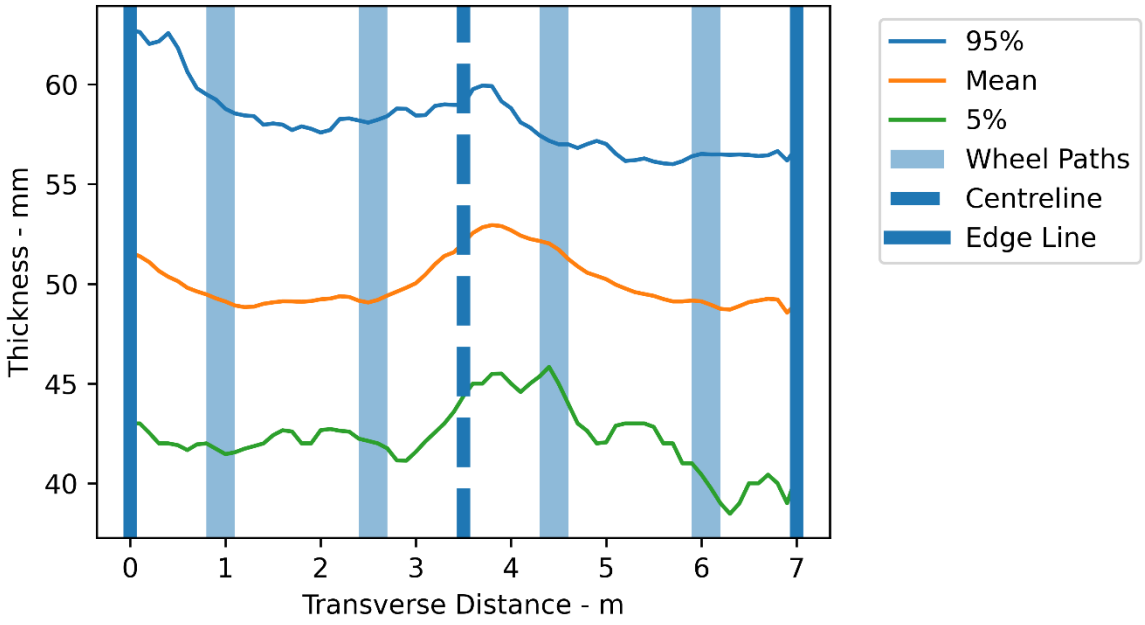

Figure 3: Transverse thickness for EPA7 (50 mm) on SB carriageway on CNC.

For the analyses of longitudinal variability and exploration of the relationships with L_{CPX}, only the thickness in the wheel paths was considered. Figure 4 shows an example of the longitudinal thickness in the left and right wheel paths. While the thicknesses in each wheel path are broadly correlated, there were regions where a sustained difference was observed (e.g., 0-150 m in Figure 4).

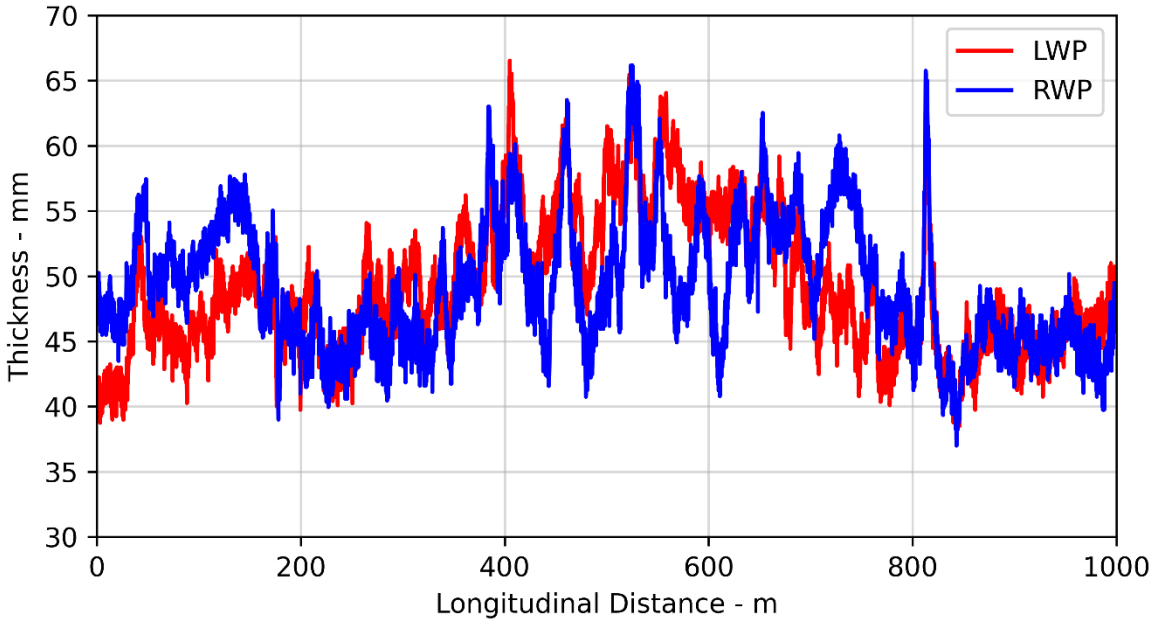

Figure 4: Longitudinal thickness of left and right wheel paths in lane 2 for EPA7 (50 mm) on the southbound carriageway on CNC.

The full thickness population was considered to be that of the left and right wheel paths (as described above). An example of the thickness distribution is shown in Figure 5 for a one-kilometre sample. In addition, the percentiles (e.g., 5th percentile) were calculated from these distributions. Note that the sample length of 2,000 m is from the combination of the two 1,000 m parallel wheel paths.

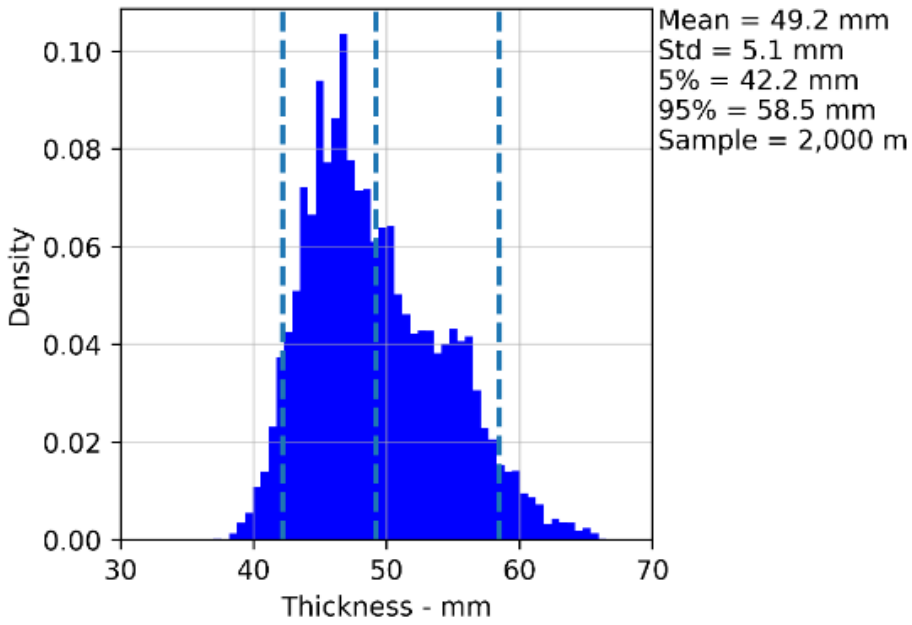

Figure 5: Wheel-path thickness distribution for the entire population for EPA7 (50 mm) on SB carriageway on CNC.

To understand how the actual thickness varies relative to that specified, the thickness distributions were calculated for each of the nine sample sections. The deltas from the specified thickness (e.g., a target thickness of 50 mm) were calculated for the 2.5th, 5th, and 25th percentiles, and the mean. Figure 6 contains boxplots of the deltas from the specified thickness for all sample sections. The mean thickness in the wheel paths was within ±5% of the specified thickness in eight of the nine sample sections. The minimum thickness (i.e., 2.5th percentile) was between 15 and 29% below the specified thickness.

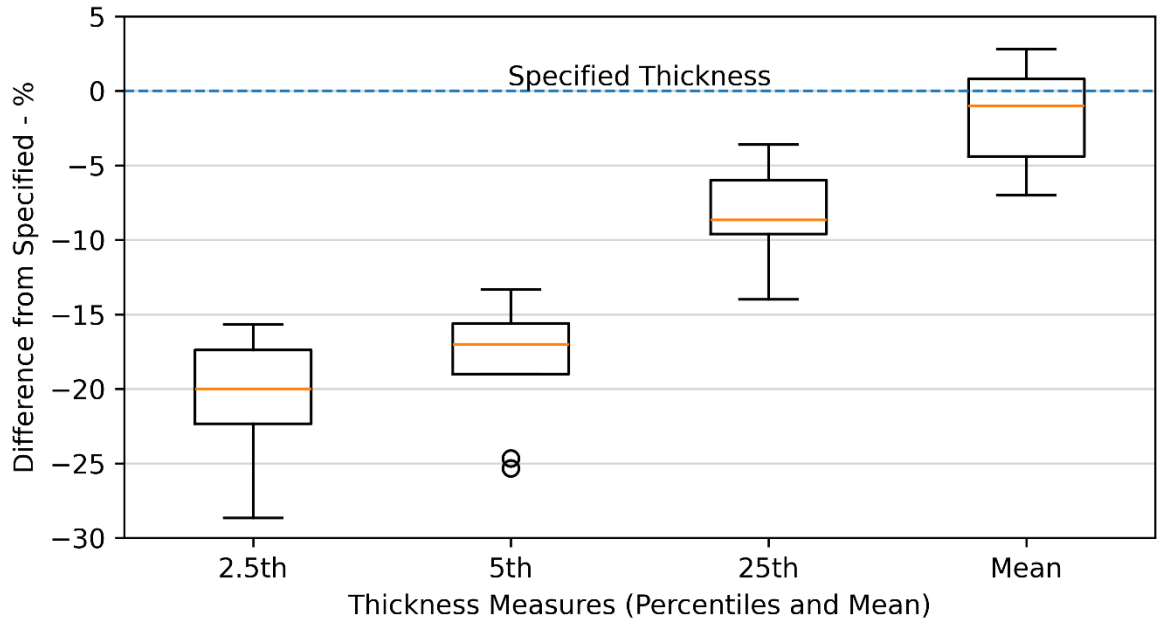

Figure 6: Deltas between percentiles and mean, and specified thickness for all sample sections.

2.2 Repeatability

The purpose of this section is to understand the repeatability of the laser survey method as the thickness is the delta of two discrete surveys. For surfaces that are known to have been static for both surveys, the deltas in elevations were used to establish the repeatability.

There were six sections of SMA on CNC that were suitable for use as reference surfaces. Their total length was 190 m (spanning both lanes). As only the left lane of PP2Ō had been paved at the time of the second survey, a one-metre-wide strip from the right lane was used as a reference. All deltas are presented as the post-surfacing survey minus the pre-surfacing survey.

The post-processing of the raw survey data required the use of physical and simulated datums; this was completed by Woods (*Mobile Laser Scanning | Woods*, 2023). Physical datums included features such as bridge footings, drains, and concrete barriers. It was assumed that the segments used in this analysis were not used for manipulating the survey results.

The analysis approach was to:

- Calculate the longitudinal profile for the mean cross-section delta.
- Calculate the transverse profile for the mean longitudinal delta.
- Generate the full distribution of point-to-point deltas for the full section and compute summary statistics.

An example of the analysis outputs for a 28 m section of SMA on CNC is shown in Figure 7. The mean delta was +0.4 mm (i.e., the post-surfacing survey was 0.4 mm above the pre survey). The variation primarily occurred longitudinally and may be related to the distance between survey datums.

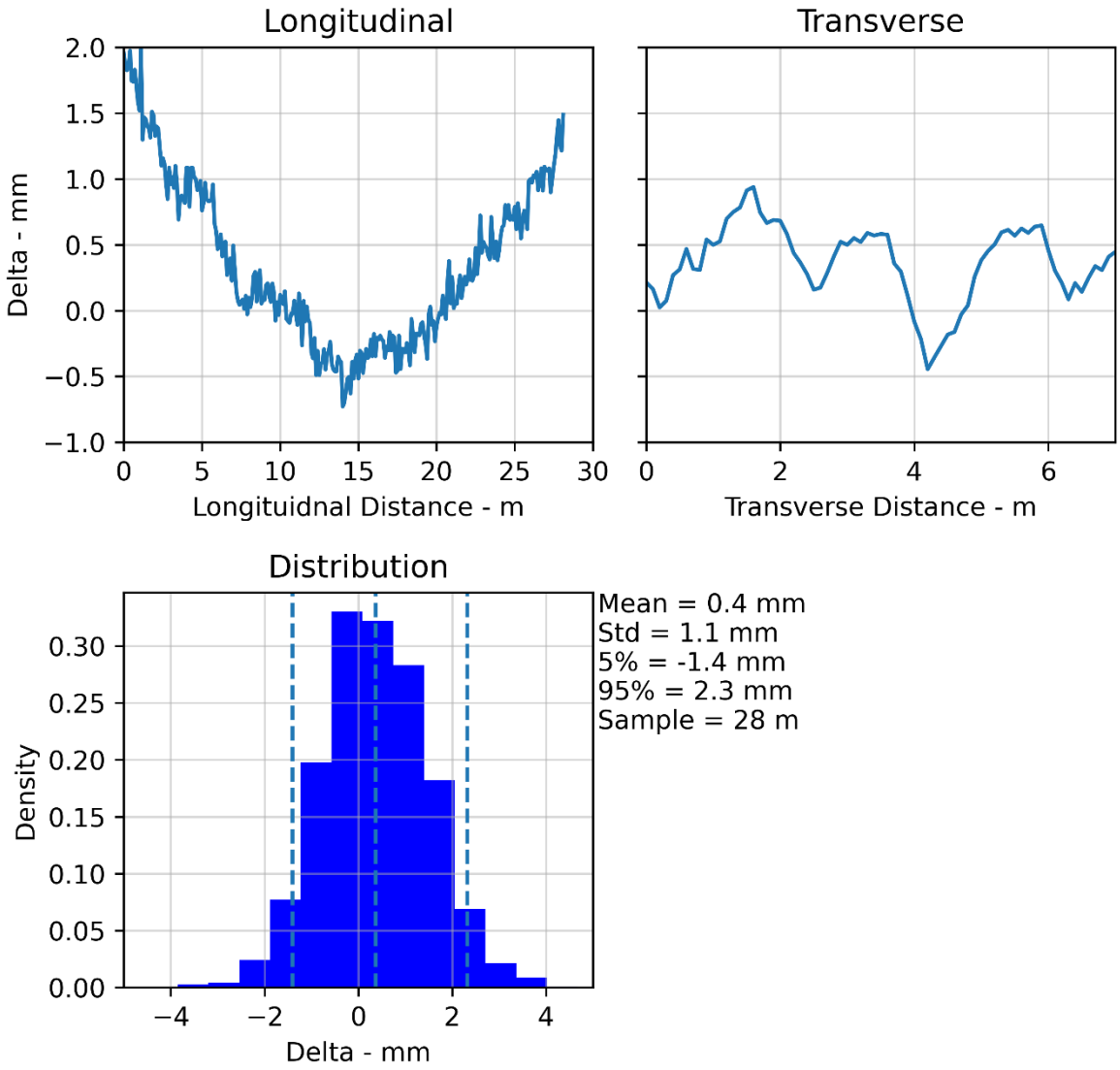

Figure 7: Example of reference surface metrics on CNC.

The overall point-to-point delta distribution for the full 190 m of SMA on CNC is shown in Figure 8. The mean delta of +0.2 mm and standard deviation of 1.6 mm indicated low inter-survey error or bias.

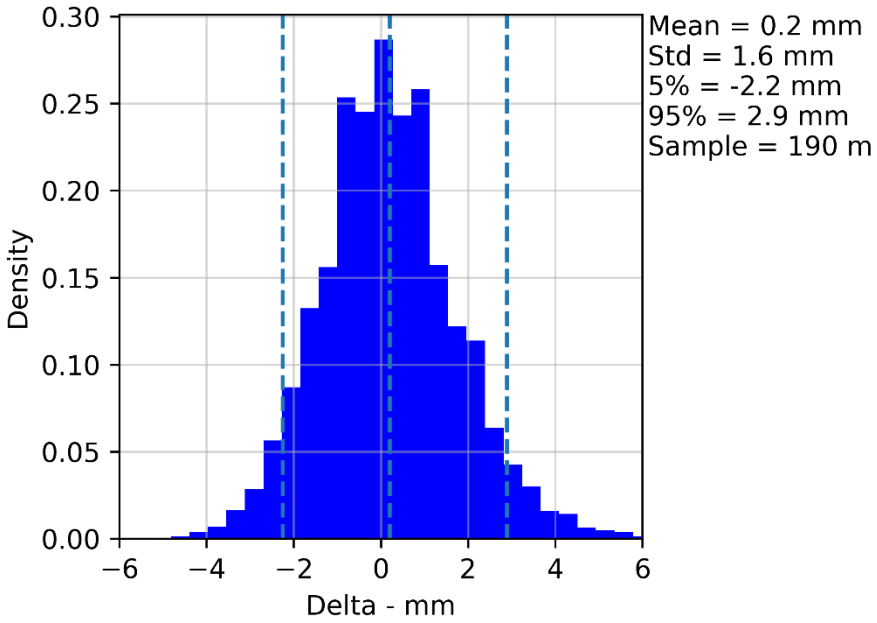

Figure 8: Delta between post- and pre-surfacing surveys for the reference surfaces on CNC.

The analysis outputs for the parallel reference surface on PP2Ō are shown in Figure 9. The mean delta was +1.7 mm (i.e., the post-surfacing survey was biased 1.7 mm above the pre-surfacing survey). The variation primarily occurred longitudinally with only a section between 300 and 400 m approaching a delta of zero. The causes of the positive bias are unknown.

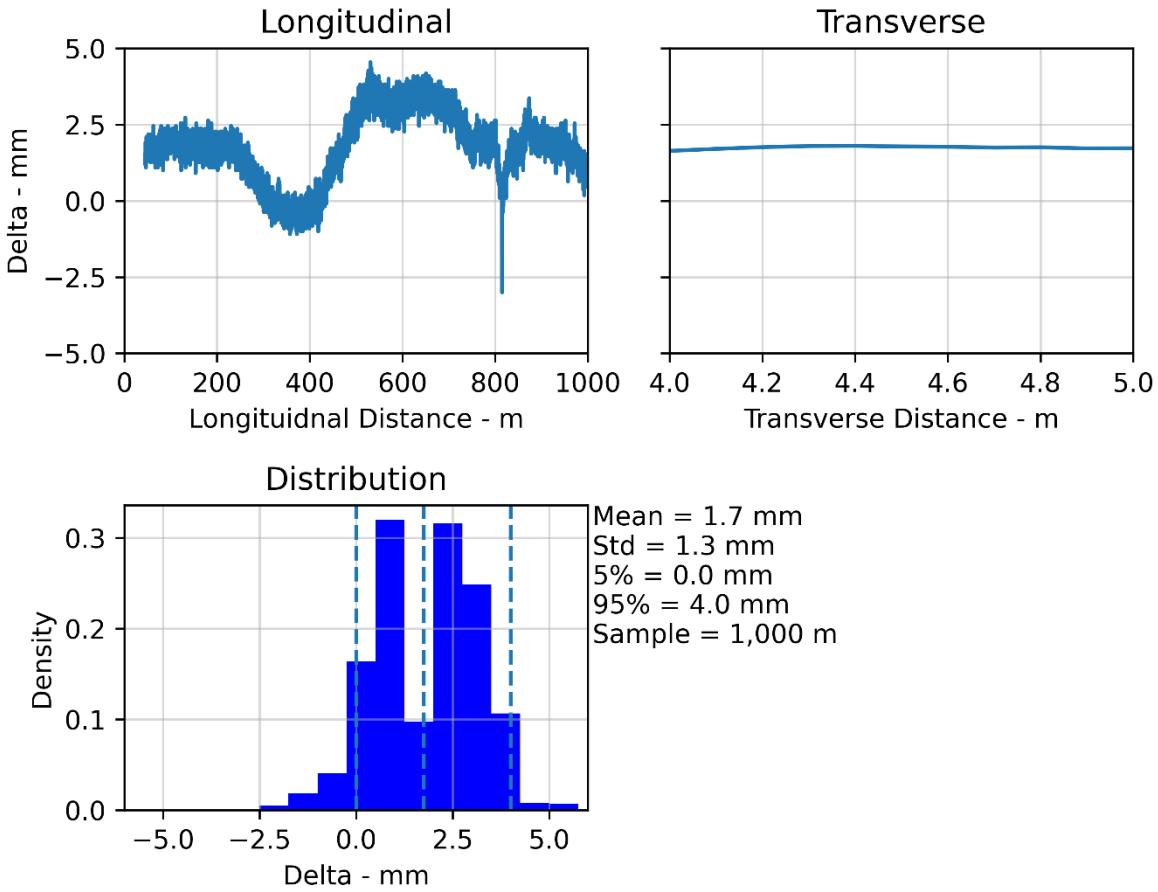

Figure 9: Delta between post- and pre-surfacing surveys for the reference surface on PP2Ō.

The key summary statistics for the reference surfaces are shown in Table 2. The delta for CNC was small (0.2 mm). The delta for PP2Ō had a positive bias of 1.7 mm and possessed a relatively tight range (4 mm). The tight range implies consistency of measurements around the shifted mean. The cause of the bias is unknown. Given the bias for PP2Ō, the MITSCAN comparison must be relied upon for validating the accuracy of the PP2Ō survey.

Table 2: Summary of reference surface statistics.

	CNC	**PP2Ō**
Mean delta	+0.2 mm	+1.7 mm
Std of delta	1.6 mm	1.3 mm
5 to 95%	-2.2 to 2.9 mm	0.0 to 4.0 mm

2.3 MIT-SCAN Comparison

The purpose of this section is to compare the laser survey results to the point measurements made using the MIT-SCAN. The MIT-SCAN is a proprietary device that utilises magnetic pulse induction to measure the thickness of road surfaces. The methodology is prescribed in (Standard Test Method for Pavement Thickness by Magnetic Pulse Induction, 2020). Aluminium disks are placed prior to the asphalt being laid, which can be subsequently used to determine the local thickness at that point.

There were 202 and 43 usable disks that overlapped with the laser surveys for CNC (Wareing, 2022) and PP2Ō, respectively. A single point measurement was extracted from the laser survey data that matched the coordinates of the MIT-SCAN disks. For CNC, the MIT-SCAN measurements were primarily intended for discrete surface mix trial sites, so do not fully span the sample sections in Table 1. The delta is reported as the laser survey minus the MIT-SCAN thickness.

Distributions of the deltas for CNC and PP2Ō are shown in Figure 10 and Figure 11, respectively. The mean deltas were 0.2 and -0.1 mm for CNC and PP2Ō, respectively. The negligible magnitudes of the mean deltas suggest excellent agreement between the two measurement methods. The bias observed for the reference surface on PP2Ō was not evident in the MIT-SCAN comparison; the reason for this is unknown.

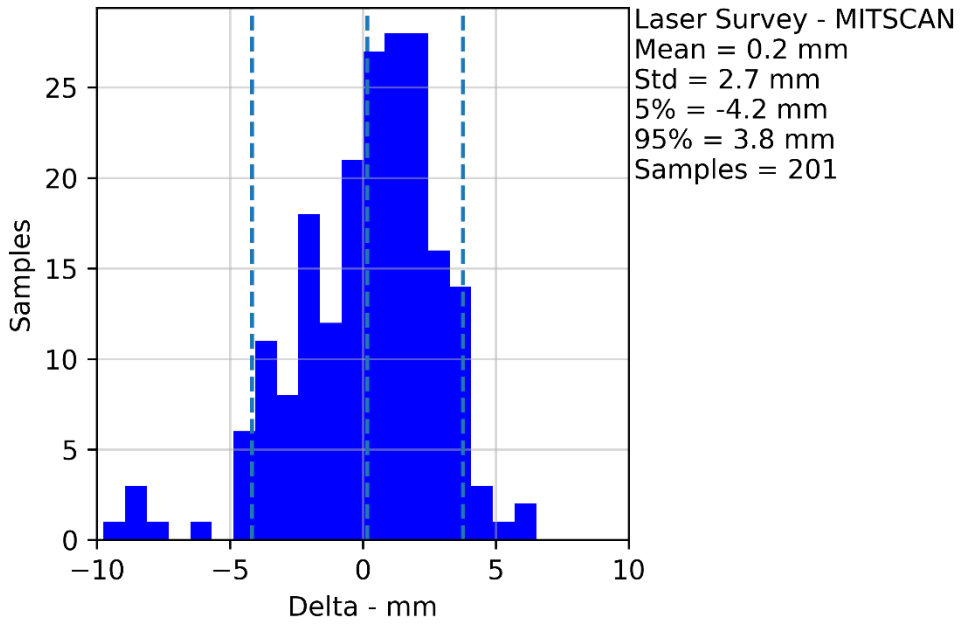

Figure 10: Delta between laser scan and MIT-SCAN thickness measurements for CNC.

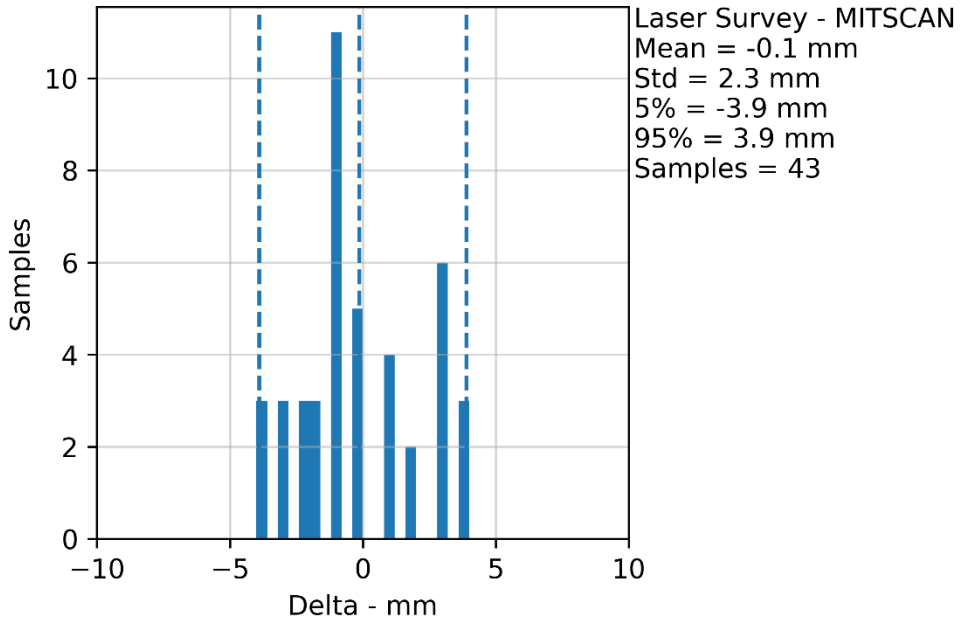

Figure 11: Delta between laser scan and MIT-SCAN thickness measurements for PP2Ō.

Figure 12 contains boxplots of the deltas grouped by specified thickness (30 and 50 mm) for CNC. There were no significant differences between the groups, suggesting the deltas are not affected by thickness in the analysed sample.

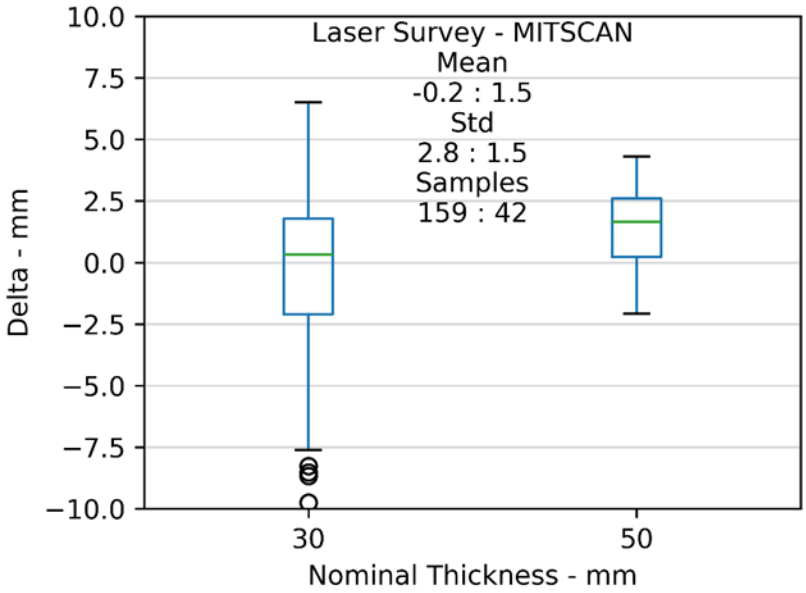

Figure 12: Deltas between laser scan and MIT-SCAN thickness measurements for CNC grouped by specified thickness.

The summary statistics for the deltas between the laser survey and MIT-SCAN thicknesses are shown in Table 3. There was excellent agreement between the two methods for both locations.

Table 3: Summary of deltas between laser survey and MIT-SCAN thickness measurements.

	CNC	**PP2Ō**
Mean delta	0.2 mm	-0.1 mm
Std of deltas	2.7 mm	2.3 mm
5-95%	-4.2 to 3.8 mm	-3.9 to 3.9 mm

2.4 Thickness and L_{CPX}

The purposes of this section are to (1) reproduce previously observed relationships between L_{CPX} and thickness as an indirect method of demonstrating the validity of the laser survey, and (2) expand the understanding of the influence of thickness on the noise spectra.

2.4.1 Thickness Influence on Overall L_{CPX}

The relationship between overall L_{CPX} and thickness was previously explored with linear or second-order polynomial models (Bell, 2022; Bull et al., 2021; IHARA & INOUE, 2003). In all of the evaluated scenarios, the models revealed negative correlations between the overall L_{CPX} and thickness.

A multivariate regression model was applied between thickness, MPD (from the high-speed data (HSD) annual survey), and the overall L_{CPX}. The longitudinal data resolutions were L_{CPX} at 4 m, MPD at 10 m, and thickness at 0.1 m. A fourth-order polynomial fit was applied to thickness and a linear fit applied to MPD. A fourth-order polynomial fit was used for thickness as a simplified approach to capturing the complex acoustic absorption relationships.

The measured overall L_{CPX} for the left wheel path of lane 2 for all EPA7 on CNC is plotted as a function of thickness in Figure 13. The multivariate model for L_{CPX}, thickness, and MPD is also included in Figure 13. The model demonstrated a very strong fit with the measured data (R^2 = 0.88).

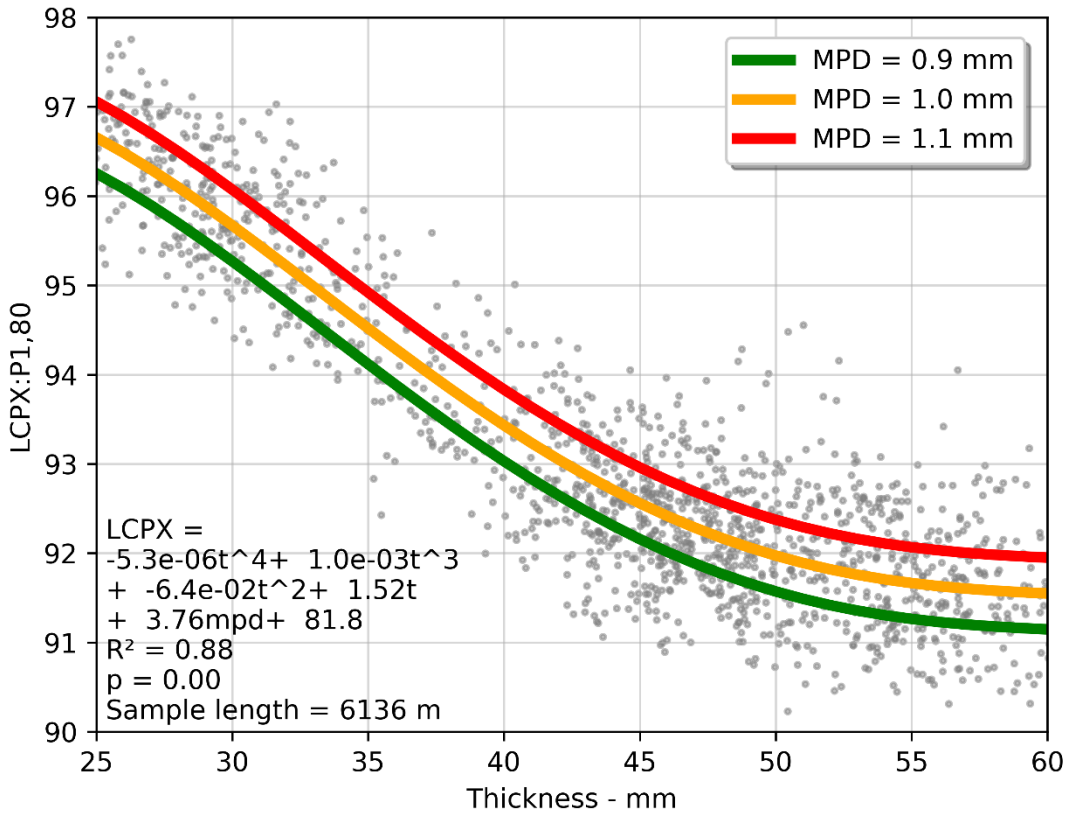

Figure 13: L_{CPX} versus thickness for the left wheel path of lane 2 of EPA7 on CNC and the multivariate model for L_{CPX}, thickness, and MPD.

The observed relationship between L_{CPX} and thickness is comparable to that previously found using the MIT-SCAN disks on CNC and the manual survey on CSM2 – see Figure 14. Significant deviations occurred below 35 mm, which may be attributable to fewer data points in that range for the MIT-SCAN and manual survey and having used only a second-order polynomial fit. Both CNC results converge with increasing thickness. The positive offset for the CSM2 fit is possibly attributable to the higher mean MPD compared to CNC (0.94 versus 0.83 mm).

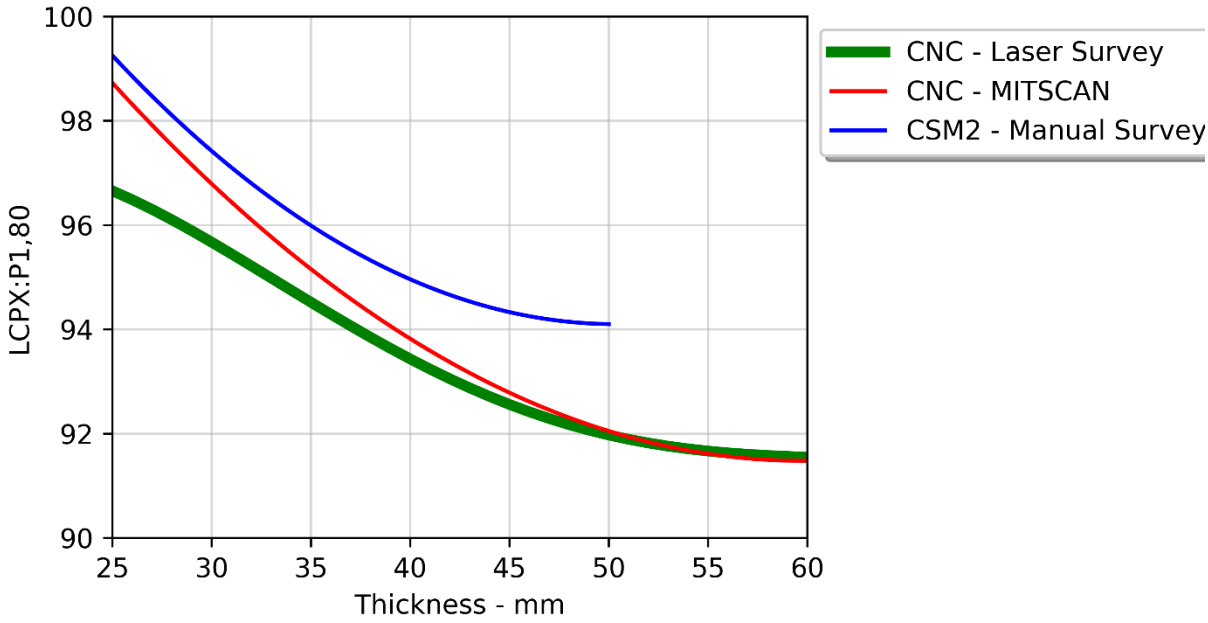

Figure 14: Model of L_{CPX} as a function of thickness for EPA7 on CNC and previous models from CNC and CSM2 from (Bell, 2022).

To explore the rate of change of L_{CPX} with thickness the derivative of the linear and polynomial models were taken. The resulting rates of change of L_{CPX} as a function of thickness are shown in Figure 15 . The fourth- and second-order regression models diverged below 35 mm; this is possibly due to the same reasons as above or edge-effects of the polynomial fits. For the analysed samples, the greatest rate of change was -2.4 dB/10 mm occurring at a thickness of 35 mm. The rate of change decreased in magnitude with increasing thickness. It is hypothesised that the diminishing impact of increasing thickness is in-part due to the peak absorption frequency shifting below the dominant generation bands. It is important to note that the observation of this phenomenon is currently limited to CPX measurements using the P1 tyre at 80 km/h and the "1" and "2" microphone positions.

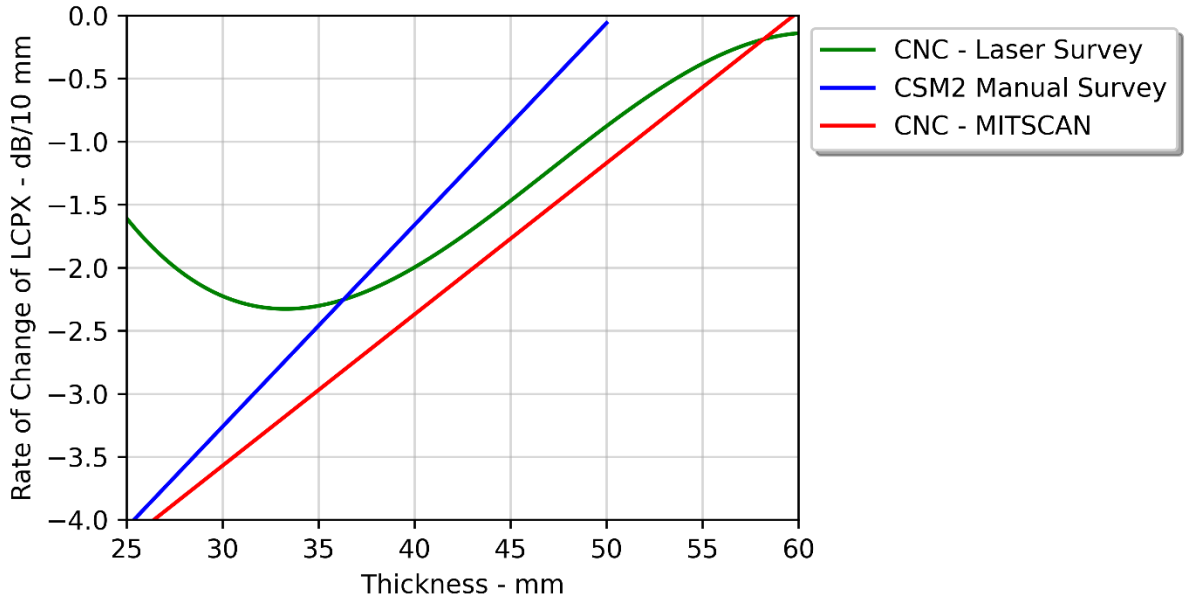

Figure 15: Rate-of-change of L_{CPX} as a function of thickness.

The relationship observed between L_{CPX} and the thickness measured using the laser survey, along with the congruence of these relationships with those predicted using alternative thickness measurement methods, suggests that the laser survey method is accurate.

2.4.2 Thickness Influence on One-Third Octave Spectra

The relationships between each one-third octave band and thickness were explored. Thickness had non-linear relationships with several of the one-third octave bands. Figure 16 shows the L_{CPX} in the 1,250 Hz band as a function of thickness. A fourth-order polynomial offered a strong fit with the observed data (R^2 = 0.81). Varying the thickness in the fitted model from 25 to 60 mm resulted in an 8.7 dB range of L_{CPX} in the 1,250 Hz band with the minimum occurring at a thickness of 43 mm.

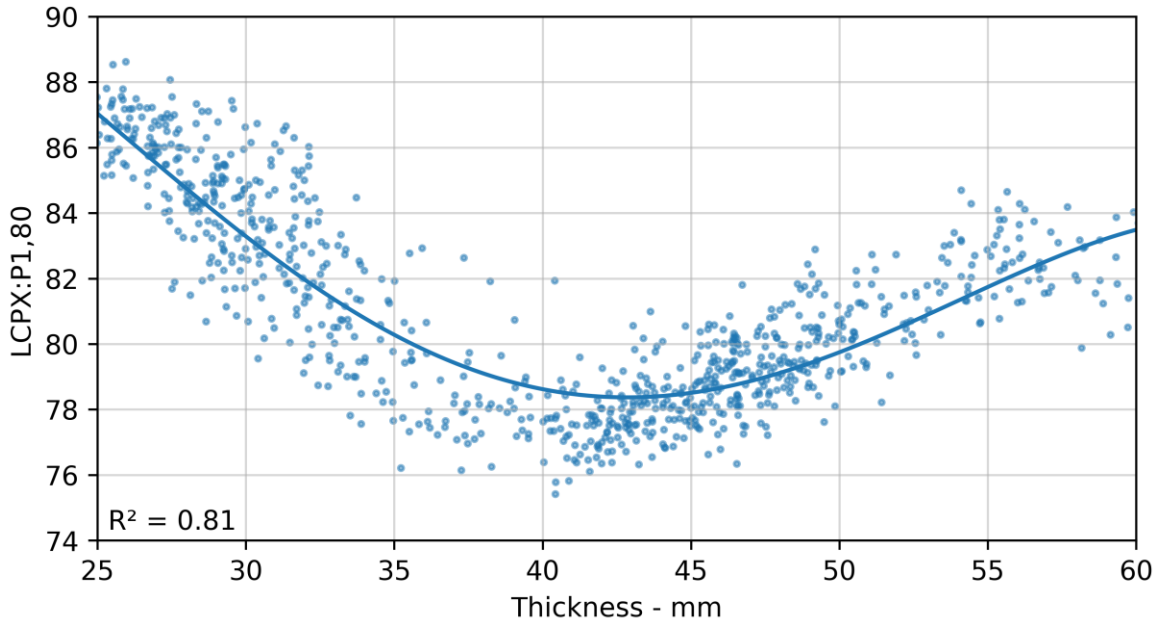

Figure 16: 1,250 Hz one-third octave band levels versus thickness for EPA7 on CNC.

A fourth-order polynomial fit was applied between each one-third octave band and thickness, the resulting predicted range for a 25 to 60 mm variation in thickness is shown in Figure 17 along with the coefficient of determinations for the models with the measured data. Thickness significantly influenced L_{CPX} from the 630 to 2,500 Hz bands. Thickness had no significant effect in the 315 to 500 Hz, and 3,150 to 5,000 Hz bands.

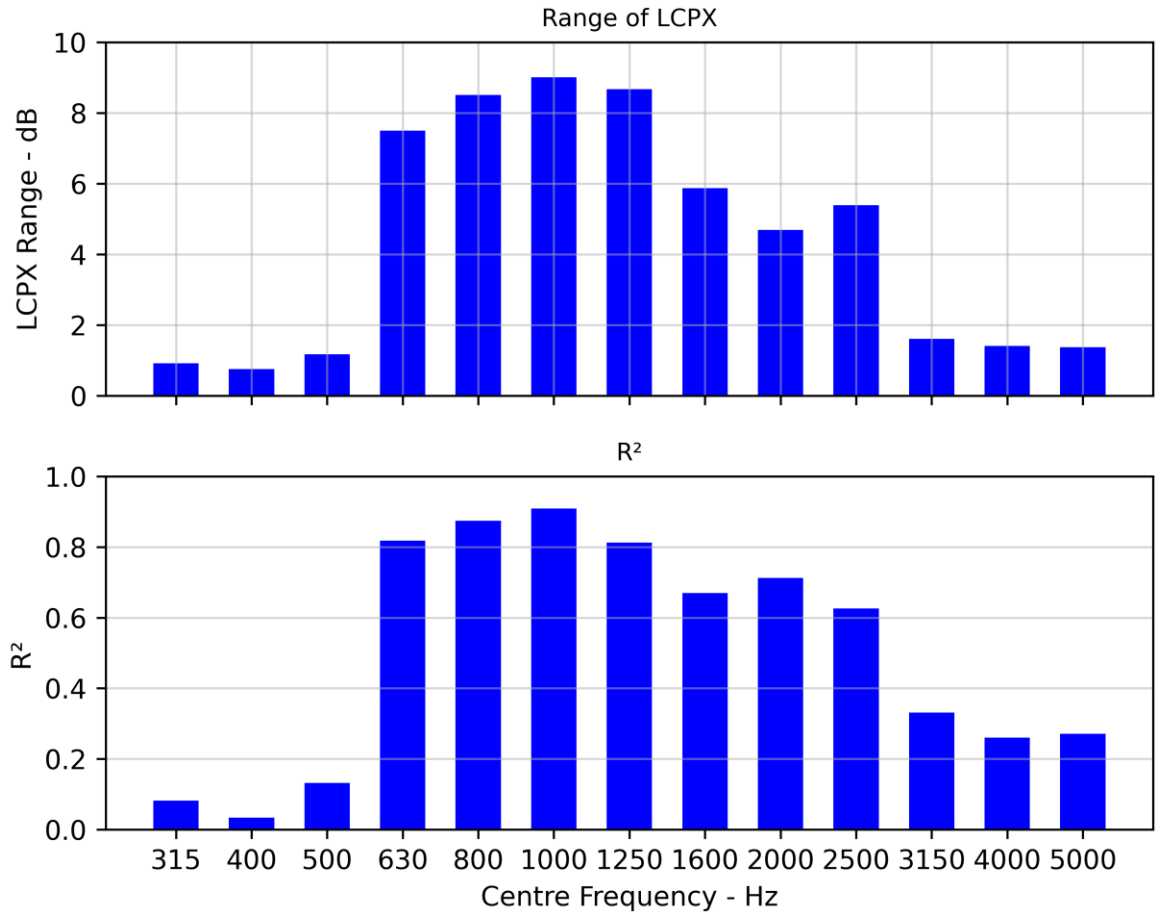

Figure 17: Range of predicted L_{CPX} due to variation in thickness for each one-third octave band.

2.5 Simulated Point Measurements

Based on the combination of the comparison of reference surfaces and MIT-SCAN measurements, and correlations with tyre/road noise, the laser survey results appear to be suitable for use in simulating point measurement scenarios (e.g., using a magnetic induction method).

The aim of this section is to determine the required point measurement spacing to ensure confidence in the verification of a specified thickness requirement. The requirement can be that a stated percentile of measured thickness must be greater than the specified thickness. An example could be written as follows: the 25th percentile of thickness must be greater than or equal to 50 mm. The point spacing must provide a representation of the thickness population that allows for the accurate (e.g., ±2 mm) estimation of the required percentile with sufficient confidence (e.g., 90%).

2.5.1 Method

The following steps were taken to estimate a range of thickness percentiles with 90% confidence.

1. The longitudinal thickness profiles in the wheel paths were calculated (see example in Figure 18).
2. The full population distribution of thicknesses for the combination of both wheel paths was calculated (see example in Figure 19).
3. The stated percentiles (2.5th, 5th, and 25th) were calculated from the full thickness population.
4. A simulated point was placed in each wheel path starting at zero m, in a range of longitudinal increments from 0.1 to 100 m (see Figure 18 for an example of 50 m point spacing).
5. A thickness distribution was created from the simulated points (see example in Figure 19) and the same stated percentiles were calculated.
6. The start position for the disks was shifted 0.1 m longitudinally along the road and the distribution and percentiles were recalculated.
7. The distribution of estimated percentiles (see example in Figure 20) was calculated (i.e., the combination of all start positions). The lower 5% and upper 95% values were calculated for each point spacing.
8. The lower 5% and upper 95% values were then plotted as a function of simulated point spacing (Figure 21).

The steps above were undertaken for each of the nine one-kilometre sample sections in Table 1. One-kilometre samples were used as this is within the typical range for the distance covered in a single paving shift.

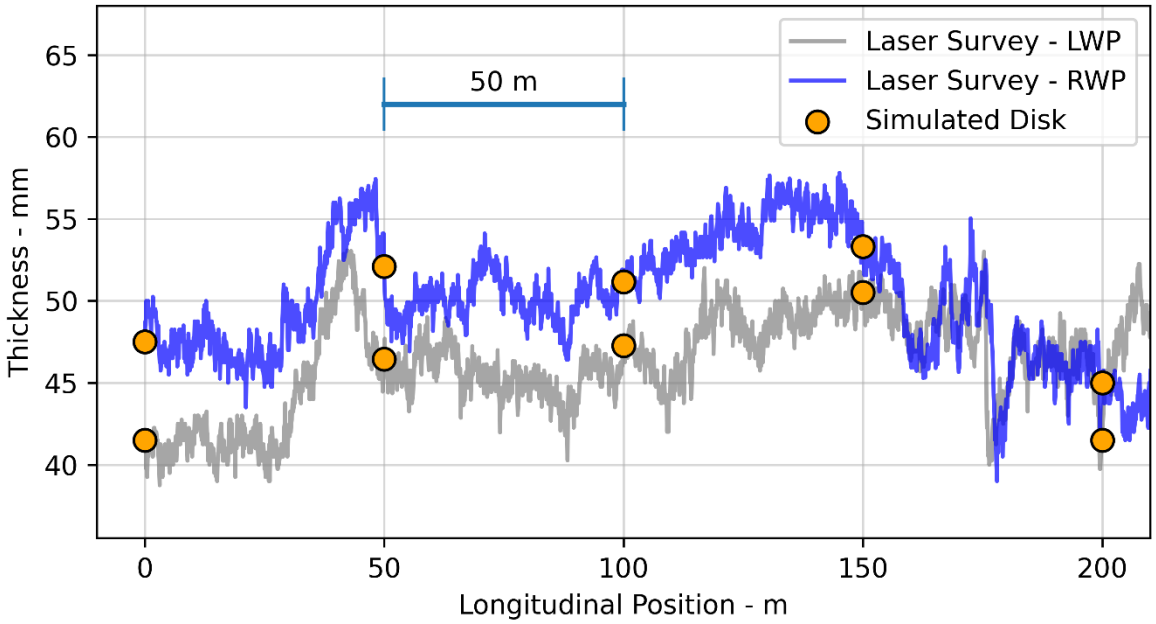

Figure 18: Example of point measurement locations ("disks") on a nominally 50 mm thick EPA7 sample on CNC.

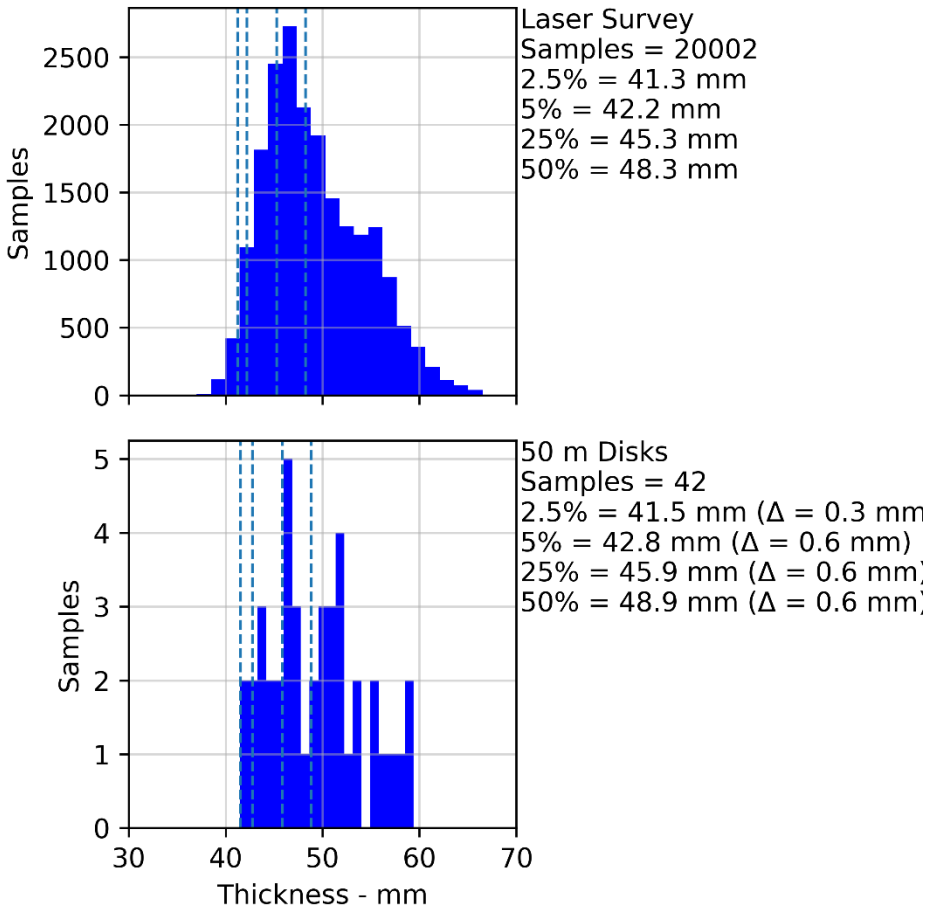

Figure 19: Example of thickness distribution achieved with 50 m point spacing compared to the full population.

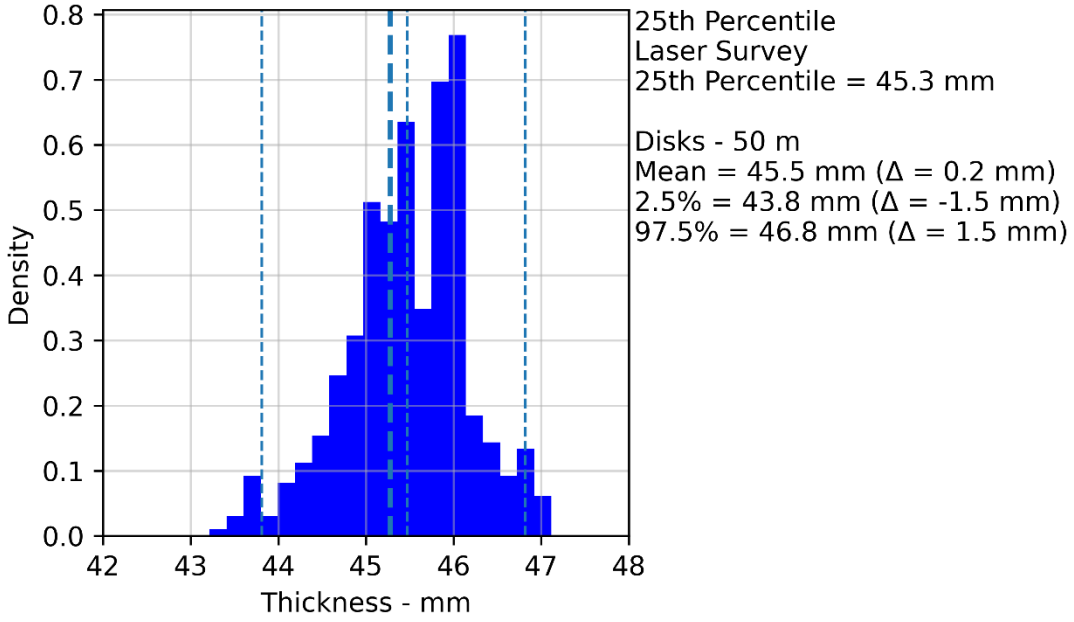

Figure 20: Example of 25th percentile estimation using 50 m point spacing for all start positions.

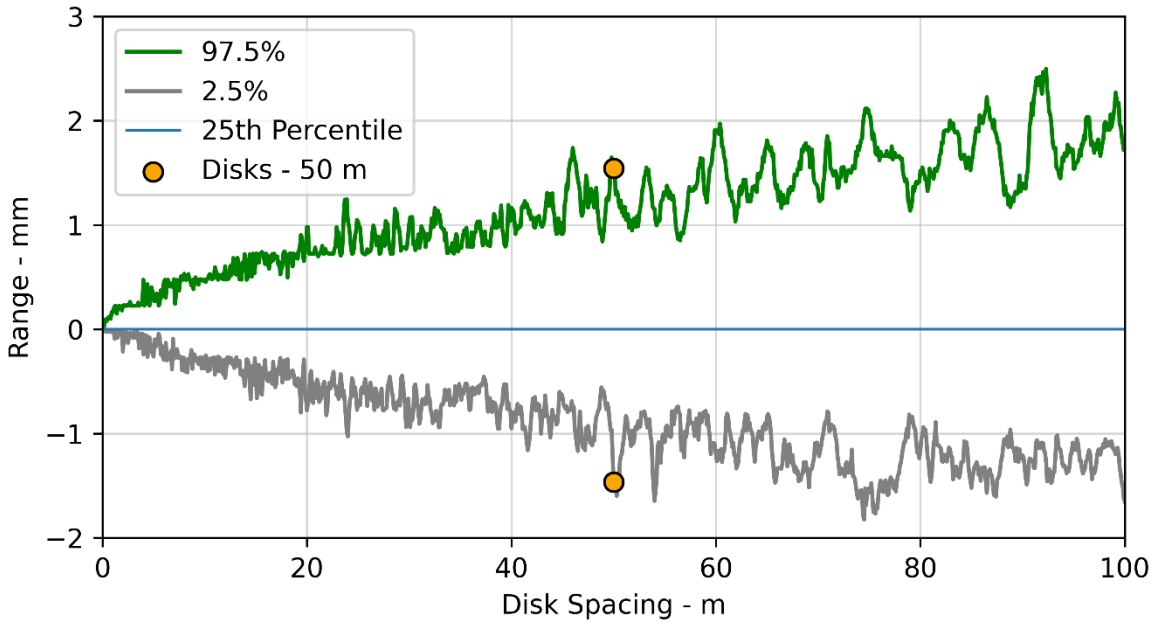

Figure 21: Estimated range of 25th percentile versus point spacing for EPA7 (50 mm) surface on CNC.

The fluctuations in the estimated range may be due to aliasing occurring at critical point spacings or randomness in the data. The wavelength spectrum for each wheel path is shown in Figure 22. The presence of discrete peaks supports the aliasing hypothesis. The actual amplitude of fluctuation (<0.5 mm) is below any practical thickness accuracy requirement and was not considered further.

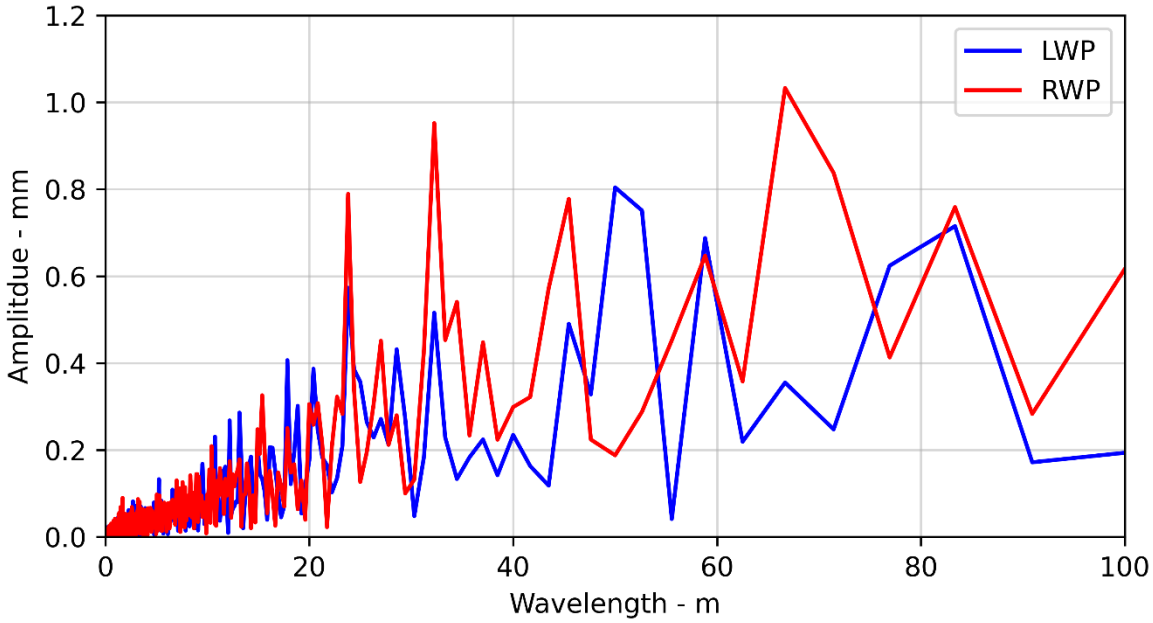

Figure 22: Wavelength spectra of longitudinal thickness in the left and right wheel paths of the EPA7 (50 mm) in lane 2 of the SB carriageway on CNC.

2.5.2 Results

Boxplots for estimating the 2.5th, 5th, and 25th percentile thickness with 90% confidence are shown in Figure 23 for point spacings of 10, 20, 50, and 100 m. To achieve 90% confidence on the estimation of the 25th percentile within ±2 mm of the true value, a point spacing of less than 100 m must be used. To achieve 90% confidence on the estimation of the 2.5th percentile within ±2 mm of the true value, a point spacing no greater than 10 m must be used. Overall, the spacing must be reduced to adequately estimate lower percentiles.

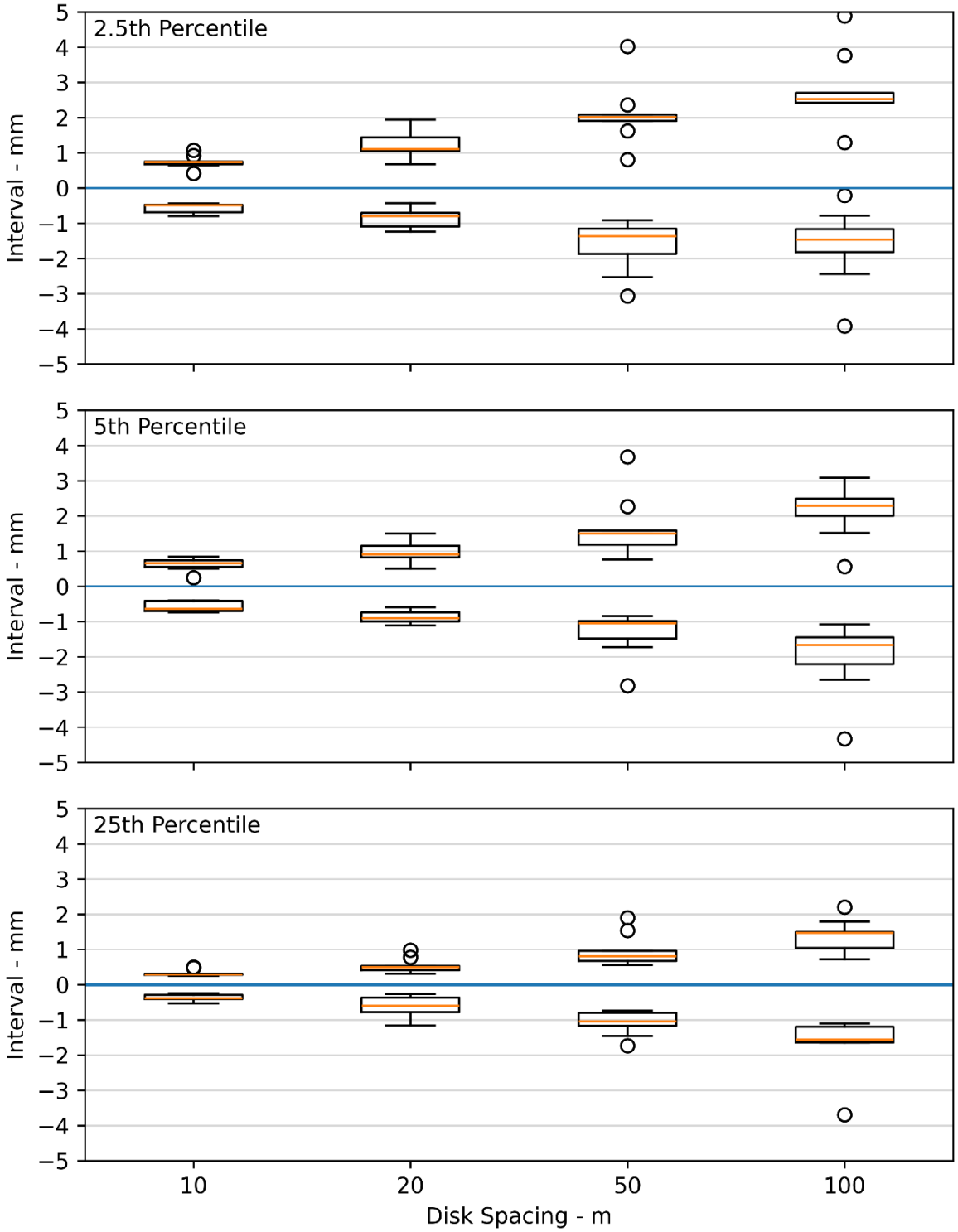

Figure 23: Percentile estimation ranges for the nine sample sections.

2.5.3 L_{CPX} and Thickness Sensitivity Analysis

A sensitivity analysis was conducted to understand the impact of the observed thickness variation on the overall L_{CPX}. The percentage difference for the 2.5th, 5th, and 25th percentile, and mean from the specified thickness for each sample section was calculated; boxplots of the results are shown in Figure 6. The 25th percentile was between 4 and 14% below the specified thickness with a mean of 8%, while the 2.5th percentile was between 15 and 29% below the specified thickness.

Using the relationship between L_{CPX} and thickness from Figure 13, the deltas from the specified low noise surface thicknesses (40 and 50 mm) were predicted. The relative deltas from the specified thickness are shown in Figure 24. The rate of change of L_{CPX} decreases with increasing thickness, which results in greater changes for perturbations in thickness around 40 mm compared to 50 mm.

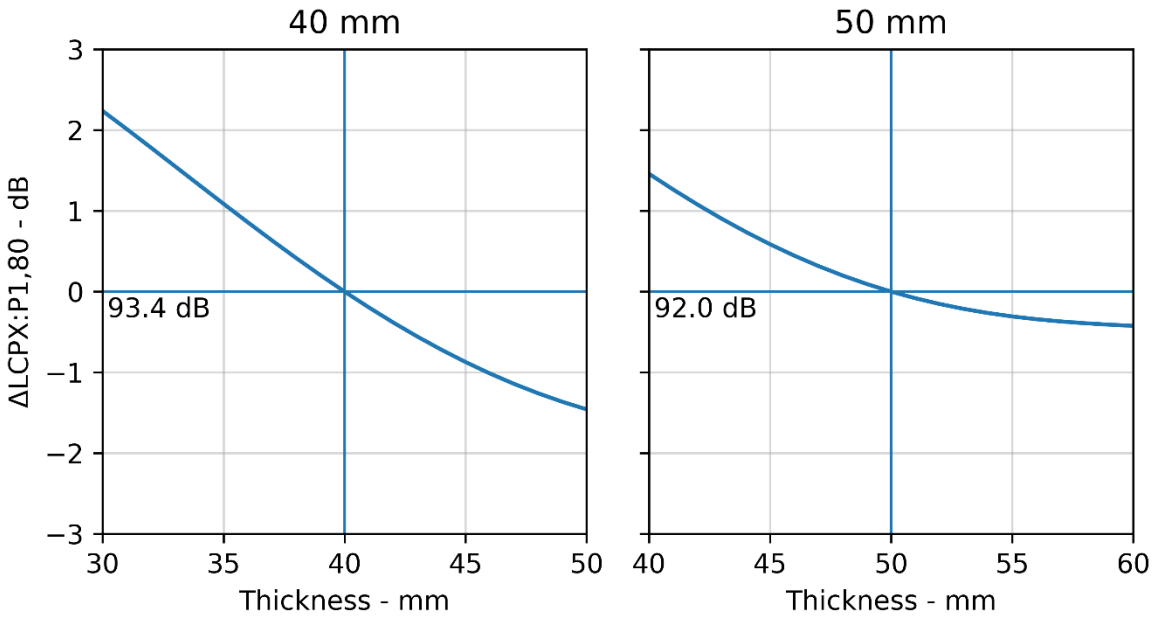

Figure 24: Relative change in overall L_{CPX} centred around 40 and 50 mm thick EPA7 surfaces.

2.5.4 Recommended Thickness Measurement Requirement

The following point measurements are recommended for determining if the specified thickness has been achieved.

Point measurements are to be made every 40 m in both wheel paths. The measurements in each wheel path are to be staggered by 20 m.

Using the observed thickness variation in the nine sample sections, the L_{CPX} levels in Table 4 would be present. The 25th percentile is the proposed thickness requirement. The 2.5th percentile is provided as an estimate of the effective minimum thickness and therefore maximum L_{CPX}.

Table 4: Estimated thickness and L_{CPX} ranges with the sample criterion.

Specified	**40 mm**		**50 mm**	
Measure	Thickness – mm	L_{CPX} - dB	Thickness – mm	L_{CPX} - dB
2.5th	34.4	94.7 (+1.3)	43.0	92.9 (+0.9)
25th	40.0 ±2	93.4 ±0.4	50.0 ±2	92.0 ±0.2
Mean	43.0	92.9 (-0.5)	53.8	91.7 (-0.3)

A comparison between the specified values and those achieved for a one-kilometre sample of EPA7 (50 mm) surface is shown in Table 5. The sample includes both wheel paths and lanes for the section on the

southbound carriageway on CNC. It is noted that as for most previous projects, the sample section was not subject to any mandatory thickness measurement requirements. The mean and 25th percentiles are 0.3 dB greater than those that would have been achieved had the recommended thickness requirements been attained.

Table 5: Thickness and L_{CPX} measures for both lanes of EPA7 (50 mm) sample on southbound carriageway of CNC.

Measure	Thickness – mm	L_{CPX} - dB	ΔL_{CPX} - dB
2.5th	40.65	93.3	+0.4
25th	46.6	92.3	+0.3
Mean	49.8	92.0	+0.3

3 Sources of Thickness Variation

To achieve a thickness requirement without a substantial increase in the mean thickness (i.e., total volume of material required) it is imperative to identify and quantify the sources of variation so they can be minimised where practical. Causes of variation in thickness include but are not limited to (1) geometric differences between the base and the top surface of the asphalt, (2) variability in construction parameters, (3) operational settings, and (4) material variability.

It is important to acknowledge that the top asphalt layer is intended and expected to partially smooth variations in the underlying layers. The variation in the underlying layers is dependent on many factors including the type and pre-surfacing trafficking. CNC has a foamed bitumen stabilised pavement, where the finished level was completed by a grader. Conversely, a structural asphalt concrete pavement is finished using a paver, which is able to achieve a relatively smoother surface. Foamed bitumen stabilised pavements must be trafficked for a period prior to final surfacing, which results in rutting; this rutting is then smoothed (i.e., removed) by the top asphalt layer.

Geometric differences between the underlying pavement and the top of the porous asphalt layer may include the smoothing of short wavelength (e.g., less than 20 m) longitudinal and transverse undulations, and the adjustment of camber. Variation in thickness due to these three factors were analysed for one km of the EPA7 (50 mm) in lane 2 of the southbound carriageway on CNC.

Construction parameters, such as roller passes and paver speed, may affect the overall thickness, compaction, and void structure. The influence of construction parameters was analysed for CNC, which is an extension of previous work (Bell, 2023). The laser survey data was not considered in the previous analysis.

During paving, the operators can adjust a variety of parameters such as the screed height and angle, feed rates, speed, etc. There are many practical considerations for why and how these parameters are adjusted. At present, there is no data available to explore the effects of these parameters and therefore this aspect is not considered further in this report.

Material variability may arise from aggregate grading, mix design tolerances, plant operation, and a range of other factors; this was not considered in this report.

It is acknowledged that thickness uniformity for noise performance might be constrained by other aspects including ride quality, underlying pavement and top surface height tolerances, equipment capabilities, and current industry practices.

The CNC project has been used to provide invaluable data for this research because relevant noise and thickness datasets were available for that project. These findings are assumed to be representative of current practices across the industry for all projects and matters raised are not anticipated to be specific to the CNC project.

3.1 Geometry

The longitudinal and transverse geometric contributions to variations in thickness were explored in isolation. The analyses were conducted in turn on a one km section of EPA7 (50 mm) in lane 2 of the southbound carriageway on CNC (see Table 1). The thickness between the solid edge line and centreline was considered (i.e., excluding the shoulder). There was significant variation in thickness across this section (the central 99% range was 39 to 65 mm). A colour map of thickness is shown in Figure 2. All findings in this section are limited to the analysed sample.

3.1.1 Longitudinal Underlying Pavement Undulation

The hypothesis is that the porous asphalt surface fills in depressions in the underlying pavement layer; this is expected to occur for shorter wavelengths (i.e., porous asphalt is not used to fill in a 200 m long depression). There is typically no requirement to smooth long wavelength elevation undulations as these do not affect ride quality. To test this hypothesis, the following steps were taken:

1. The base layer elevation and thickness were extracted for the left wheel path along the sample section.
2. A high-pass filter was applied to the base layer to remove long wavelength changes (such as those due to true elevation changes). A cut-off wavelength of 50 m was used for filtering the pavement elevation. 50 m was selected by iteration to achieve the best fit with the measured data.
3. Relationships between the underlying pavement height and thickness were explored.

The underlying pavement and top surface heights, and porous asphalt thickness are shown in Figure 25. The horizontal dashed lines correspond to the specified height (i.e., zero for the pavement and 50 mm for the top surface). Figure 26 contains a scatter plot of the pavement height versus the thickness; a linear fit was a poor predictor of the measured data (R^2 = 0.08). A noteworthy qualitative feature of the scatter plot is the apparent presence of local relationships (e.g., top left corner), which implies that discrete segments may exhibit correlations.

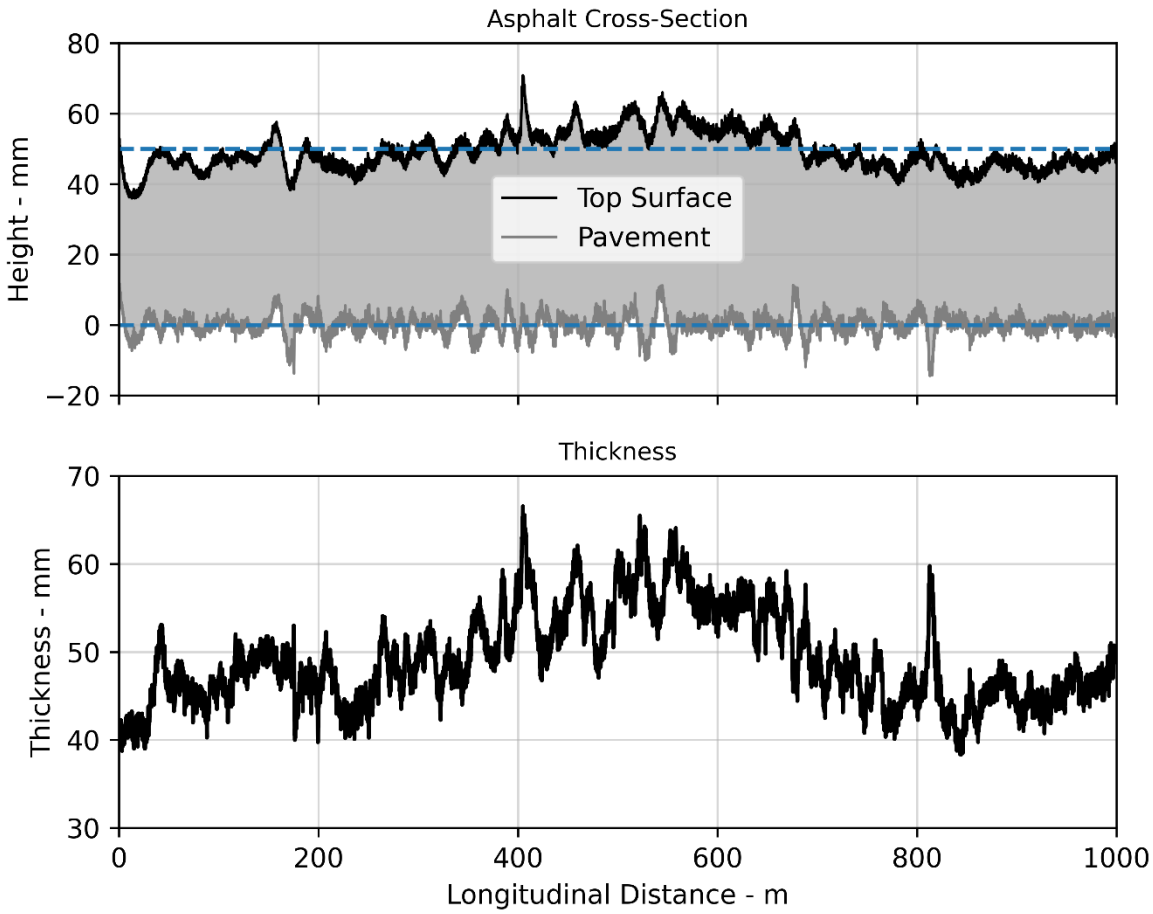

Figure 25: Relative height from the pavement and thickness for the sample section.

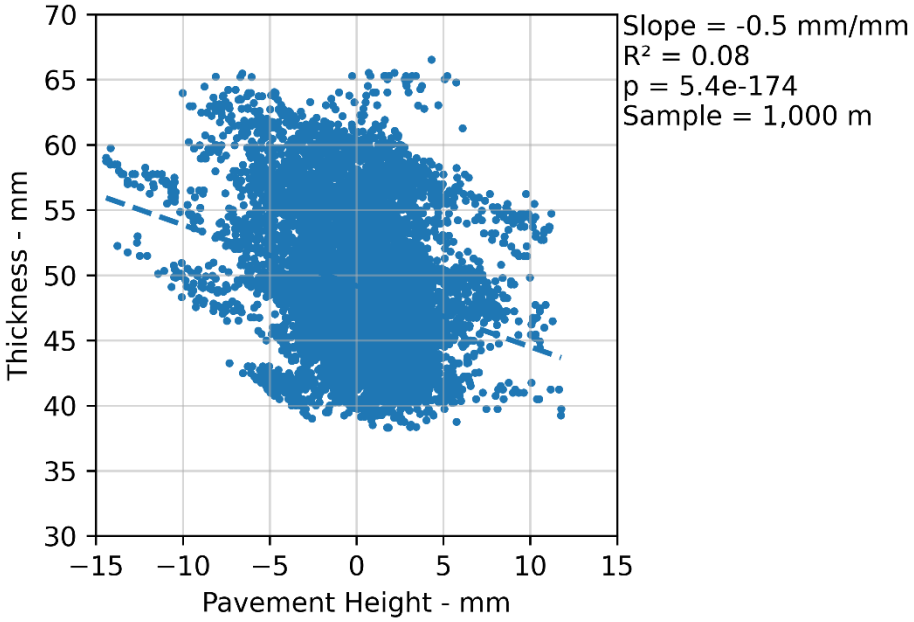

Figure 26: Thickness versus local pavement height for the sample section.

To explore if discrete segments possessed a correlation between the underlying pavement height and thickness, a 20 m analysis-window was traversed along the one km sample section. An example 20 m subsample is shown in Figure 27 and a scatter plot of pavement height versus thickness in Figure 28. When a linear fit was applied between thickness and pavement height for this subsample there was strong agreement with the measured data (R^2 = 0.81) and a slope of -0.6 mm/mm. The negative slope of the linear fit indicates that for every 1 mm increase in height of the underlying surface, the thickness of the asphalt reduces by 0.6 mm - thus partially smoothing undulations in the underlying surface.

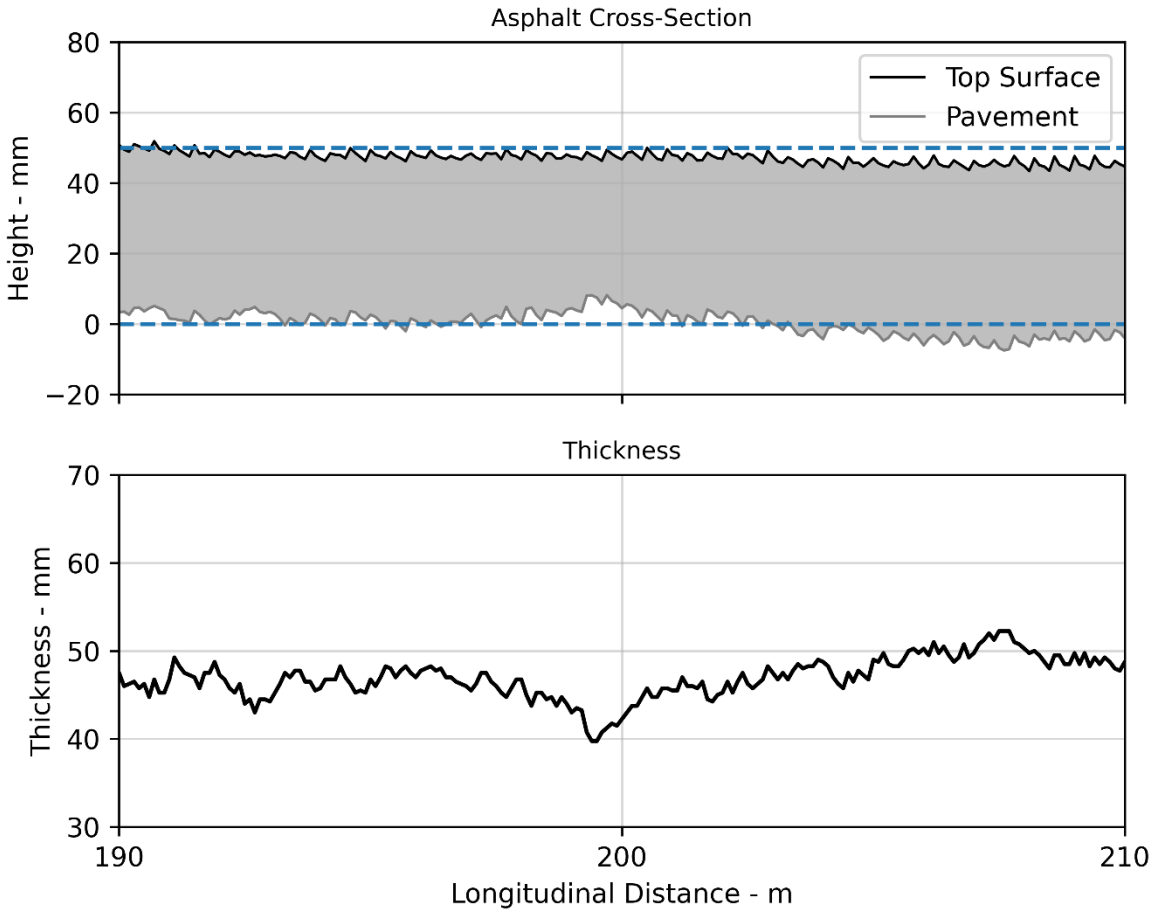

Figure 27: Relative surface height and overall thickness for the 20 m sub-sample.

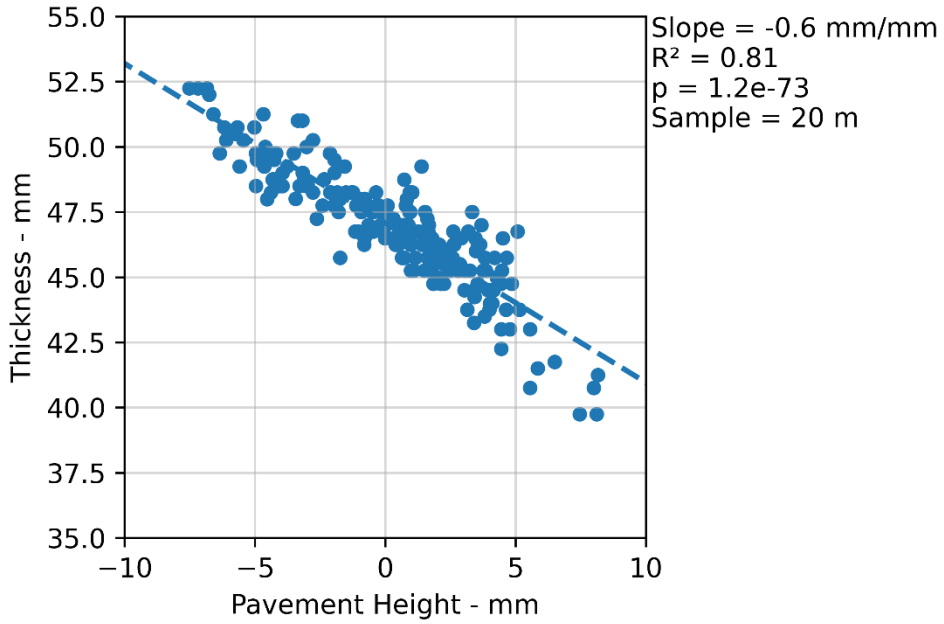

Figure 28: Thickness versus pavement height for the 20 m sub-sample.

Figure 29 contains the coefficient of determination (R^2) for each 20 m subsample plotted longitudinally for the one km sample. Where the thickness and pavement height have a high R^2 (suggesting good correlation), it is expected that asphalt was being used to fill in longitudinal undulations in the underlying pavement. Some regions within the analysed segment exhibited a correlation between thickness and pavement height, while others did not. The apparent poor correlation may be due to either there being minimal variation or another more dominant source of variability.

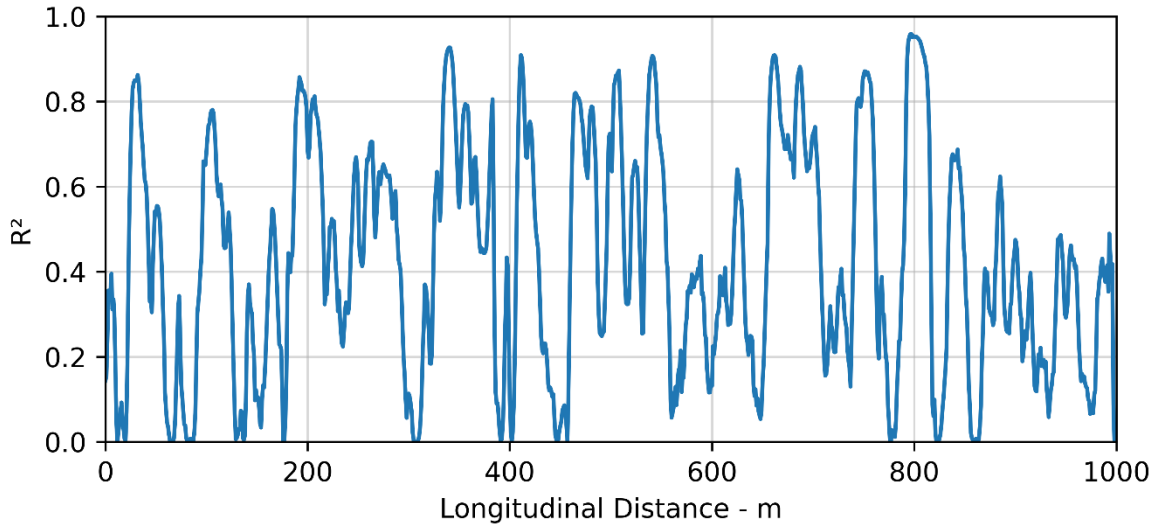

Figure 29: R^2 for a linear fit between pavement height and thickness for each 20 m sub-sample along the sample section.

The distribution of the slopes from the linear models (between pavement height and thickness) is shown in Figure 30. The mean slope was -0.7 mm/mm, with 5% exceeding -1.15 mm/mm. These relationships support the hypothesis that the asphalt layer is partially smoothing longitudinal undulations in the underlying pavement in the analysed sample. The slope ranged from less than negative one, indicating over-correction, to zero, where the asphalt thickness remained unaffected by underlying irregularities. The different scenarios for the slope are described below.

- A slope less than negative one would indicate that the asphalt layer is over-correcting for undulations in the underlying pavement (e.g., when the slope is -2 mm/mm, a local increase of 2 mm in the underlying pavement height results in a 4 mm decrease in the thickness of the asphalt layer).
- A slope of negative one would indicate that the asphalt layer is smoothing the undulations in the underlying pavement (e.g., a local increase of 2 mm in the underlying pavement height results in a 2 mm decrease in the thickness of the asphalt layer).
- A slope between negative one and zero would indicate that the asphalt layer is partially smoothing undulations in the underlying pavement (e.g., when the slope is -0.5 mm/mm, a local increase of 2 mm in the underlying pavement height results in a 1 mm decrease in the thickness of the asphalt layer).
- A slope of zero (i.e., uncorrelated) would indicate that the asphalt layer thickness is not influenced by undulations in the pavement.

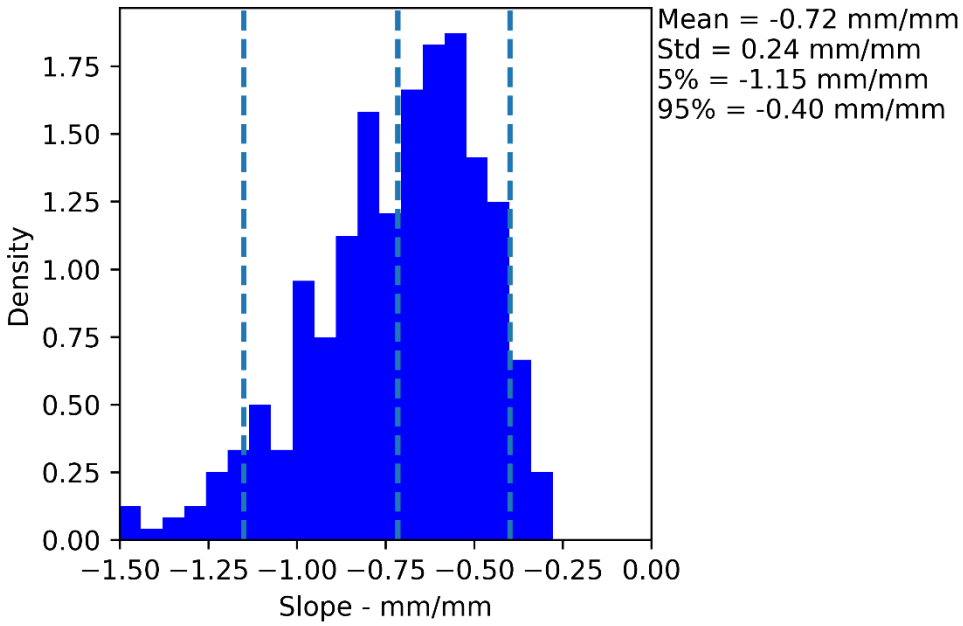

Figure 30: Distribution of the slopes from the linear models between pavement height and thickness.

When considering the longitudinal strip in the wheel path, smoothing undulations in the underlying pavement accounted for a significant portion of the variation in thickness. However, there remains a large, long-wavelength variation that is not due to the underlying pavement – this is shown in Figure 31. The two lines correspond to the longitudinal thickness with and without the shorter wavelength (<50 m, removed using a low-pass filter).

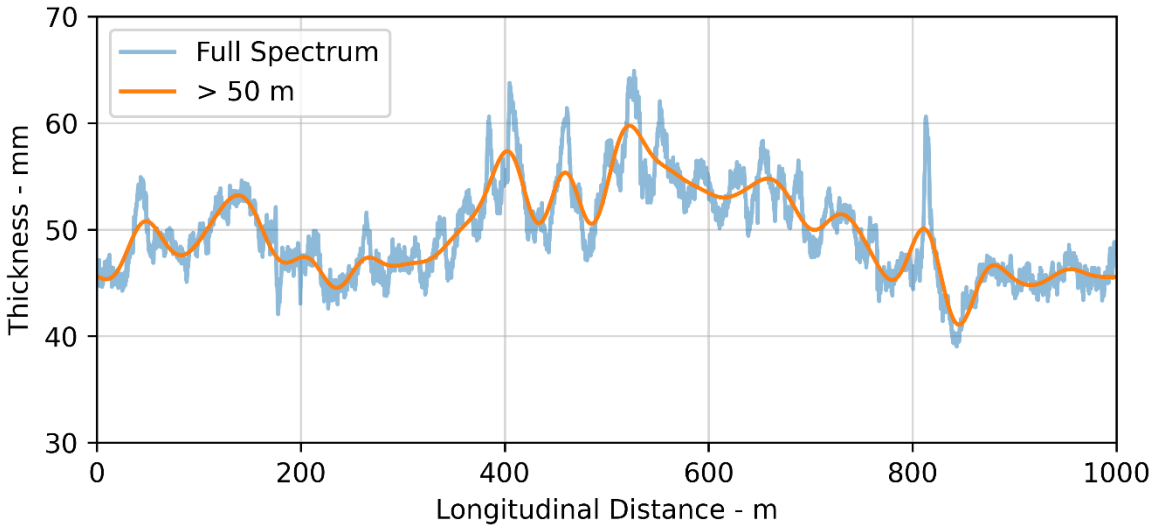

Figure 31: Residual longitudinal thickness variation for the sample section.

3.1.2 Transverse Variation

When considering the transverse thickness, only the area between the solid edge line and centreline was used from the same sample as the previous section (i.e., the shoulder was excluded). Note that the section is straight with no super-elevation or major elevation changes. The mean transverse thickness along with the transverse range are shown for the sample in Figure 32. The mean transverse thickness range was 11.9 mm with the 95th percentile at 19.0 mm. The transverse and longitudinal variations were similar for the analysed sample.

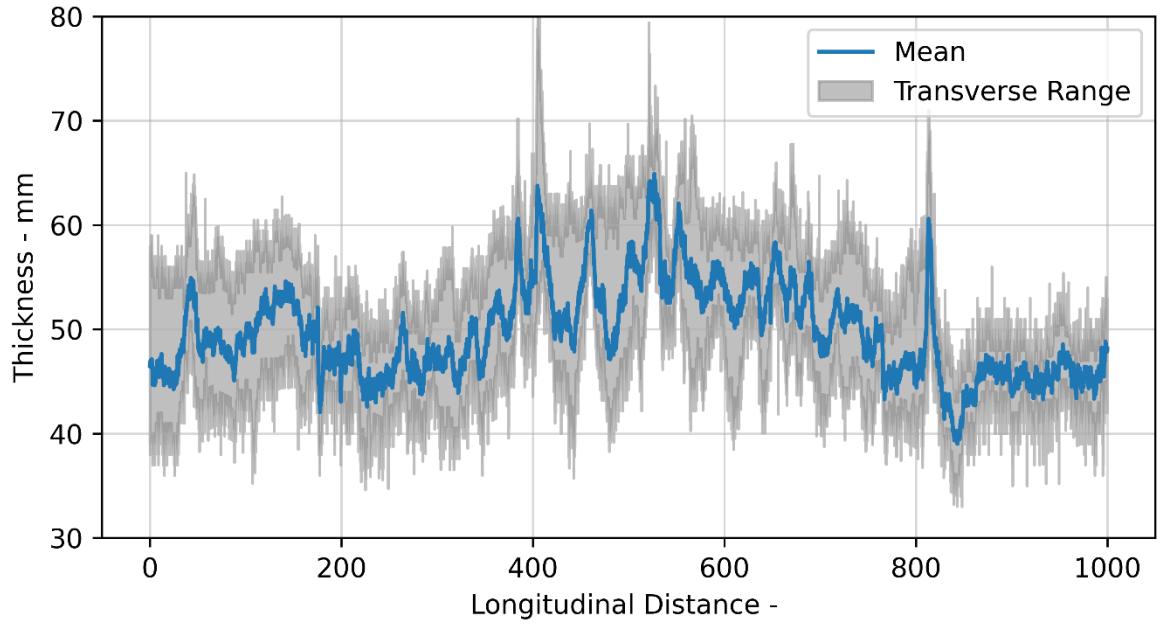

Figure 32: Longitudinal mean thickness and transverse range for the sample section.

Presumed geometric factors that could influence transverse thickness include the difference in mean camber between the underlying pavement and top surface, and smoothing transverse undulations in the underlying pavement. The impact of each of these factors was explored by first analysing the effect of the difference in camber, and then removing the camber and analysing the transverse undulations.

Camber Adjustment

Any difference between the camber of the pavement and top surface of the asphalt will result in transverse thickness variations. The three archetypal scenarios for linear cross-sections are schematically shown in Figure 33. For two flat surfaces, if the underlying pavement and top surface are parallel, there is no transverse variation. If the surfaces are not parallel, there will be a transverse thickness variation of $L \tan \Delta\theta$, where L is the cross-section width, and $\Delta\theta$ is the difference between the camber of the underlying pavement and top surface. For example, for a 3.5 m wide lane and a camber difference of 0.2° there will be a minimum transverse thickness variation of 12 mm. Assuming that the minimum thickness is maintained, this would be equivalent to adding an additional 6 mm of asphalt across the entire width of the lane.

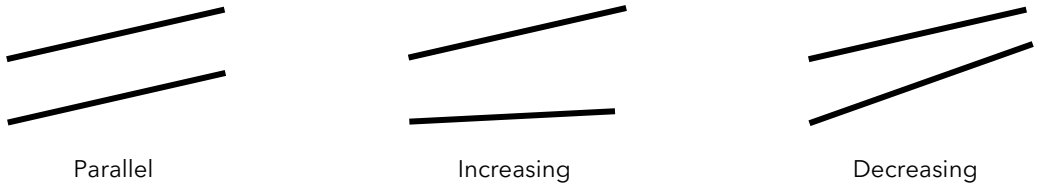

Figure 33: Simplified camber correction scenarios.

To determine the camber of the underlying pavement and top surface, the mean slopes were calculated. The camber distributions for the underlying pavement and top surface for all cross-sections in the sample section are shown in Figure 34. The mean values for both surfaces were equal (1.73°). The allowable range for chipseals is 3.0-4.0% (1.72-2.29°) (Richard Fanning, 2021). The range of cambers reduced after surfacing with a 0.05° reduction in the standard deviation and a 0.09° reduction in the 5-95th percentile range; this suggests that the asphalt layer is reducing the camber range.

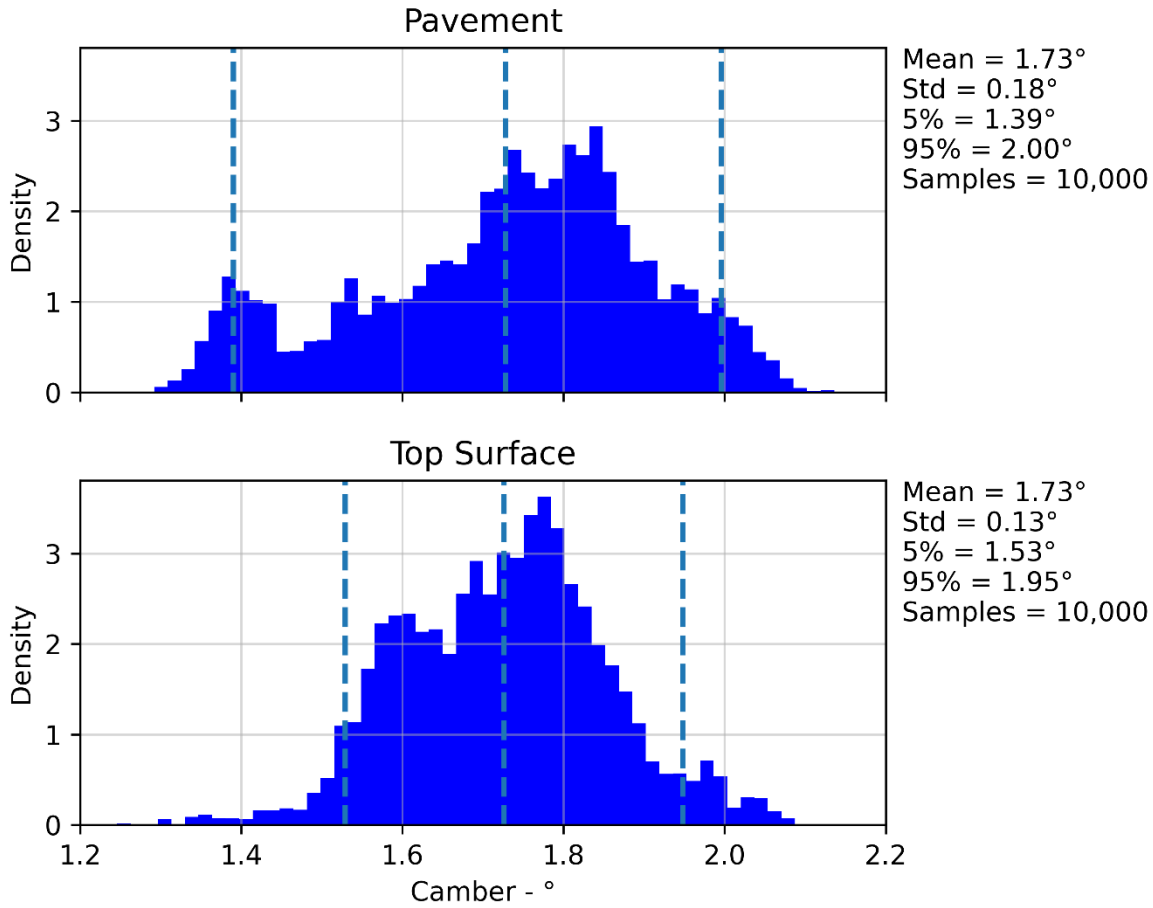

Figure 34: Camber distributions for pavement and top surface for the sample section.

Figure 35 contains a scatter plot of the underlying pavement versus the top surface cambers (paired by location). The axes values have been normalised to the mean camber for the sample (i.e., ō = 1.73° for both). A linear fit between the two variables has a positive slope of 0.45 °/°, which suggests that surfacing approximately halved the delta between the camber of the pavement and the assumed target of 1.73° (e.g., if the camber of the underlying pavement was 2.23°, the resulting camber of the top surface of the asphalt would be 1.96°).

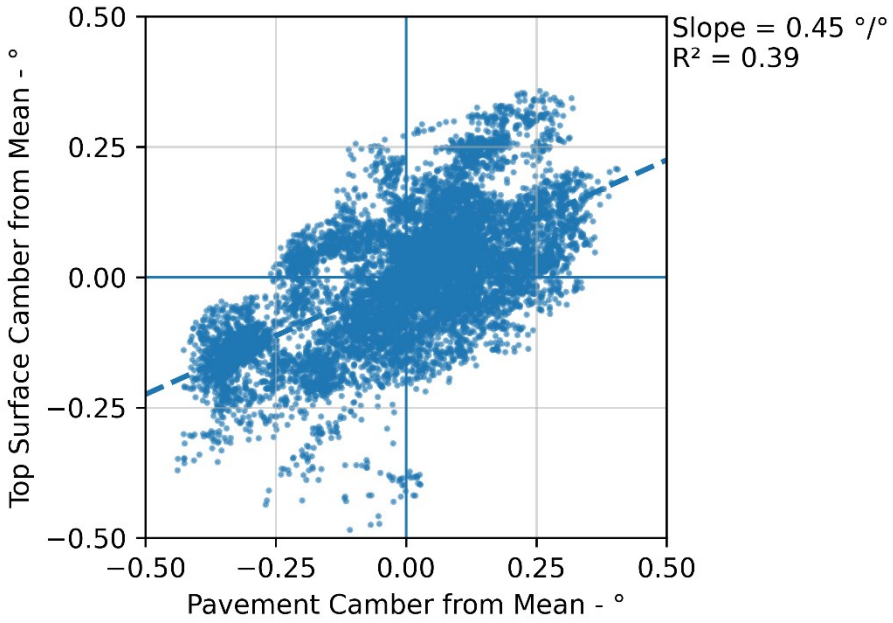

Figure 35: Delta from mean camber for pavement versus top surface.

Figure 36 contains a scatter plot of the deltas between the underlying pavement and top surface cambers versus the transverse thickness range, and a histogram of the distribution. The red lines on the scatter plot indicate the theoretical minimum difference for two linear surfaces using $L \tan \Delta\theta$, where L equals 3.5 m. The measurement points are predominantly encapsulated by the theoretical minimum range. The distribution shows that 51% of the sample had a camber difference of at least 0.1°, and therefore a minimum transverse variation of 6 mm, while 17% had a camber difference of at least 0.2° and therefore a minimum transverse variation of 12 mm.

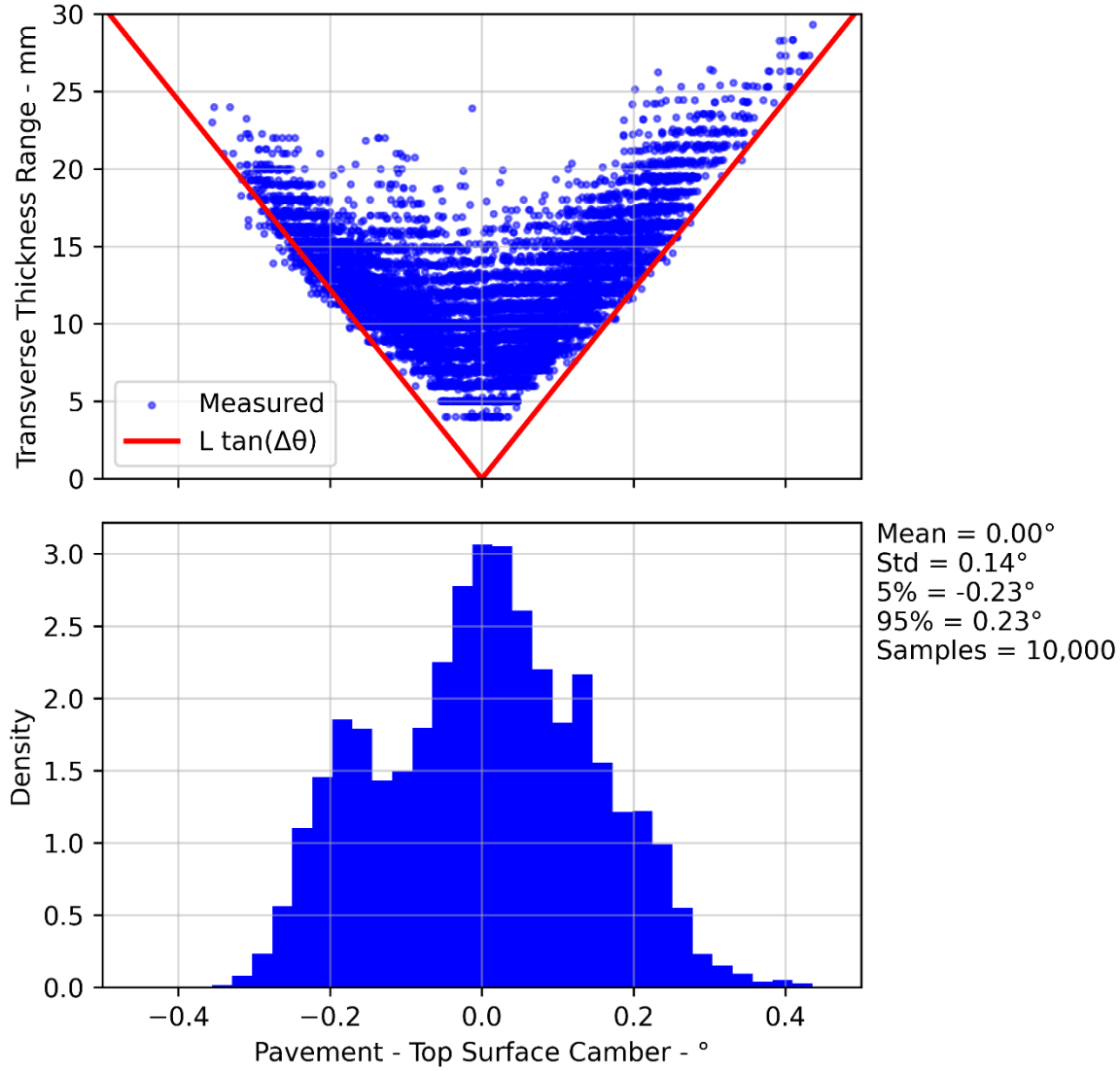

Figure 36: Camber correction versus transverse thickness range and correction distribution.

Adjusting or correcting the camber from the underlying pavement causes a significant increase in the transverse thickness range. If the minimum thickness was being maintained this would represent a significant increase in asphalt utilisation (7% for the sample section).

Transverse Undulations

The difference in camber between the top surface and pavement was removed from each cross section. The resulting profiles allowed for the quantification of the variation in thickness due to transverse undulations of the underlying pavement. The height of each cross-sectional profile had the camber removed by applying a linear fit and removing the mean slope. An example of a cross-sectional profile with (top) and without (middle and bottom) camber is shown in Figure 37. Note that the two lower plots show the cross-section first (middle plot)) with the pavement being "flattened" and then with the top surface of the asphalt being made parallel with the pavement (i.e., the difference in camber is removed).

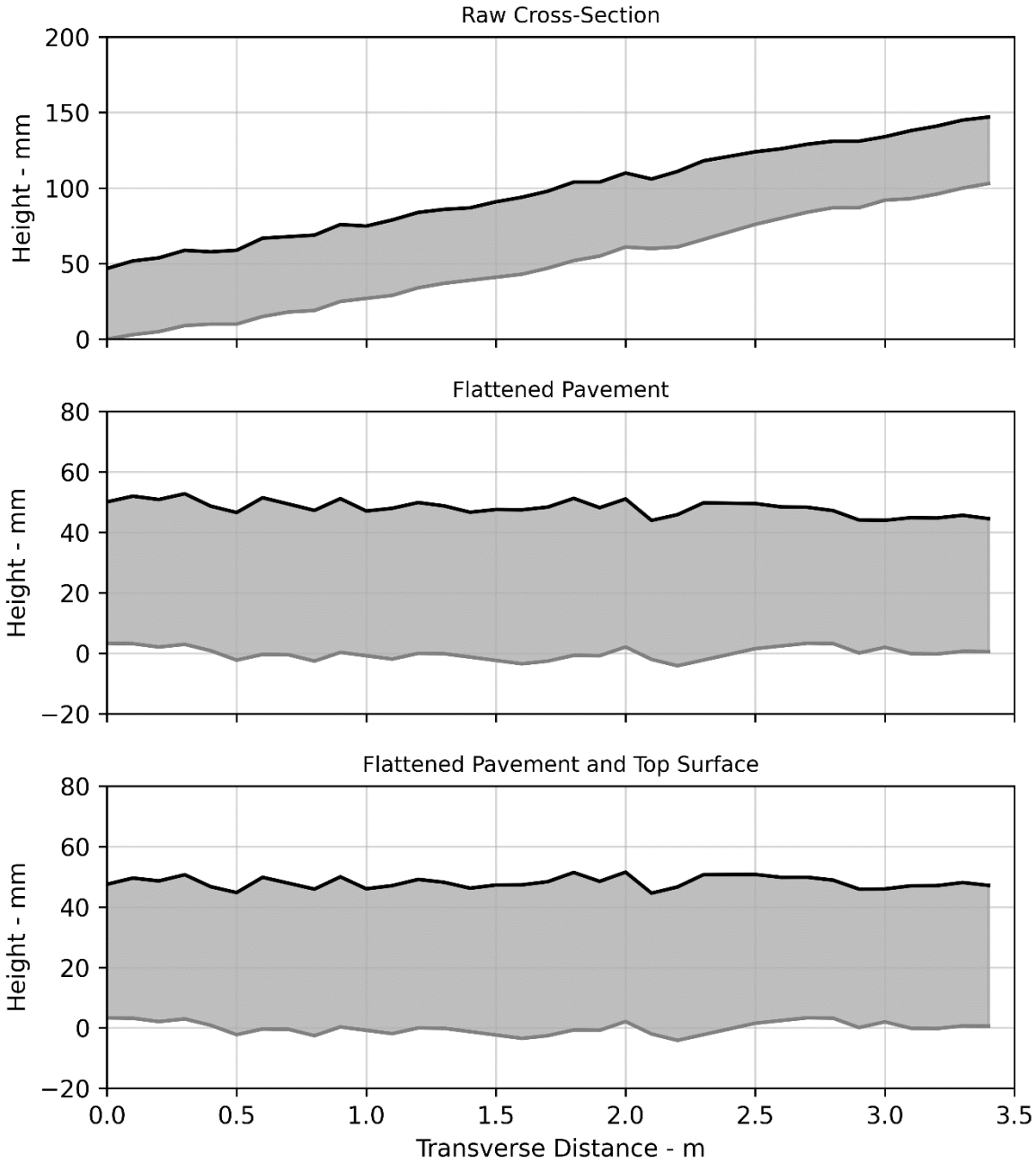

Figure 37: Transverse cross-section of asphalt layer showing pavement and top surface and the removal of camber.

Figure 38 contains a scatter plot of the flattened underlying pavement height versus thickness for the example cross-section shown above. A linear fit between underlying pavement height and thickness exhibited good agreement with the measured data (R^2 = 0.81) and a negative slope of -0.7 mm/mm, which supports the hypothesis that the asphalt layer was smoothing transverse undulations. The slope of -0.7 mm/mm is comparable in magnitude to that observed for the smoothing of longitudinal undulations. Smoothing of transverse undulations was present in the majority of the one-kilometre sample.

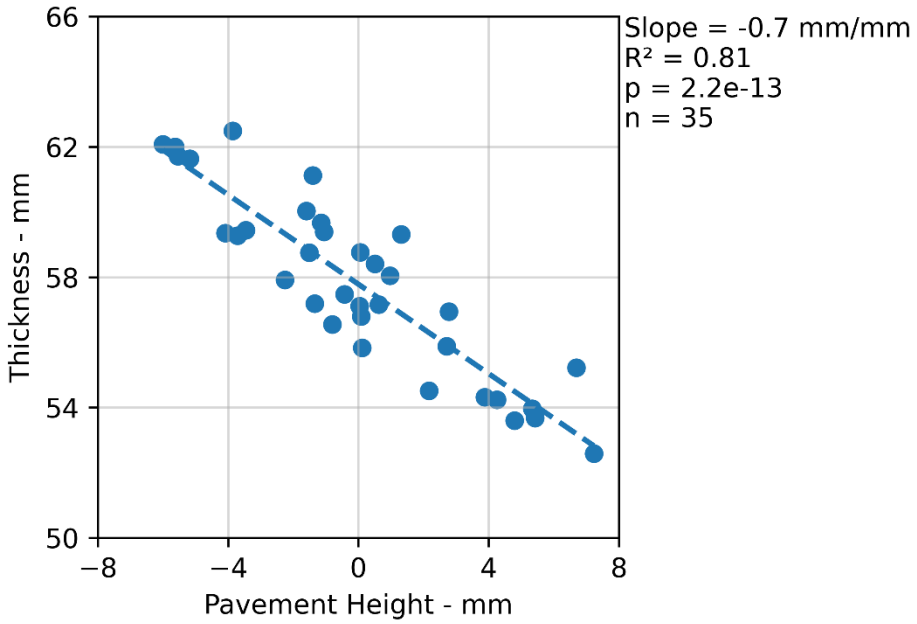

Figure 38: Scatter plot of thickness versus transverse pavement height for a single cross-section

Residual Transverse Variation

The variation from camber adjustment and transverse underlying pavement undulations were removed from each cross-section to explore the residual variation. The distribution of the range in transverse thickness for each scenario is shown in Figure 39. The effects of removing camber adjustment and transverse undulations were combined. The mean range reduced from 11.9 mm to 5.3 mm, which represents a significant reduction in transverse variation.

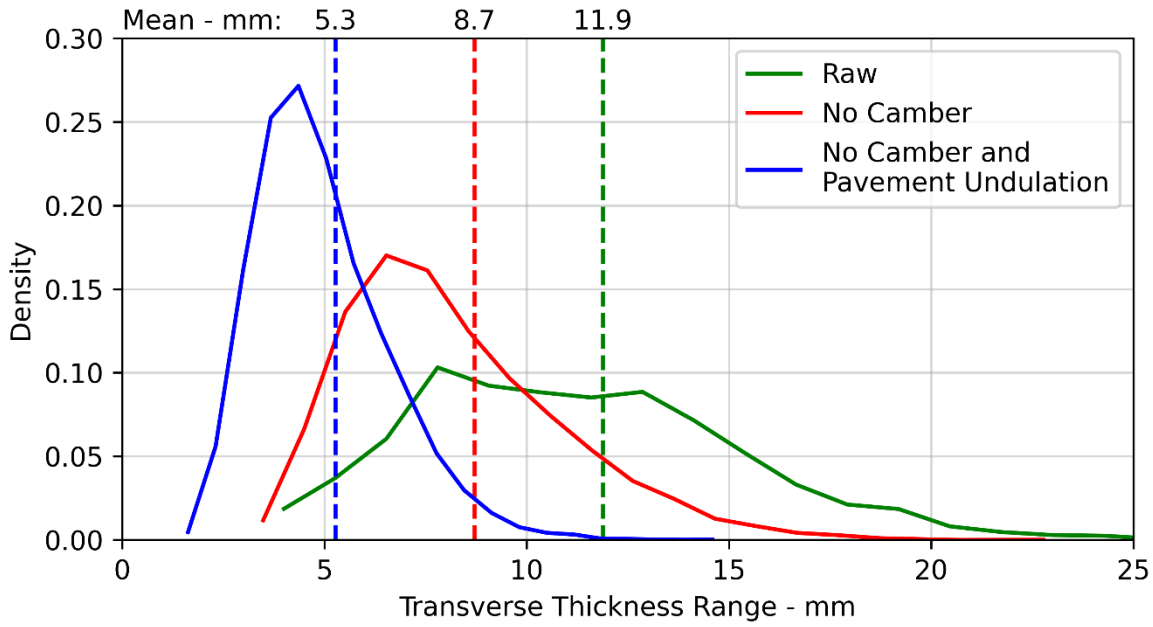

Figure 39: Distributions for transverse thickness ranges for the raw thickness, removal of camber adjustment, and removal of transverse pavement undulations.

The residual mean transverse profile is shown in Figure 40. The cause of the U-shaped profile is unknown; it may be due to post-surfacing compaction by traffic, the profile of the screed, a survey artefact, or another factor. It is unknown whether this profile is unique to the analysed sample. Given that the primary benefits of thickness occur in the wheel paths it is recommended that this phenomenon is explored further to determine if the profile can be affected by construction controls, thus reducing asphalt utilisation.

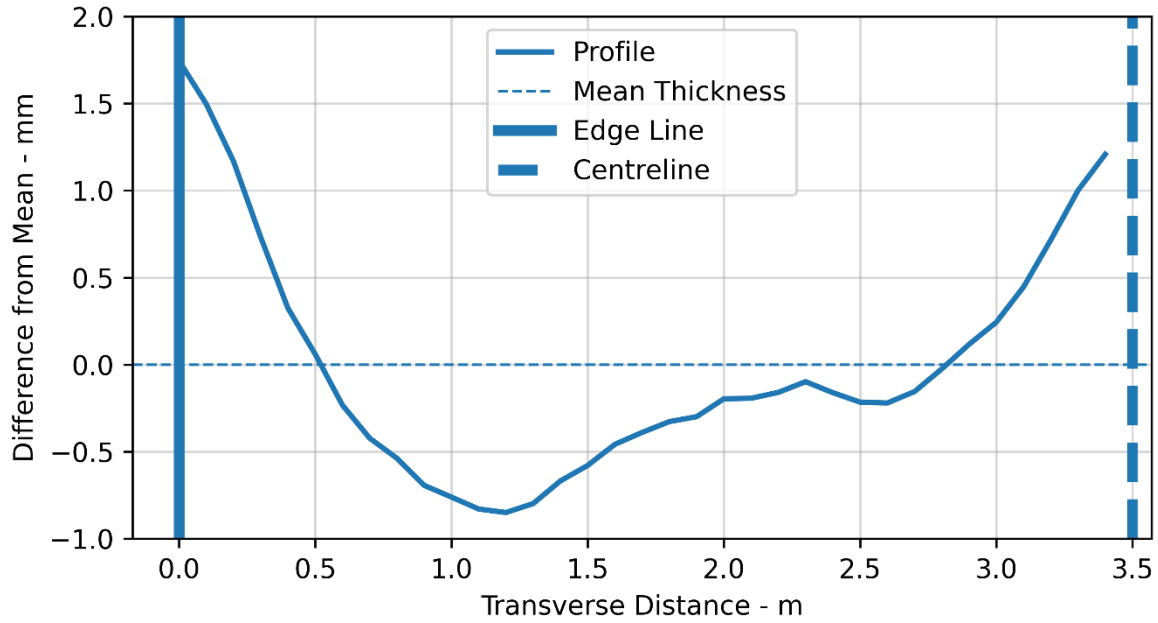

Figure 40: Residual mean transverse thickness profile about the mean after the removal of camber adjustment and transverse pavement undulations.

3.2 Construction

The influence of construction metrics on noise, texture, and thickness were previously explored for CNC (Bell, 2023) and WBB (Bull, 2019). For CNC, previously only discrete point measurements of thickness were available using the MIT-SCAN. The investigation of the influence of construction metrics on thickness was repeated here using the continuous thickness data and a machine learning (ML) model.

The purpose of monitoring the construction was to identify whether the typical variability in routine processes influences noise or the physical surface properties that affect it. A targeted parametric experiment would be more appropriate to quantify the true relationships between construction parameters, and the resulting thickness and tyre/road noise.

A Random Forest algorithm was used to create a regression model using the available construction metrics against the resulting thickness. The data was split 70:30 between training and testing. The outputs of the model included the overall coefficient of determination, parameter influence ranking, and single-variable influence plots. A separate model was created for each lane for the individual surface types (PA7, PA10, PA7 LV PA7 HS, and SMA7).

An example of the results for one surface type are presented followed by a high-level summary of reoccurring trends.

The applicability of the results is limited to non-epoxy modified porous asphalts as the addition of epoxy significantly alters the temperature-dependent properties and workability of the material. In addition. The results are not generalisable and are limited to CNC.

3.2.1 Example Results

The left lane (lane 2) of the PA7 (30 mm) on the southbound carriageway on CNC was used to provide an example of the outputs from the analysis. Longitudinal plots of L_{CPX}, MPD, and thickness are shown in Figure 41 for the sample section. The mean thickness was 29.0 mm with a standard deviation of 3.2 mm.

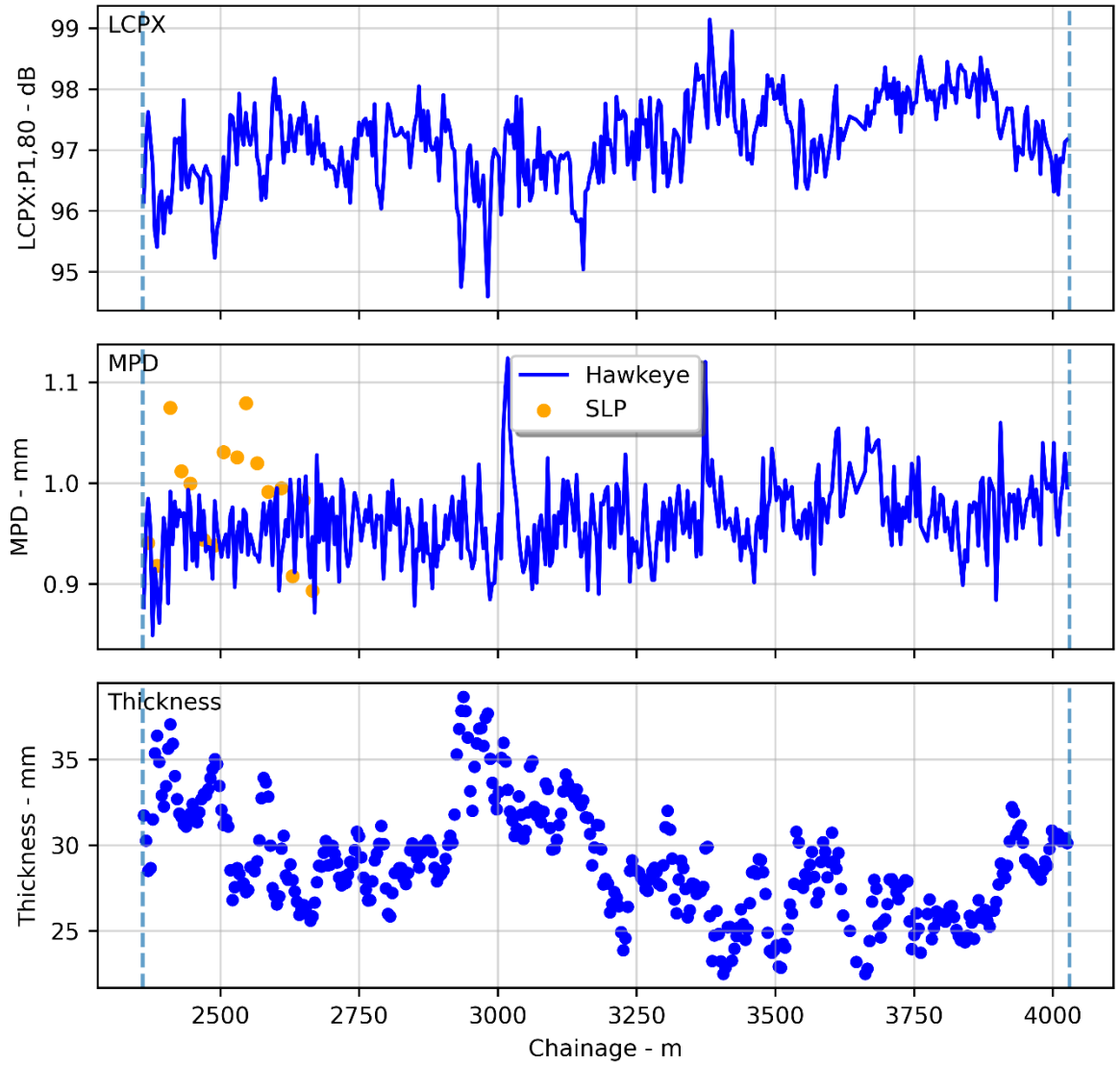

Figure 41: Longitudinal plots of L_{CPX}, MPD, and thickness for PA7 (30 mm).

The ML regression model between construction metrics and thickness achieved an overall coefficient of determination of 0.59. The variable influence rankings are shown in Figure 42. The variables with the greatest influence were lane width, time to rolling, mean paver speed, and roller passes. When a linear multivariate model was fitted to the data using the top four independent variables an adjusted R^2 value of 0.50 was achieved. As expected, the machine learning model offered a better fit to the data and was able to extract more complex relationships.

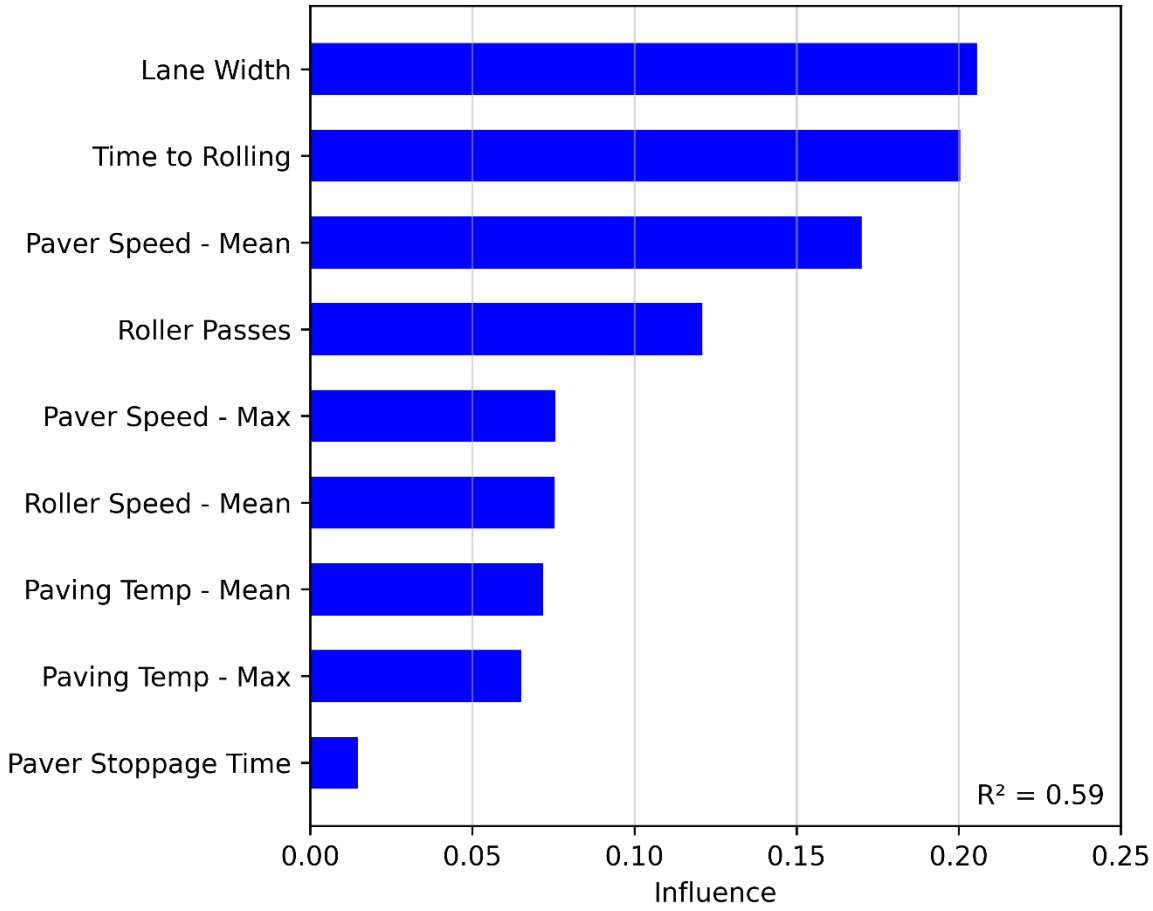

Figure 42: Example of ranked feature importance scores for construction metrics on PA7 (30 mm) thickness.

The specific influence of each variable is shown in Figure 43. Lane width was positively correlated with thickness, which is likely secondary to an underlying mechanism. Thickness was positively correlated with time between paving and rolling. There was a step-down relationship between mean paver speed and thickness. The observed positive correlation between roller passes and thickness is counter-intuitive and is unlikely to be causal. Note that the average number of roller passes was used, which is the number of times the roller went over the section of lane multiplied by the roller width and divided by the paved width.

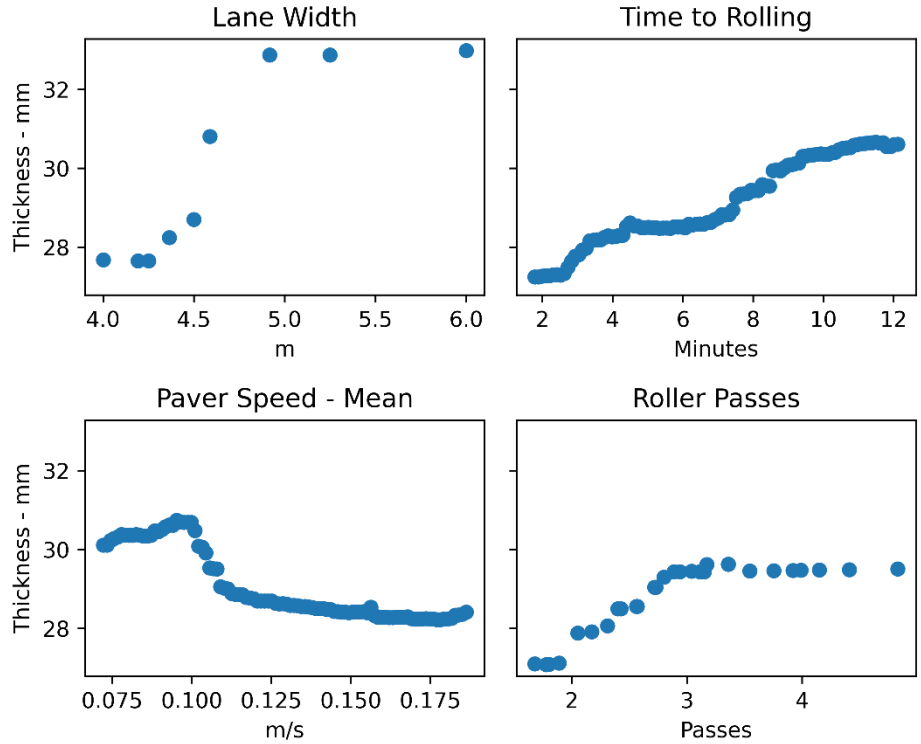

Figure 43: Example of partial parameter variation for PA7 (30 mm).

3.2.2 Results

The reoccurring trends of the relationships between construction metrics and thickness are shown in Figure 44. A positive correlation with time to rolling was observed; this is hypothesised to be a secondary relationship to rolling temperature (this data was not captured for the CNC project). The time available for compaction is a function of mix, base, and ambient temperatures [ref: state of practice for cold weather compaction]. Thickness exhibited step-down relationships with paver speed and paver stoppages. Thickness exhibited a step-up relationship with lane width. The latter three relationships are hypothesised to be primarily driven by the paver being stopped or moving at a very low speed.

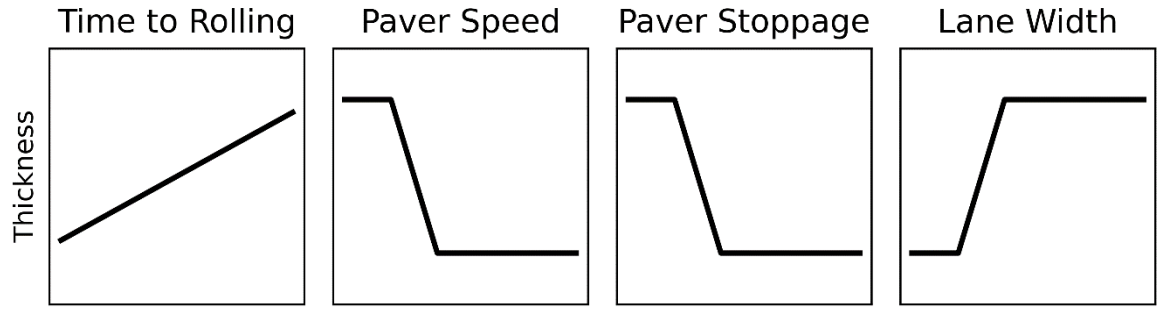

Figure 44: Indicative trends between construction metrics and thickness.

It is hypothesised that paver speed, paver stoppages, and lane width changes are linked. When the paver starts and stops there is likely a section that cools more before being ejected by the paver and then rolled. There may be an increased likelihood of the paver needing to stop or slow when the lane width is being changed as the transverse feed rates require tuning. A collaborative review with construction experts is recommended to develop an understanding of these phenomena.

4 Future Work

The following areas are suggested for future investigations based on the findings in this report.

Tyre/Road Noise Research:

- **Expanded Multivariate Model**
  Description: Reproduce the multivariate regression model with texture data captured using the CPX trailer and void fraction from the NDM.
  Purpose: Development of a predictive model based on measurable properties of the surface, which will enable parameter optimisation.
- **Surface Absorption**
  Description: Explore how thickness and surface absorption influence the wayside noise level.
  Purpose: Determine far-field influence of thickness and surface absorption.
- **Mechanisms**
  Description: Explore the dominant generation frequencies and how they change with speed, vehicle type, tyre type, etc.
  Purpose: Demonstrate that surface type and thickness effects maintain relative noise performance for a wider range of fleet vehicles.

Thickness Variability:

- **Operational Settings**
  Description: Work with either contractors or equipment suppliers to record operational settings.
  Purpose: Quantify how operational settings affect final surface thickness.
- **Thickness Variation Minimisation**
  Description: Work with contractors to identify practical methods of reducing thickness variability.
  Purpose: Minimise asphalt usage while achieving noise requirements.
- **WBB Construction Data**
  Description: Review construction data from 2019 WBB project (specifically rolling temperature).
  Purpose: Identify whether and how construction parameters influence surface properties that affect tyre/road noise.
- **Additional Thickness Variability Analysis**
  Description: Expand analysis of thickness variability to use the full CNC laser survey data.
  Purpose: Increase confidence in recent findings and explore other sources of variability.

5 Conclusions

This investigation used high spatial resolution thickness data captured using a mobile laser survey to (1) quantify the variability of the asphalt layer thickness, (2) expand the understanding of the relationship between tyre/road noise and thickness, (3) define measurement requirements for the qualification of thickness, and (4) explore sources of variability.

Nine one-kilometre sections of porous asphalt were analysed from the CNC (8) and PP2Ō (1) projects. The 25th percentile thicknesses in the wheel paths were on average 7% below the specified values (where the statistical metric (e.g., mean, minimum, etc.) of the specified values were not defined). It is hypothesised that the variability observed within these samples is typical of low-noise asphalt surfaces in New Zealand.

The relationship between overall tyre/road noise and thickness was revisited and expanded upon. The overall noise level was negatively correlated with thickness, with a maximum observed rate of change of -2.4 dB/10 mm occurring at 35 mm. It was observed that there are non-linear relationships between thickness and the one-third octave bands from 630 to 2,500 Hz. It was shown that there is a local minimum (i.e., not occurring at the maximum thickness) noise level in the thickness range from 25 to 60 mm in the 1,250 to 2,500 Hz bands.

The laser survey data was used to simulate point measurements at various spacings within the nine sample sections. The resulting confidence intervals for estimating the 2.5th, 5th, and 25th percentile thicknesses were calculated. The 25th percentile thickness can be estimated within ±2 mm with 90% confidence if disks are placed in each wheel path with a spacing less than or equal to 50 m.

Variations in thickness are caused by a variety of factors including geometric differences between the underlying pavement and required top surface levels, construction processes, and operational settings. Of the analysed factors, the greatest variability was due to geometric differences that appeared to arise from road camber adjustment and the smoothing of longitudinal and transverse undulations.

There appears to be an opportunity to optimise asphalt utilisation to reduce cost and environmental impact. This might be achieved through future collaborative investigations with pavement design engineers, construction contractors, and equipment suppliers.

Part II Porous Asphalt Ageing

1 Introduction and Background

When considering the low-noise performance of porous asphalts, the long-term characteristics must be studied as they are typically used to mitigate effects of sustained noise exposure. With the inclusion of additives (e.g., epoxy) to the bituminous binder, the service life of low-noise surfaces in New Zealand is expected to substantially increase (Herrington, 2014; OECD, 2008). Waka Kotahi has routinely measured the CPX level on several surfaces from early in their operational life, which enables the temporal analysis of noise over this initial period of up to five years (long-term monitoring will be undertaken).

The noise performance of a porous asphalt surface degrades due to several mechanisms, (1) reduction of inter-connected voids due to clogging and post-construction compaction, and (2) changes to the surface texture (Ahmed, 2015; Gardziejczyk, 2016; Sandberg, 1999). High traffic speed and volume locations might be less susceptible to clogging due to self-cleaning by tyres during heavy rain; therefore lower speed and volume locations and road shoulders may experience more severe clogging (Van Heystraeten & Moraux, 1990). The loss of noise performance has been observed to occur at mid to high frequencies and had a greater increase in the outer lane of dual carriageways (Ahmed, 2015). The expected rate of increase of noise is 1 dB per year in Swedish conditions but depends on many environmental factors (Sandberg & Ejsmont, 2002).

Clogging can potentially be managed by periodic cleaning of the road surface (Sandberg, 1999; Vítězslav Křivánek et al., 2015). A Swedish study demonstrated an 83% increase in the quantity of interconnected voids after cleaning, however no significant change in the CPX level was measured (Ahmed, 2015). It has been demonstrated in a Czech study that a reduction of approximately 1 dB could be achieved by cleaning the surface (Vítězslav Křivánek et al., 2015). The Swedish and Czech authors recommended that porous surfaces are cleaned every two to three years (Sandberg, 1999; Vítězslav Křivánek et al., 2015).

A 2017 study considered the long-term acoustic performance of porous asphalt surfaces in New Zealand using a close-proximity method (Lester et al., 2017). The study, focusing on high-speed environments (80 to 100 km/h), measured the acoustic performance of 150 PA sections of different ages across four regions in New Zealand. Findings indicated a steady, albeit slow, deterioration in acoustic performance over 8 to 10 years, amounting to an overall increase of 2 dB.

A 2021 study utilised a cross-sectional method to explore the age-related change in close proximity noise level of PA10 (30 mm) across New Zealand's state highway network. The measurements were made using the Waka Kotahi CPX trailer. A small statistically significant age-related increase of 0.14 dB/year ±0.13 dB/year was observed (Jackett, 2021).

A study of 19 years' of texture data on hot-rolled asphalt in the UK (Edmondson et al., 2021) showed an overall linear increase in texture depth with time. The rate of change was found to be seasonal and loading dependent.

This investigation has two components:

- Measurement system stability: Reviewing how the CPX trailer has changed over time and the resulting impact on the reported noise levels.
- Surface CPX levels: Using CPX and HSD data to analyse how the noise and texture of low-noise surfaces have changed over time.

2 Measurement System

This section provides a brief overview of the main changes to the Waka Kotahi CPX measurement system from 2018 to 2023. Changes include:

- Tyre sets and hardness.
- Wheel enclosures and corrections.
- Microphones.

Figure 45 shows a graphical timeline of the changes. Vertical dashed lines represent when a change occurred (i.e., new tyres, new enclosure corrections, or new microphones). The specific physical enclosure configurations are in Table 13 in the appendix.

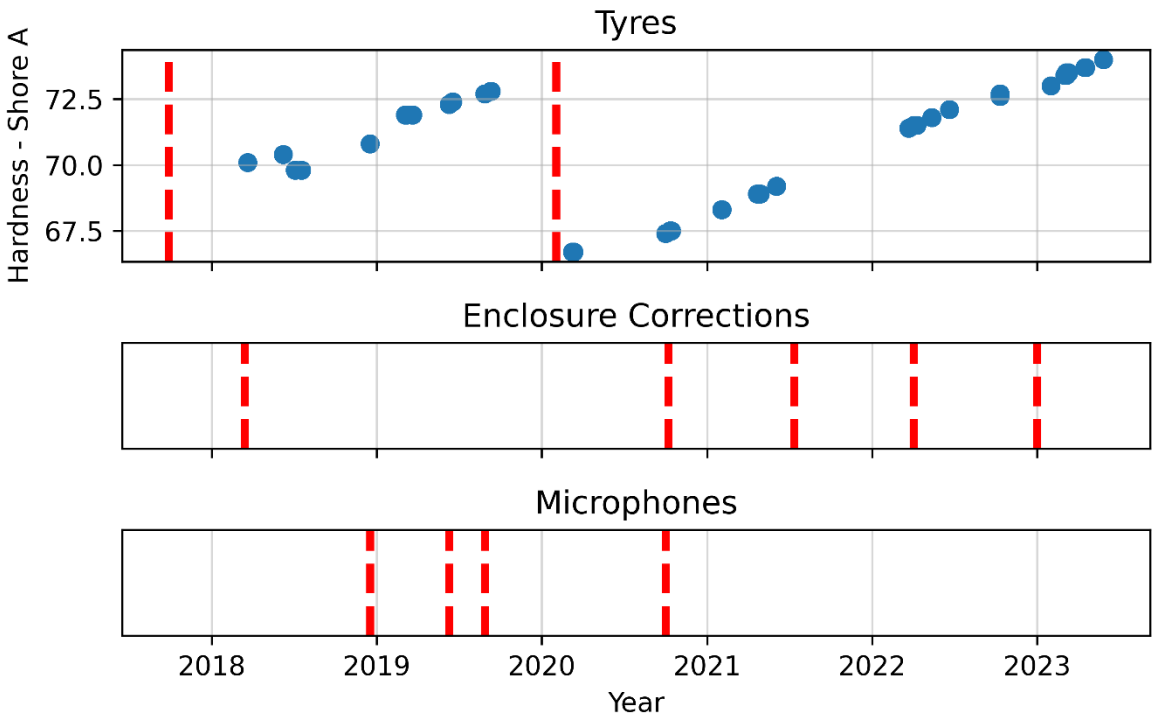

Figure 45: Timeline of changes to the Waka Kotahi CPX measurement system.

Two sets of P1 tyres have been used over this period. The hardness was linearly interpolated between adjacent measurements. The trend of hardness increasing over time is expected.

The enclosure corrections by frequency band are shown in Figure 46. It is expected that changes in the values occurred due to either discrete physical changes to the trailer (e.g., removal of the rubber skirts) or the slow degradation of the absorption material. The temporary elevation of the correction for the 1,000 Hz band in 2022 indicated an erroneous reading and was not considered further in the chronological analysis.

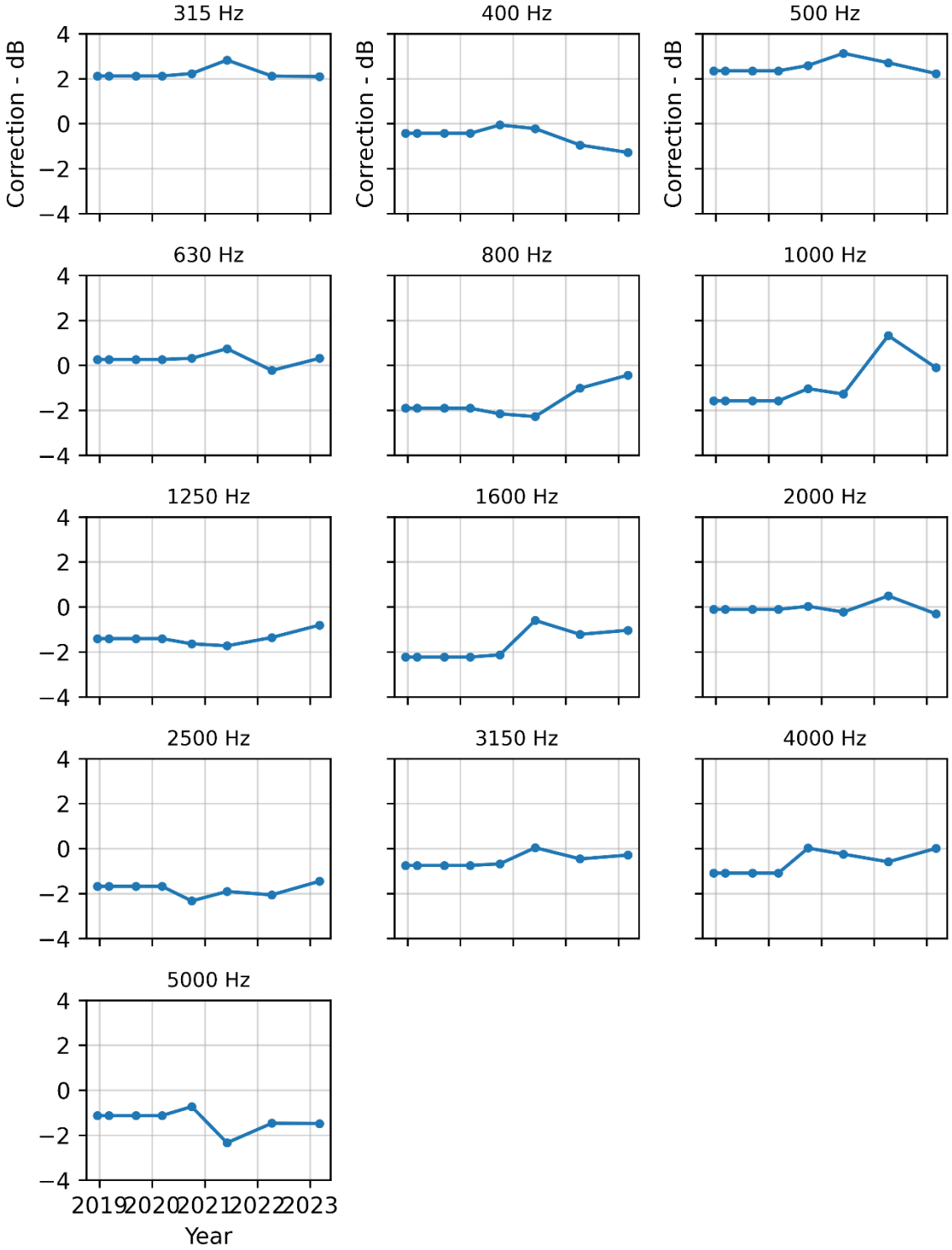

Figure 46: Enclosure corrections versus time.

Multiple sets of microphones have been employed. In addition, the process for applying the sensitivity was changed with the adoption of the latest GRAS microphones in 2020. Prior to this, the field calibration was

used to calculate sensitivity; this process has been updated to only use the factory sensitivity with the field calibration being used to establish no large changes have occurred. It was assumed that the calibration method does not have any significant impact on the measured levels.

Each measurement is corrected for temperature, speed, and tyre hardness. The corrections are applied following the procedure in the CPX standard (*ISO 11819-2*, 2017) . The corrections due to speed and hardness are considered in Part IV; the findings have not been included in the ageing analysis. The correction due to temperature is out of scope of this investigation.

3 Method

Two approaches were used for the analysis: (1) chronological, and (2) cross-sectional. These are described in-turn below.

3.1 Method One – Chronological Analysis

The following steps were taken:

1. Reference surfaces that are assumed to have experienced minimal changes over the analysis window were identified (SMA).
2. The reference surfaces were used to identify changes in the CPX levels due to the measurement system and any residual effect of hardness, speed, and temperature correction.
3. Subsections of surfaces that have been routinely measured were analysed and any changes due to the measurement system were either adjusted or omitted.
4. The rate of change of the overall and one-third octave band levels were calculated for each sample.

Details of the sample sections are shown in Table 6. The SMA surfaces were used as references.

Table 6: Details of surfaces used in the ageing analysis.

Surface	Location	ID	Road ID*: Start-End	Length - m	Construction
EPA10 (30 mm)	S2G	1	3664: 3640-3880	240	Mar-2017
EPA10 HV (30 mm)	S2G	2	3664: 3320-3620	300	Mar-2017
EPA14 (30 mm)	S2G	3	3664: 3040- 3300	230	Mar-2017
EPA7 (30 mm)	Memorial Bridge	4	3736: 6895-7260	360 m	Apr-2018
		5	3736: 7322-7660	320	Apr-2018
	WBB	6	1715: 4864-5126	240	Nov-2018
EPA7 (40 mm)	WBB	7	1715: 4585-4845	240	Nov-2018
		8	1715: 2998-4272	1,260	Nov-2018
		9	3650: 45-500	440	Nov-2018
		10	1716: 3095-5750	2,640	Nov-2018
EPA7 (50 mm)	WBB	11	1715: 4292-4566	260	Nov-2018
SMA10 (40 mm)	Groynes Off-Ramp	12	3653: 50-250	200	Mar-2017
	WBB	13	1715: 2715-2775	60	Oct-2017

*Road ID to Reference Station mapping can be found in Table 15 in the appendix.

The primary limitation of the chronological method is the dependence on the stability of the measurement system and the ability to identify and correct for it with a reference surface that is assumed to be immutable.

3.2 Method Two – Cross-Sectional Analysis

For a single surface specification, several examples of different ages were measured and compared. The analysis was conducted on PA10 (30 mm) surfaces for measurements made in 2023. The advantage of this approach is that any temporal changes to the measurement system are minimal.

Table 7: Road IDs and lengths of samples included in the 2023 cross-sectional analysis.

Road ID	Length - m	Road ID	Length - m	Road ID*	Length - m
1202	2360	3564	4620	3690	420
1203	5200	3588	1080	3691	440
3271	2780	3589	1120	3735	2980
3277	1180	3650	200	3736	2580
3278	1680	3656	200	3843	360
3279	1260	3663	2380		
3563	3800	3664	1360		

*Road ID to Reference Station mapping can be found in Table 15 in the appendix.

The primary limitation of the cross-sectional analysis method is that physical variations between locations cannot be excluded. For example, differences in thickness are likely to cause greater variation than age between sites.

4 Results and Discussion

4.1 Chronological Analysis

4.1.1 Reference Surfaces

Two separate sections of SMA10 (40 mm) were selected for use as reference surfaces (see Table 6). The bridge section on WBB offered the greatest time span and measurement quantity but is relatively short with only two 20 m segments; it is also subject to greater trafficking (13,000 vehicles per day), which will likely result in physical and associated acoustic changes as the service life increases. The Groynes off-ramp is longer and will experience less trafficking (3,300 vehicles per day). However, fewer historic measurement runs had been undertaken, which limited the ability to use the surface as a reference.

The mean L_{CPX} level and MPD (from the annual HSD survey) over time is shown in Figure 47 for the reference SMA10 (40 mm) on WBB. The raised level for 2022 is attributable to the temporarily elevated enclosure correction in the 1,000 Hz band. When the 2022 measurement was excluded, the overall range was 0.5 dB across the five years of measurements. The MPD appeared stable over the analysed period.

Figure 47: Changes in L_{CPX} and MPD for the reference SMA10 (40 mm) bridge deck on WBB.

The one third octave band spectra are shown for each measurement (as age) in Figure 48. The individual band levels are shown as a function of age in Figure 49. The primary deviations occur in the 1,000 Hz bands for the 2022 measurement, and the 1,600 Hz band for the 2021 measurement. The raised level for the 1,000 Hz band was likely due to the temporarily elevated enclosure correction. The cause of the elevated level in the 1,600 Hz band could not be discerned from the available data.

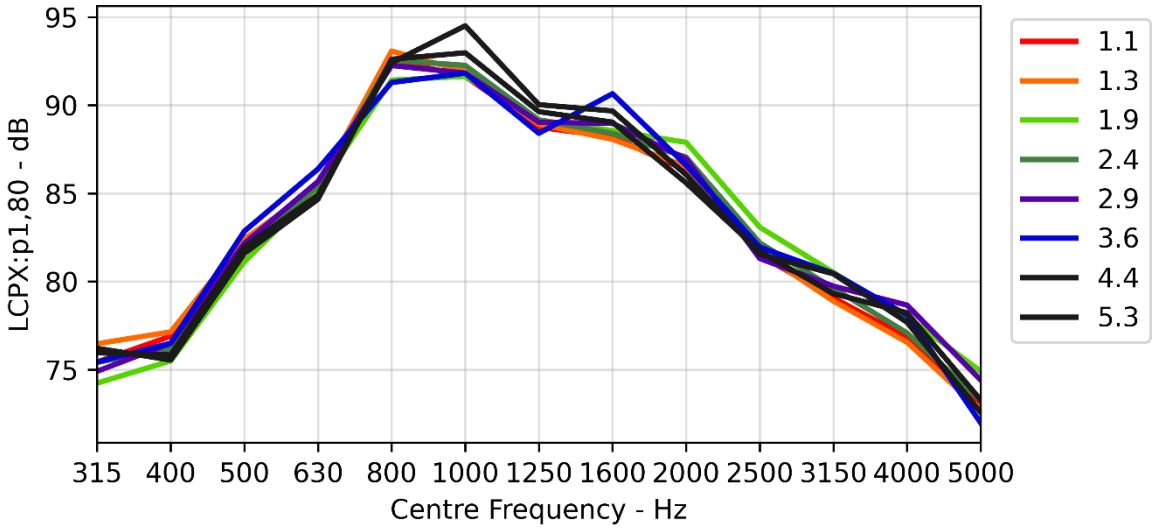

Figure 48: One-third octave band L_{CPX} levels for the reference SMA10 (40 mm) bridge deck on WBB.

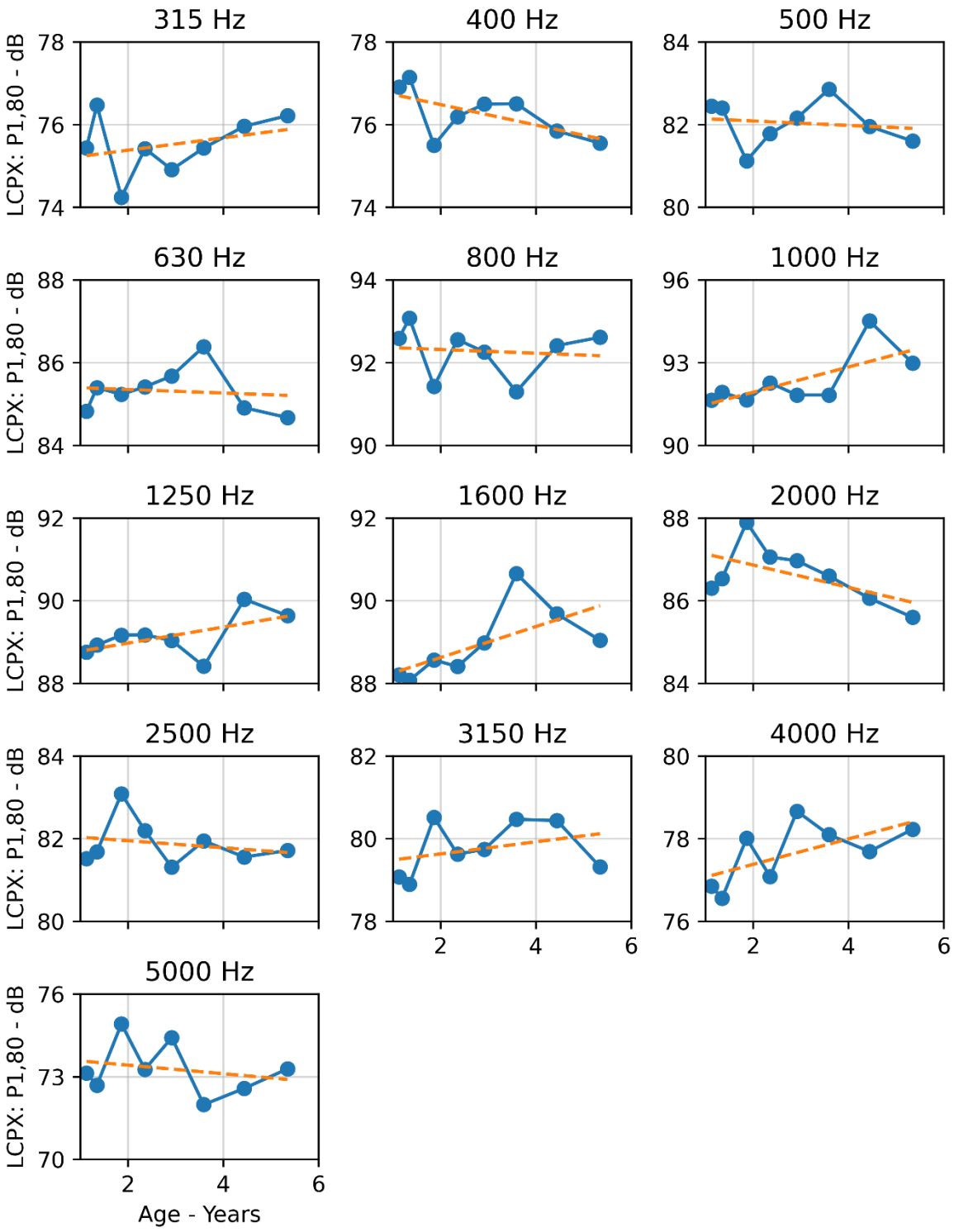

Figure 49: Changes in one-third octave band levels for the reference SMA10 (40 mm) bridge deck on WBB.

The mean L_{CPX} and MPD over time is shown in Figure 50 for the reference SMA10 (40 mm) on the Groynes off-ramp. As above, the elevated level for 2022 is attributable to the temporarily raised enclosure correction in the 1,000 Hz band. When the 2022 measurement was excluded, the overall range was 1.0 dB across the four measurement sessions.

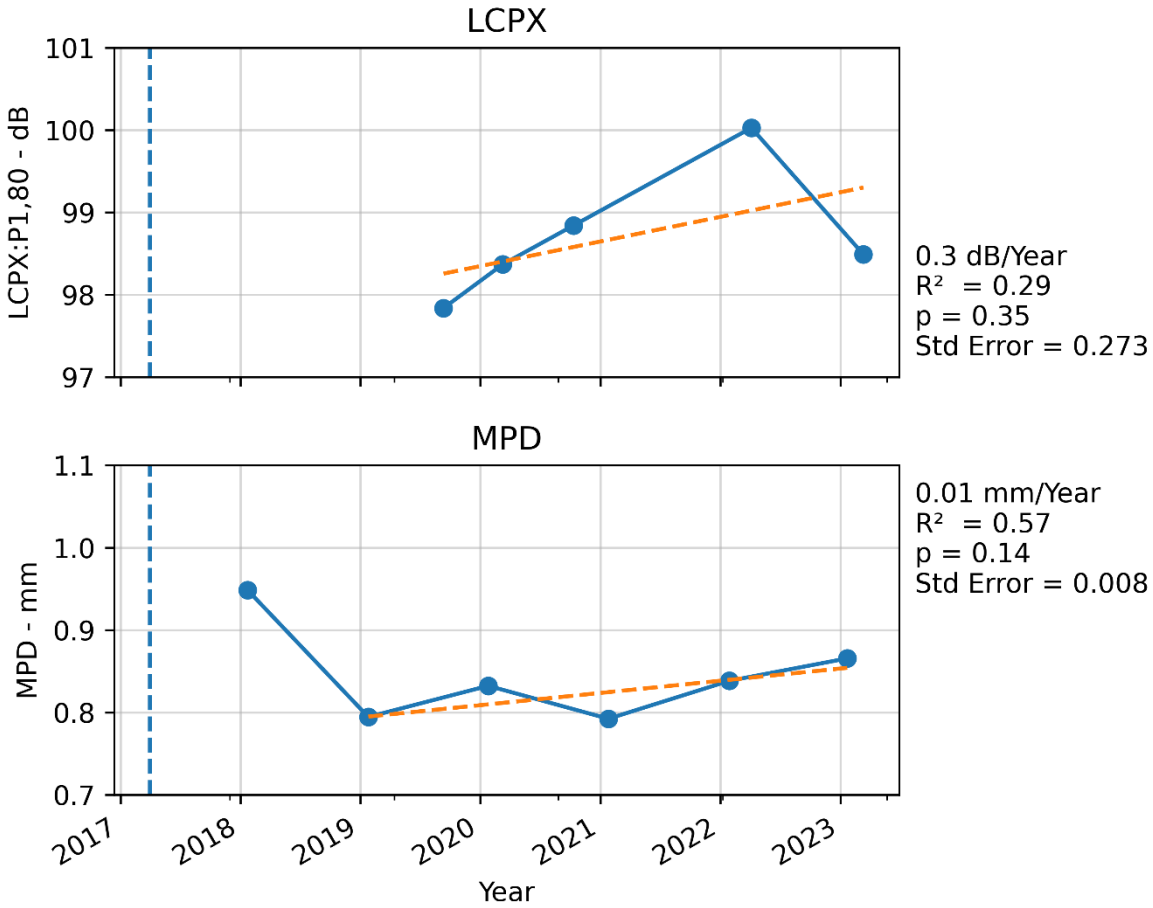

Figure 50: Changes in overall L_{CPX} and MPD for the reference SMA10 (40 mm) on north-bound Groynes off-ramp.

After excluding the erroneous 2022 measurements, the bridge decks on WBB exhibited a 0.1 dB/year increase. The limited data for the Groynes off-ramp indicated a 0.1 dB/year increase, these rates will likely be a combination of measurement system drift, inter-measurement repeatability, and physical changes to the surfaces (i.e., ageing). It was assumed that the SMA on the lightly trafficked Groynes off-ramp experienced minimal physical changes over the analysis period. Other than 2022 no major year-to-year anomalies were observed, suggesting that inherent CPX repeatability was low (WBB bridge deck: sd = 0.3 dB, n = 7). There were insufficient data to determine if a correction for measurement system drift is required. For the chronological analysis, measurements undertaken with the 2022 enclosure correction set were excluded.

Based on the extended length and low trafficking, it is recommended to routinely measure the Groynes ramps and at least one other location to develop a more comprehensive set of reference measurements that can be used for the rapid evaluation of the measurement system.

4.1.2 Mean Rate of Change

The results for the EPA7 (50 mm) on WBB sample are first presented. This is followed by a summary of the mean rates of change for all samples and then a targeted discussion of these results. Some supplementary figures are included in the appendix and are referenced within the text.

The mean levels over time for the left lane of the EPA7 (50 mm) trial section are shown in Figure 51. Linear regression was used to determine the rate of change of the mean levels. Only measurements completed more than one year after surfacing were included to exclude any short-term transient effects. There were only four measurement sessions available for the regression, which limited the robustness of the resulting statistics. For the given example, the mean L_{CPX} increased at +0.3 dB/year and the mean MPD was decreasing at -0.03 mm/year.

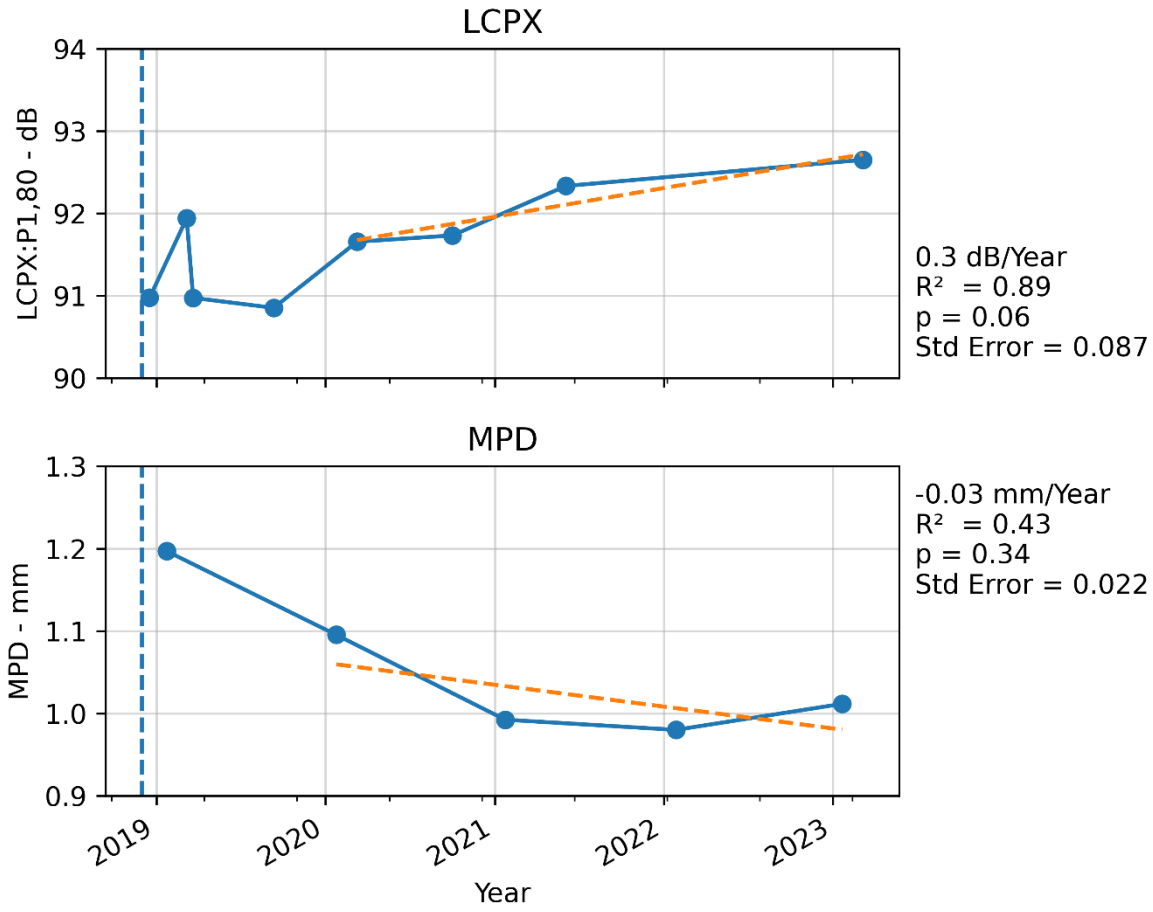

Figure 51: Changes in overall L_{CPX} and MPD for EPA7 (50 mm) on WBB.

The one-third octave band spectra for each age and the rate of change with time for the EPA7 (50 mm) sample are shown in Figure 52 and Figure 53, respectively. There was a positive rate-of-change with time in all bands from 800 Hz. The shapes of the one-third octave band spectra are indicative of reducing thickness. In addition, the increase in the high frequency bands may suggest increasing air flow noise due to reduced permeability.

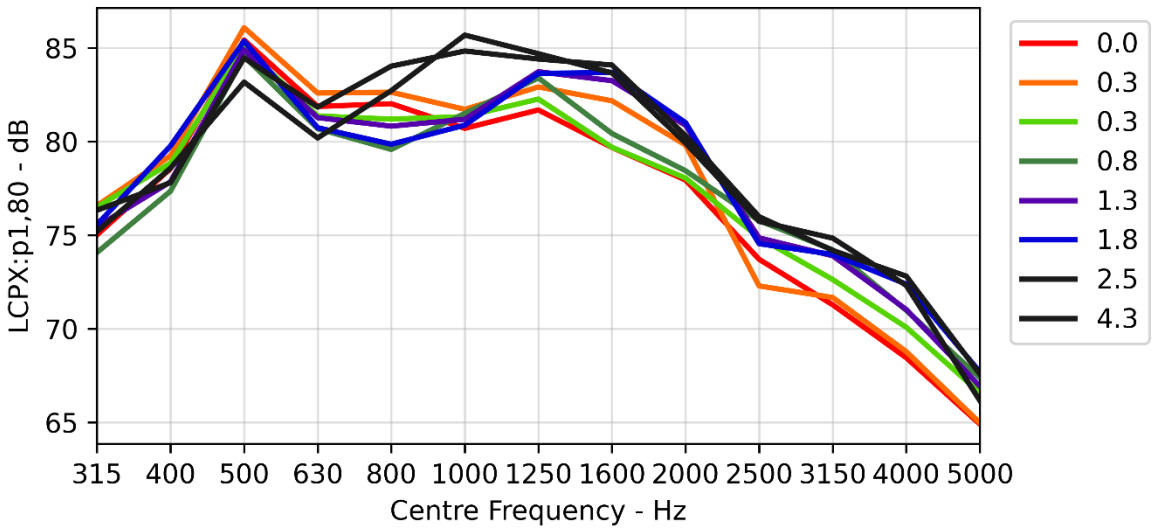

Figure 52: One-third octave band L_{CPX} levels for EPA7 (50 mm) in lane 2 on WBB over time.

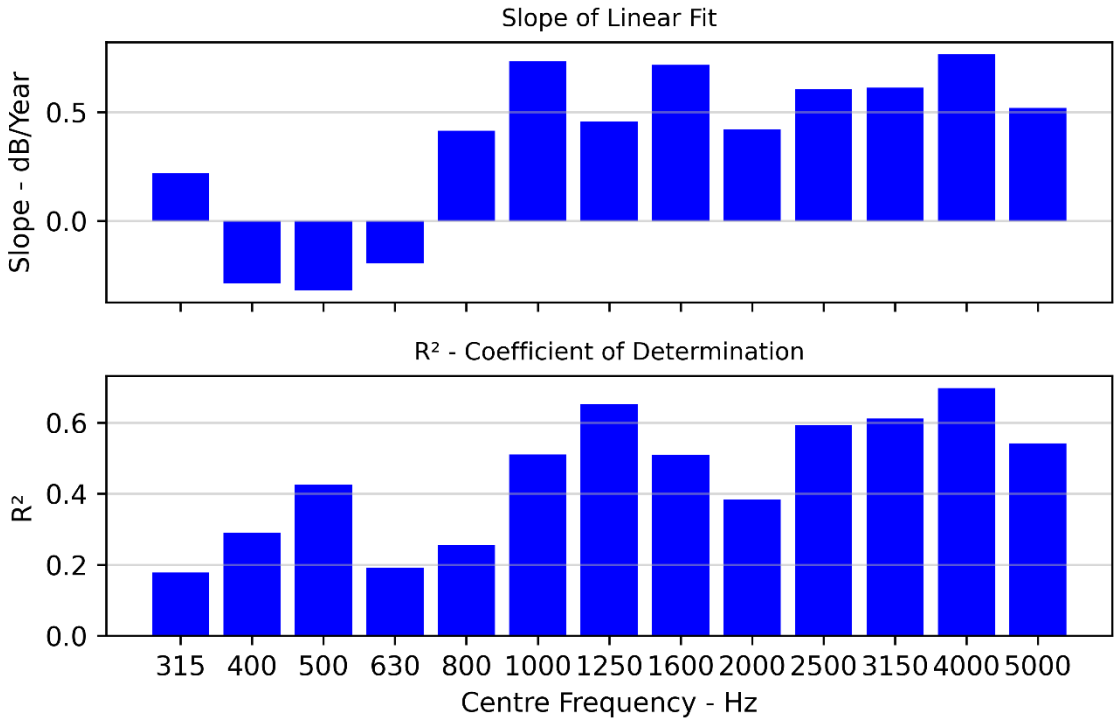

Figure 53: Rate-of-change of one-third octave band levels with time for EPA7 (50 mm) in lane 2 on WBB.

The mean rate of change of L_{CPX} and MPD for each sample are shown in Figure 54 and Figure 55, respectively. Aside from the SMA10 (40 mm) reference surfaces and EPA10 (30 mm), the overall trend was a positive rate of increase of mean L_{CPX} in lane 2 (left lane) and a zero or slightly negative rate in lane 1 (right lane). The MPD exhibited a negative rate across all samples, excluding the EPA10 (30 mm).

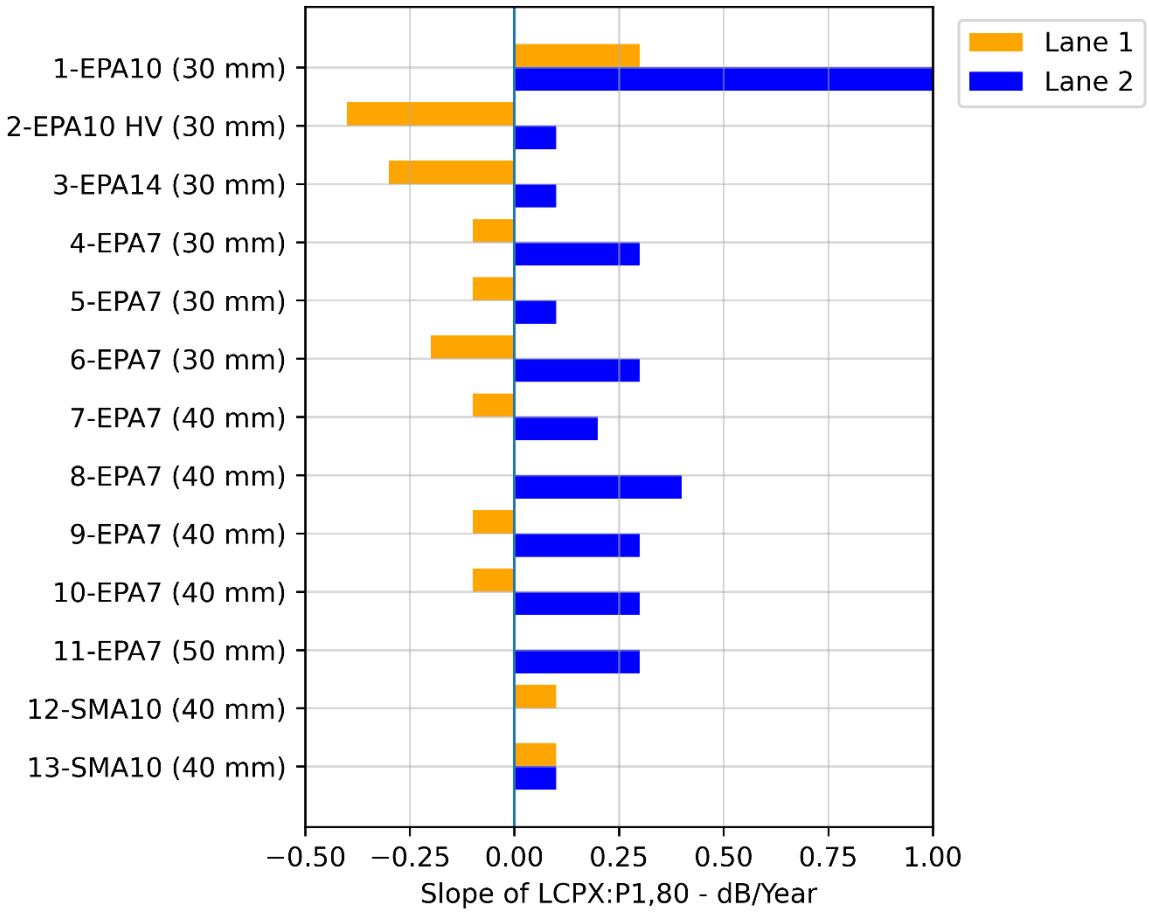

Figure 54: Mean rate-of-change of L_{CPX} with time by surface.

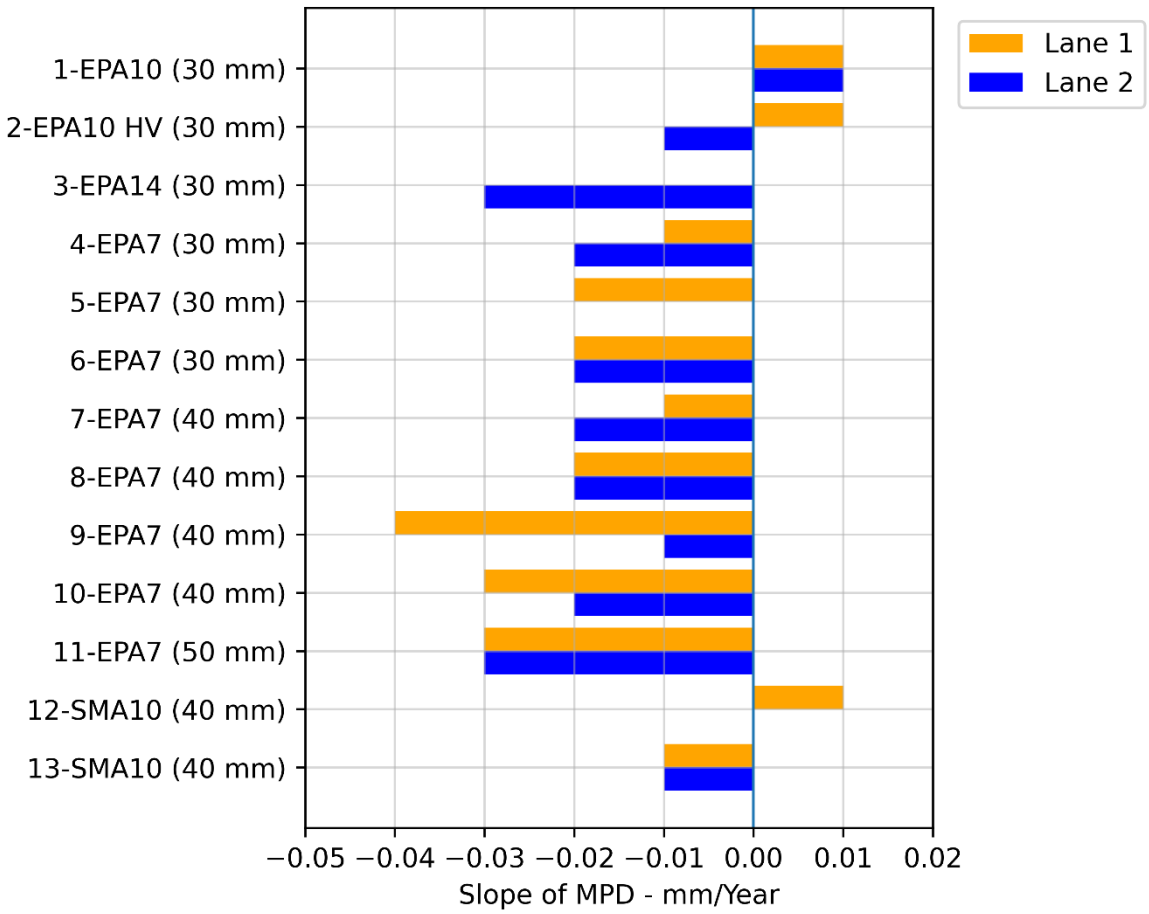

Figure 55: Mean rate-of-change of MPD with time by surface.

Several noteworthy results and findings are discussed below.

Lane 1 versus 2

In all of the evaluated locations, the rate of increase in lane 2 (the left and outer lane) was greater than lane 1 (the right or inner lane). Lane 2 typically exhibited a positive rate of increase, while lane 1 was either stable over time or had a small negative rate of change. The L_{CPX} for Lane 2 has more influence on the wayside noise level due to its physical proximity and greater trafficking. For the EPA7 (50 mm) on WBB (sample 11, lane 2 exhibited a positive rate of change of 0.3 dB/year ±0.1 dB/year (n = 4), while lane 2 was relatively stable over the same period (0.0 dB/year ±0.2 dB/year, R^2 = 0.01). It is important to acknowledge that while the overall L_{CPX} for lane 2 was observed to be increasing, the rate is low in absolute terms.

EPA10 (30 mm) on S2G

Lane 2 of the EPA10 (30 mm) sample on S2G had a significantly greater rate of increase (+1.0 dB/year ±0.1 dB/year, n = 9) compared to the other sample sections (+0.1 to +0.4 dB/year). The rate of change varies significantly along the sample, with the greatest rate being immediately adjacent to the SMA and an approximately linear decrease along the length (see Figure 85). It is hypothesised that the higher degradation in acoustic performance is due to it being immediately adjacent to the SMA of a roundabout and vehicles tracking debris from the impermeable surface. The EPA10 (30 mm) on S2G ageing may not be indicative of the typical performance of porous asphalts. Further investigations would be required to understand the ageing mechanisms at this site and their generalisability to other locations.

EPA10 HV and EPA14 (30 mm)

Both the EPA10 HV (30 mm) and EPA14 (30 mm) had similar rates of change; with a small positive rate in lane 2 (left lane) and a large negative rate in lane 1 (right lane). These sections are adjacent on S2G and experience identical trafficking. In all cases, the rate of change by frequency had a similar trend with negative rates in the low-frequency bands and positive rates in the high-frequency bands (see Figure 86 and Figure 87). The negative rates in the low-frequency bands are consistent with the change expected when a surface has reducing texture (Bell, 2022), while the increasing rates in the high frequency bands support a loss of voids and/or thickness. The overall levels for both surfaces are dominated by lower frequency bands (500-800 Hz) and therefore the reduction in these bands resulted in an overall decrease.

EPA7

The samples of EPA7 demonstrated the same characteristics over time; with increasing levels in lane 2 (left lane) and minimal changes in lane 1 (right lane). The samples were drawn from two sites (WBB (5,040 m) and Memorial Bridge (680 m)). The observations are limited to these two locations and are not generalisable. For lane 1, the frequency bands 1,250, 1,600, 4,000, and 5,000 Hz increased (see Figure 88 for example), which may suggest an effective decrease in thickness and/or a decrease in air flow permeability.

Initial L_{CPX} Level

It was hypothesised that the rate-of-change of L_{CPX} with time is inversely proportional to the initial level (i.e., segments that have a lower initial level increase more rapidly). For sample 10 of the EPA7 (40 mm) the initial L_{CPX} and the rate of change were negatively correlated with a linear fit resulting in an R^2 of 0.36 with the measured data for this single sample (see Figure 89). This sample was selected as it is 2.6 km long, with regular CPX measurements. The underlying factors contributing to the observed weak correlation remain unidentified. Future research should investigate this relationship further.

4.2 Cross-Sectional Analysis

All measurements taken in Q1 of 2023 in lane 2 of PA10 (30 mm) surfaces (20 different sites) were included in the cross-sectional analysis. The mean L_{CPX} versus age is shown in Figure 56. There was a positive correlation between L_{CPX} and age with a linear fit having a slope of +0.3 dB/year ±0.1 dB/year. The linear fit had an R^2 of 0.23, indicating only a fraction of the observed variance is likely due to age. Based on previous analyses, variations in thickness and texture are likely the dominant sources of dissimilarity in L_{CPX} between sites.

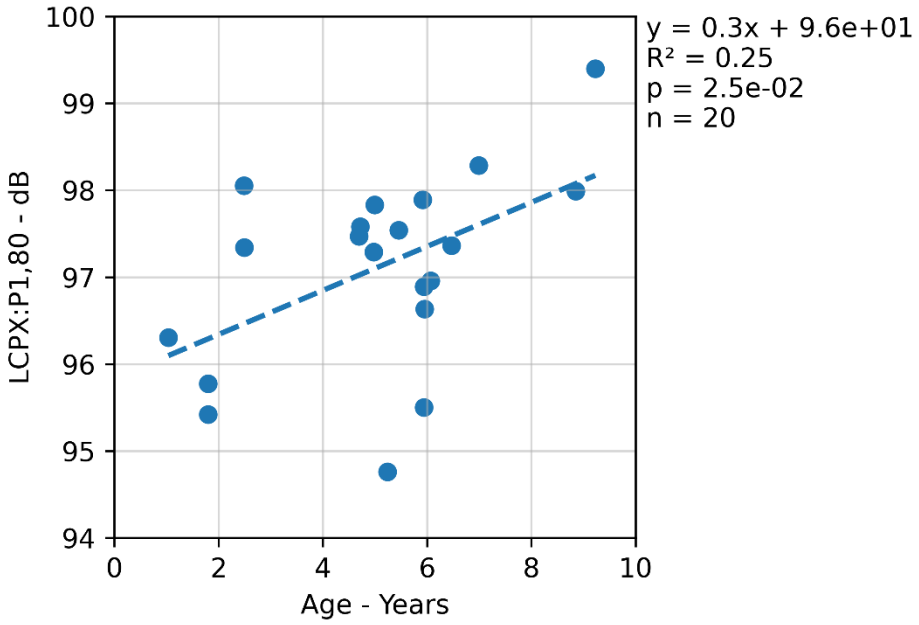

Figure 56: L_{CPX} versus age for all PA10 (30 mm) measured in Q1 2023.

The mean rates-of-change by one-third octave band are shown in Figure 57. All bands from 1,000 Hz up exhibited a positive rate of change, which is consistent with the results of the chronological analysis.

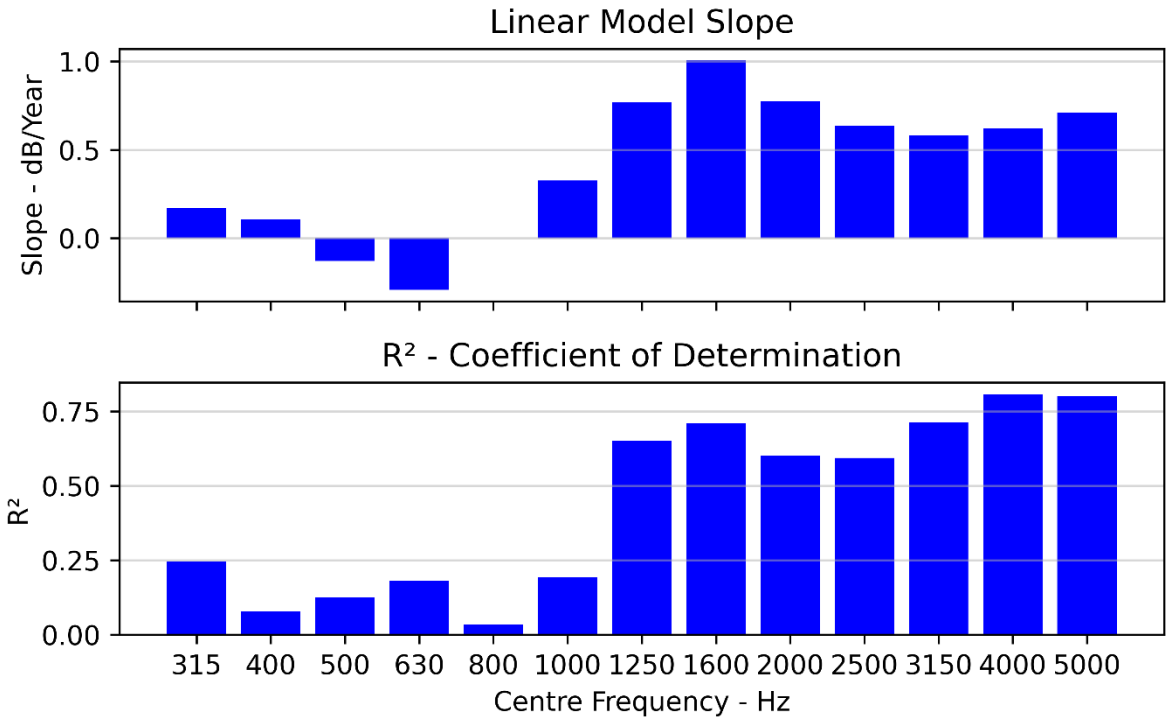

Figure 57: Mean rate-of-change of one-third octave band levels for all PA10 (30 mm) measured in Q1 2023.

4.3 Summary of Chronological and Cross-Sectional Analyses

Availability of data did not allow for the direct comparison of the two methods for the same surface mix (e.g., PA10 (30 mm)), therefore only overall trends could be compared. The chronological and cross-sectional methods yielded similar results for the age-related change in close-proximity noise level of porous asphalt. Both methods showed a positive rate of increase in the left lane of dual carriageways. Both methods showed positive rates of change in the high frequency bands, which may indicate changing void characteristics from the collection of debris or compaction from traffic, or another mechanism. The chronological analysis revealed negative rates of change in the low frequency bands for multiple surfaces and locations; this was not evident in the cross-sectional analysis for PA 10 (30 mm).

Two previous studies have demonstrated age-related degradation of the close-proximity noise level for porous asphalt on New Zealan's state highway network using cross-sectional analyses (Jackett, 2021; Lester et al., 2017). The +0.3 dB/year mean rate of change for PA10 (30 mm) observed in this study is similar to the +0.14 dB/year and +0.2 dB/year that was observed by Jackett and Lester (Jackett, 2021; Lester et al., 2017), respectively.

The chronological approach enables detailed, site-specific studies of aging effects, which are not feasible with the cross-sectional method. This allows for in-depth analysis of phenomena such as the observed elevated rate of increase in noise for EPA10 (30 mm) on S2G, aiding in uncovering specific causes of noise performance degradation. Assuming that the measurement system is stable and corrections for factors like speed, tyre hardness, temperature, and enclosures are known, the chronological method could offer valuable insights in future research.

5 Future Work

The following areas are suggested for future investigations based on the findings in this report.

- **Void Reduction**
  Description: Explore whether compaction or clogging is responsible for a majority of the porous asphalt ageing effect.
  Purpose: Understanding the mechanism of ageing may enable mitigation of the loss of noise performance through mix design, maintenance, etc.
- **Lane 1 versus Lane 2**
  Description: Explore the causes of the difference between the left and right lanes on dual carriageways.
  Purpose: The cause(s) of the difference may enable further noise optimisations over the service life of the surface.
- **Ongoing Ageing Monitoring**
  Description: Update the analysis following the 2023/2024 annual survey; this may also include updating the CPX Data Viewer to support detailed ageing analyses.
  Purpose: Expanding ageing analysis beyond five years.
- **Targeted Ageing Study**
  Description: Conduct a targeted location study of sites experiencing greater rates of change (e.g., porous asphalt adjacent to impermeable surfaces). Also explore whether the underlying pavement type influences the rate of change with time.
  Purpose: Increase the understanding of how critical design and usage parameters influence ageing.
- **Remediation Methods and Efficacy**
  Description: Conduct a review of available technologies and their efficacy for restoring the age-related loss of noise performance.
  Purpose: Identify methods of reversing the loss of low noise performance over time.

6 Conclusions

Changes in the tyre/road noise measured by the Waka Kotahi CPX system were analysed using data collected from 2018 to 2023. The primary focus was to establish how the overall level and frequency spectra have changed for various porous asphalt low-noise surfaces.

Two analysis methods were used: the first considered chronological data for the samples of various surface types, and the second considered data from the same nominal surface type within a single measurement season. The chronological approach first required demonstration of the long-term stability of the measurement system. It was found that one set of enclosure corrections strongly influenced a period of measurements, which were omitted from the subsequent analyses. The remainder of the reference measurements showed good repeatability and low drift over time.

Both methods yielded similar results, which was a positive rate of change for the overall level in lane 2 (left lane) driven by increases in the mid to high-frequency bands. Surfaces with initially high noise levels and texture exhibited decreasing overall levels as the low-frequency bands were decreasing with time, the overall noise level for surfaces with higher texture is dominated by these bands.

The observed direction of the results is consistent with published literature but with lower magnitudes. A potential cause of the increasing levels is a reduction in voids, which may be either reducing the effective thickness or air flow permeability. The voids may be reducing due to a combination of compaction from trafficking and the collection of debris.

The positive rates of change are low and there is presently no indication that the relative levels between surfaces will experience a significant variation. The present approach of reducing the noise level through increasing the thickness of the porous asphalt layer is probably not affected by these findings (i.e., a 50 mm surface would likely remain quieter than a 40 mm surface in the same location).

Part III Epoxy-Modified Porous Asphalt

1 Introduction

To extend the service life of porous asphalts, a reactive epoxy resin and curing agent are added to the bituminous binder. The epoxy modified binder hardens slowly over time, resulting in a greater stiffness than conventional asphalt. The mix designs are typically identical (Herrington, 2014). Bituminous binders oxidise as they age causing the binder to become brittle over time. This eventually causes the surface to begin to lose stones or "ravel". The inclusion of epoxy in the binder slows down the bitumen oxidation process, thereby extending the life of the porous asphalt surface beyond its typical eight-year lifespan. It is common to use epoxy on 40 mm thick, porous asphalt surfaces and it has been used for all 50 mm porous asphalt surfaces.

The objective of this analysis was to use available data to determine the effect that the addition of epoxy has on tyre/road noise.

The effect of the epoxy modification on tyre/road noise had not previously been assessed for adjacent and contemporaneous surfaces using the CPX method. The presence of both conventional and epoxy-modified porous asphalt surfaces within the CNC project enabled an indicative comparison of the tyre/road noise. The availability of high-resolution thickness measurements, the effectively concurrent surfacing, and identical trafficking enabled the isolation of thickness, age, and traffic loading.

A critical limitation of the analysis in this report is that it was confined to the CNC project and is not generalisable to other sites. All findings are specific to the processes, parameters, and conditions of CNC. With each sample only having a size of one, the analysis was vulnerable to anomalies that could not be identified (e.g., inter-batch variation, paving equipment, operators etc.). The ability to conduct quantitative statistical analyses was constrained by the use of a single sample. All findings must be considered as indicative and require further research to understand the influence that the epoxy-modification has on tyre /road noise.

The effect of the epoxy-modification was partially explored for other sites using the available CPX data from 2018 to 2023. The data from other sites was confounded by thickness, texture, age, trafficking, etc., which likely has a greater effect on tyre/road noise. No results from this analysis were included in this report.

This part contains a description of the data, presentation and discussion of the results, and a series of recommendations for future investigations.

2 Data

The 2022 CNC project contains both epoxy-modified and conventional porous asphalt. This project contains an excellent source of contemporaneous trial sections. In addition, high-resolution thickness data was present for the entirety of each section. To reduce the dominant thickness influence, the samples were filtered to 30 mm ±3 mm. The available sample lengths with and without thickness filtering are given in Table 8.

Table 8: Lengths of samples with and without epoxy modification.

Thickness	PA7 (30 mm) Length* – km	EPA7 (30 mm) Length* - km
All thicknesses	10.5	3.1
30 mm ±3 mm	6.5	1.8

*Total lane length (i.e., two lanes)

The analysis used measurement data of tyre/road noise, texture, thickness, and void fraction. The sources of data and measurement dates are given in Table 9.

Table 9: Data, sources, and measurement dates.

Data	Source	Measurement Date	Surface Age Months
Tyre/road noise	Waka Kotahi CPX trailer	Apr 2022 Mar 2023	1 12
Texture	WDM HSD survey	Dec 2023	9
Thickness	Woods laser survey	-	-
Void fraction	Road Science NDM	Nov 2023	21

3 Results and Discussion

To analyse the effect of the addition of epoxy, the following was completed:

- Comparison of the overall L_{CPX} at one and 12 months after surfacing.
- Comparison of the MPD measured as part of the HSD annual survey.
- Comparison of the void fraction measured using an NDM.
- Comparison of the one-third octave spectra one and 12 months after surfacing.
- Comparison of the change in overall L_{CPX} with thickness.

All components of the analysis, excluding the effect of thickness, used only lane segments with a thickness of 27 to 33 mm in the left wheel path. It was assumed that the 27 to 33 mm range sufficiently isolated the effect of the epoxy modification from the dominant thickness relationship. It was also assumed that most differences in MPD and void fraction were linked to the epoxy modification.

While the sample lengths of 6.5 and 1.8 km for 30 mm ±3 mm PA and EPA, respectively, were divided into 4 m segments, the sample size for each category remains effectively one. All statistical tests were completed using the quantities of segments (e.g., 6.5 km yields 1,625 segments) rather than distinct sites (i.e., one).

Boxplots of the L_{CPX} at one and twelve months after surfacing are shown in Figure 58 and Figure 59, respectively. Boxplots of the MPD nine months after surfacing are shown in Figure 60. Boxplots of the void fraction measured 21 months after surfacing a shown in Figure 61

The EPA offered a mean reduction in L_{CPX} of up to 1 dB, which was present immediately after surfacing and remained one year later. The EPA had a small reduction in mean MPD and void fraction of 0.05 mm and 1%, respectively.

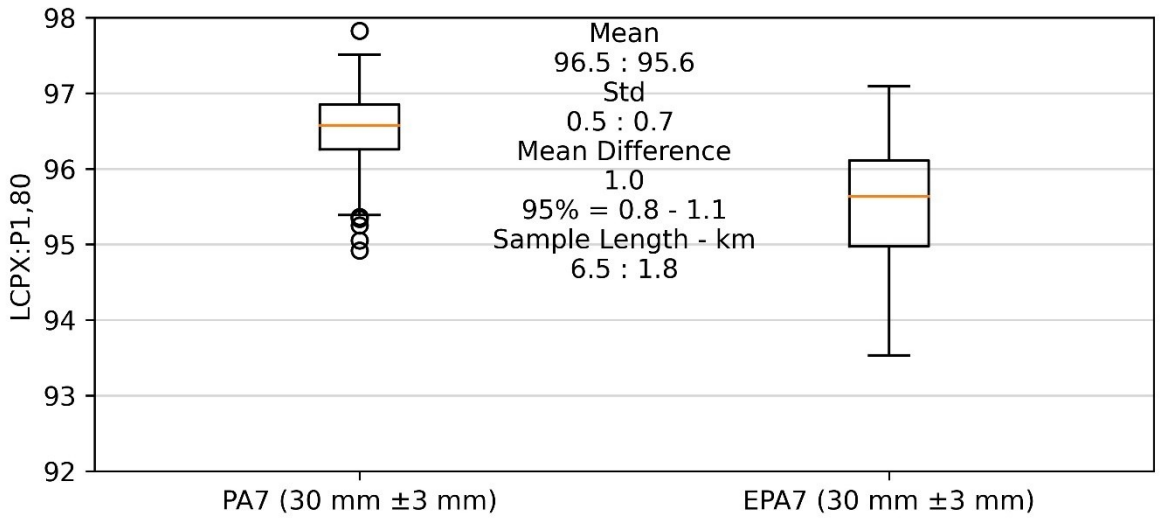

Figure 58: Overall L_{CPX} for PA7 and EPA7 on CNC for a thickness of 30 mm ±3 mm one month after surfacing.

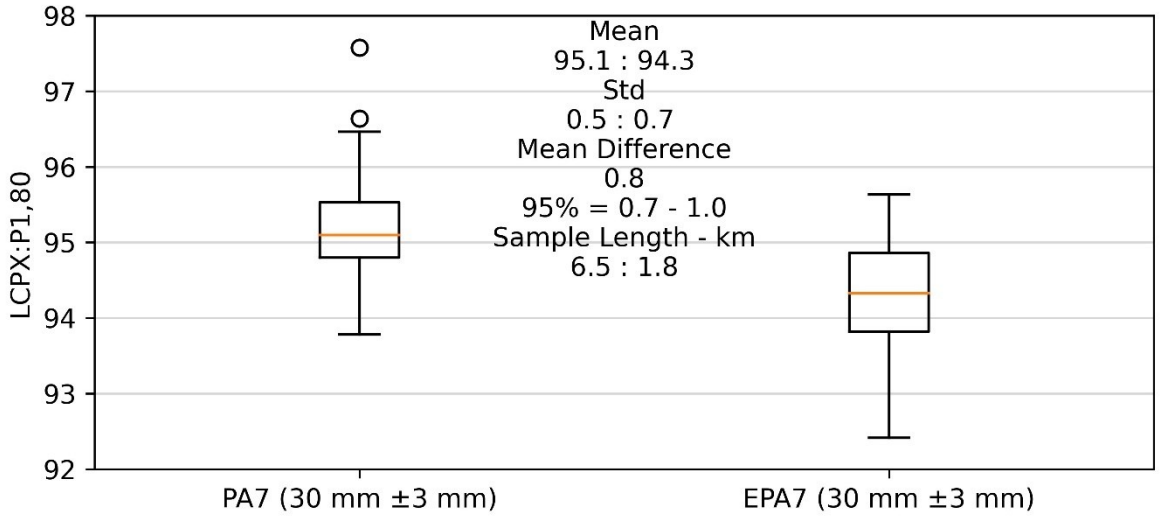

Figure 59: L_{CPX} for PA7 and EPA7 on CNC for a thickness of 30 mm ±3 mm 12 months after surfacing.

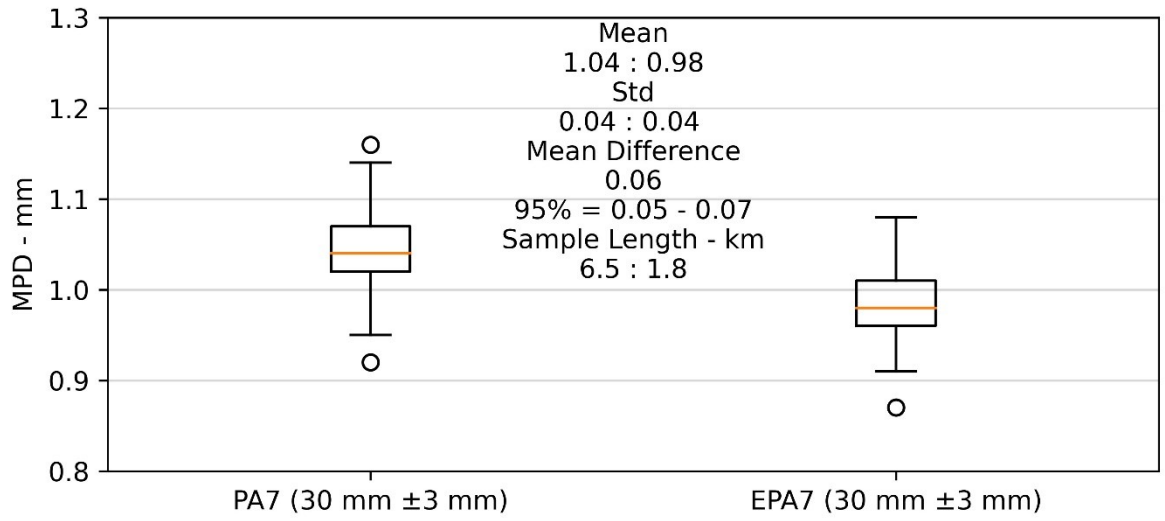

Figure 60: MPD for PA7 and EPA7 on CNC for a thickness of 30 mm ±3 mm.

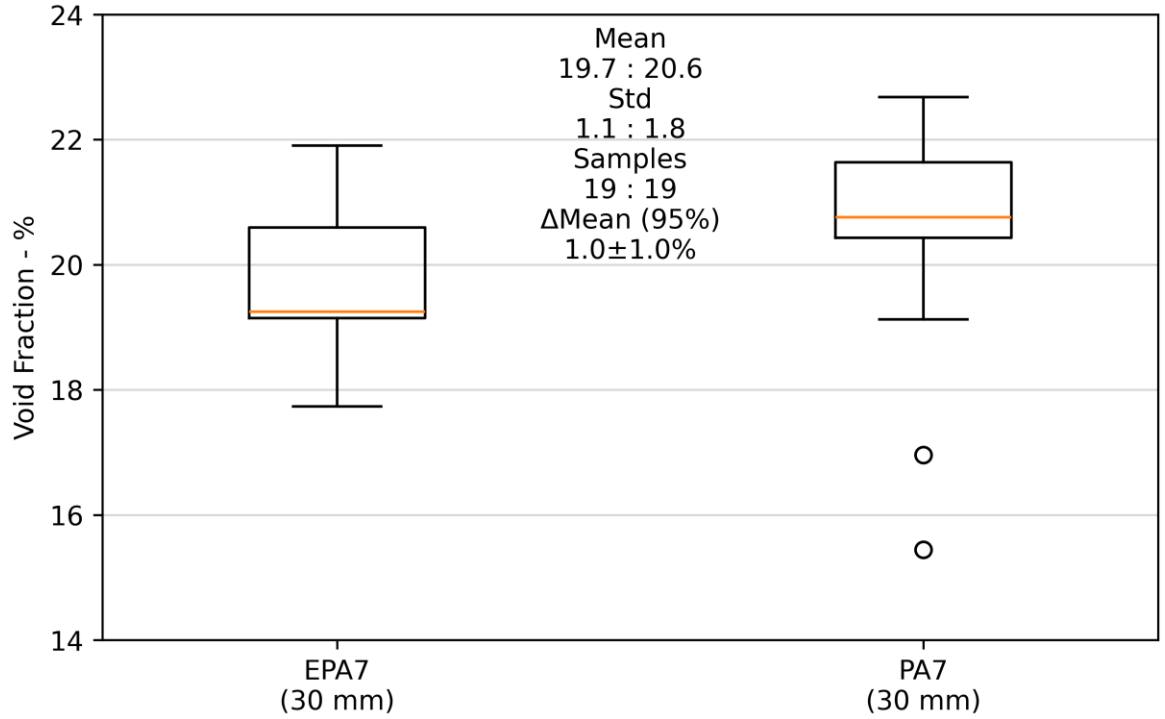

Figure 61: Void fraction for PA7 and EPA7 on CNC.

The one-third octave spectra and the deltas (PA minus EPA) are shown in Figure 62. The greatest delta occurred in the 1,600 Hz band, with significant deltas in the 1,000, 1,250, 4,000, and 5,000 Hz bands.

The absence of deltas in the lower frequencies (< 1,000 Hz) indicate that texture is not a dominant source of variation in L_{CPX} between PA and EPA. A more detailed review of texture (i.e., parameters other than MPD) would likely be required to identify potential texture differences (e.g., surface void shape, etc.)

The deltas in the 1,000 to 1,600 Hz bands are likely due to acoustic absorption. As thickness is common across the samples, the other factors that can influence absorption are interconnected void quantity, void shape, and air flow resistance (which is primarily a function of void quantity and shape). Directly measuring the acoustic absorption will confirm this hypothesis and potentially indicate which void characteristic is causing it.

It is expected that a greater mean void fraction would typically result in increased air flow permeability and lower noise levels at high frequencies (i.e., 4,000 and 5,000 Hz). However, the opposite was observed where the PA had greater high frequency levels and a marginally higher void fraction. A potential cause could be that the air flow resistance is greater due to smaller or fewer interconnected voids.

It is recommended to explore the void characteristics further to attempt to identify the mechanism(s) driving the difference in tyre/road noise.

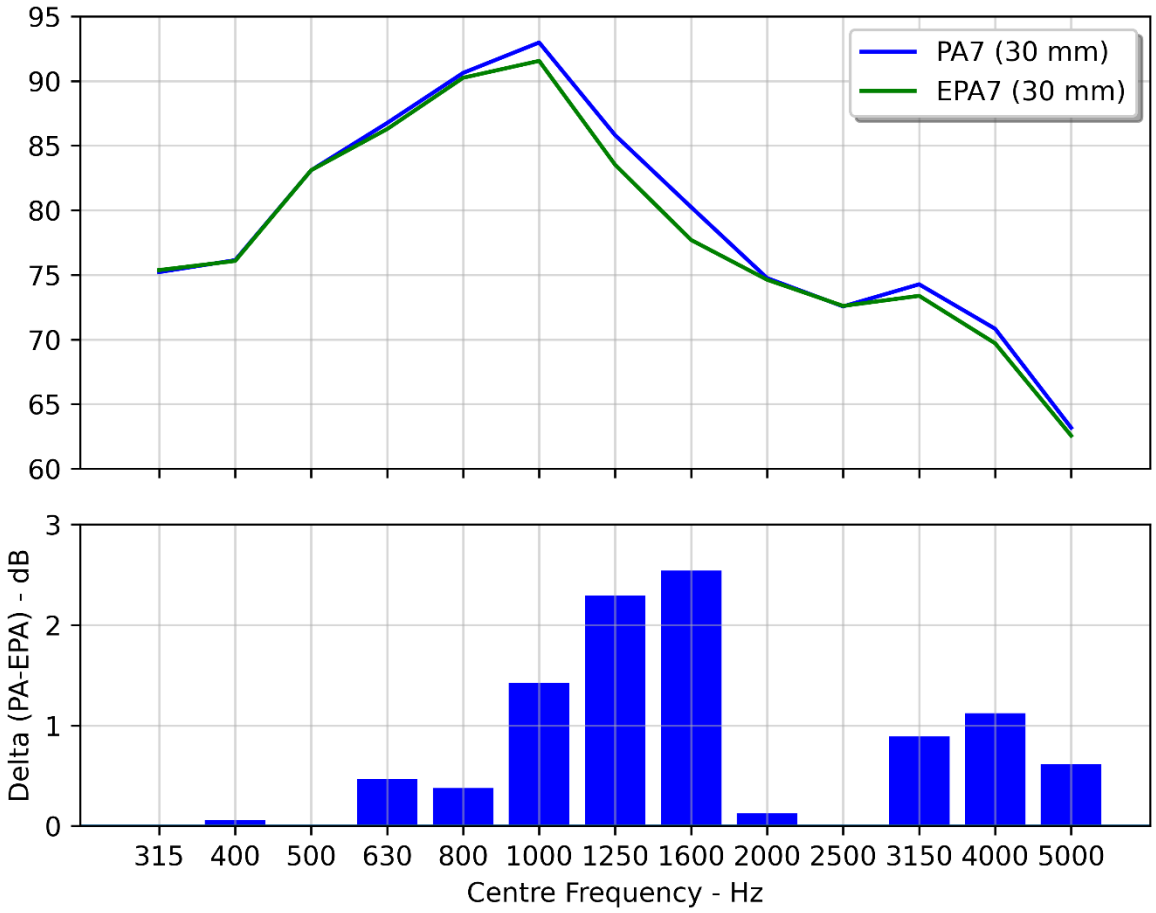

Figure 62: One-third octave band L_{CPX} spectra for EPA7 (30 mm) and PA7 (30 mm) on CNC one month after surfacing.

The influence of thickness on the effect of EPA was analysed by grouping the samples in thickness bins from 22 to 38 mm with widths of 1 mm (e.g., 25 mm ±0.5 mm). Figure 63 contains a plot of L_{CPX} as a function of thickness for EPA and PA. The mean rate of decrease with thickness for PA is -1.2 dB/10 mm, compared to -2.0 dB/10 mm for the EPA. The increasing delta with thickness supports the hypothesis that the difference is arising from a physical property that affects acoustic absorption.

While the EPA7 exhibited the expected relationship with thickness, the PA7 had a lower rate of change. The consequence of this was the divergence of the overall levels with increasing thickness. From the limited data, the delta increased to 2 dB at a thickness of 40 mm. It is recommended that this relationship is explored further in a future study.

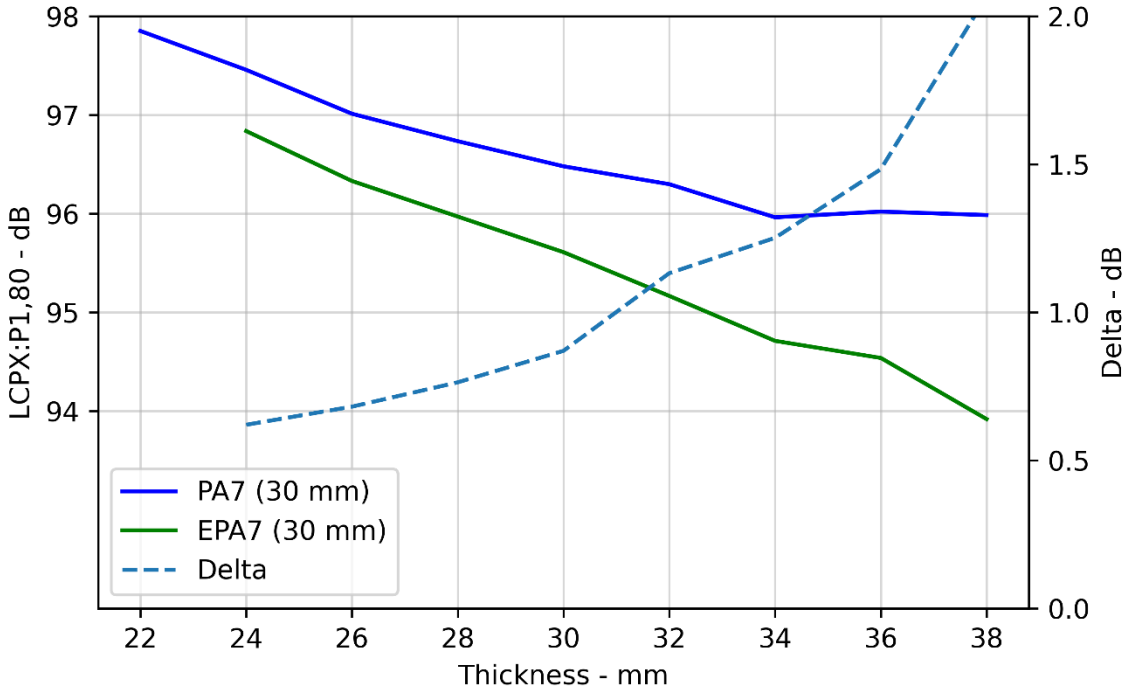

Figure 63: L_{CPX} versus thickness for PA7 and EPA7 one month after construction.

4 Future Work

The following areas are suggested for future investigations based on the findings in this report.

- **Field Void Fraction Measurements**
  Description: Expand the NDM measurements set with a range of thicknesses and shoulder measurements.
  Purpose: Increase the confidence of the delta observed by the initial NDM measurements. Explore whether the void fraction delta increases with increasing thickness. Confirm whether compaction is due to trafficking or construction.
- **Acoustic Absorption**
  Description: Measure in situ acoustic absorption across a range of thicknesses.
  Purpose: Test hypothesis that absorption is the mechanism underlying the delta in tyre/road noise levels. Indicate the physical mechanism causing the delta (e.g., air flow resistance, void shape, etc.).
- **Cores**
  Description: Extract core samples to explore void structure using NDI methods such as x-ray tomography.
  Purpose: Determine if field samples have different void characteristics.
- **Short-Term Workability**
  Description: Use CAPTIF track to conduct controlled early life compaction under trafficking measurements.
  Purpose: Characterise workability window to inform construction processes.

5 Conclusions

Sections of epoxy-modified and conventional PA on CNC were analysed to explore the effect of epoxy on tyre/road noise. For a thickness of 30 mm ±3 mm, the EPA was measured to be an average of 1.0 dB quieter than the PA. The frequency spectra showed that the delta in L_{CPX} was driven by differences in the mid (1,000-1,600 Hz) and high (3,150-5,000 Hz) bands. It is hypothesised that the surfaces have differences in acoustic absorption, stemming from changes in the void characteristics. For CNC only, there was a small difference of 1 dB in the overall noise level for PA7 and EPA7 with a thickness of 30 mm ±3 mm.

The presented findings are limited to the analysed sections on CNC and are not generalisable. Further research is required to confidently determine the effect of the epoxy-modification on tyre/road noise.

Part IV CPX Speed and Tyre Hardness

1 Introduction

There are numerous parameters that affect tyre/road noise. Speed and tyre hardness were identified as critical parameters for both their general influence on road noise and their relevance in the CPX method. Although the CPX standard attempts to correct measurements for perturbations of speed and tyre hardness from specified values, it applies these corrections uniformly across all one-third octave bands. This approach likely oversimplifies the true nature of these relationships. Also, it is unknown whether the noise level deltas between various surface designs are consistent across the full range of traffic speeds.

The objectives of this analysis included:

- **Speed**
  - Determine the accuracy of the speed correction for various surfaces, including frequency dependence.
  - Confirm the effect of speed on CPX levels for different surface designs.
- **Tyre hardness**
  - Determine the accuracy of the tyre hardness correction and its frequency dependence.
  - Confirm the effect of hardness on CPX levels for different surface designs.

This part provides a brief background of the key parameters and their normalisation process as per the CPX standard. It then outlines the methods used for measurement and the variations observed in the parameters. The findings are then presented concurrently with an in-depth analysis.

2 Background

The correction method prescribed in the CPX standard is described along with the interpretation and application by Waka Kotahi. A limited literature review was completed to determine the current understanding of how speed and hardness influence tyre/road noise.

2.1 Speed

The relationship between tyre/road noise level, *L*, and vehicle speed is commonly represented in the form shown in Equation 1 (Sandberg & Ejsmont, 2002).

$$L \propto 10n \log v$$ Equation 1

Where:

n Speed exponent

v Speed – km/h

The CPX standard utilises the speed relationship to normalise results to a reference speed following Equation 2.

$$\Delta L_{CPX} = 10n \log \frac{v}{v_{ref}}$$ Equation 2

Where:

v_{ref} Reference speed – km/h

Note that within the CPX standard, the correction coefficient B is equal to $10n$. It should also be noted that the correction is subtracted from the measured level to normalise the result to a specified speed (e.g., 80 km/h).

The standard states that the speed correction coefficient is a function of the surface type. Table 10 contains the specified values and surface descriptions. Waka Kotahi currently utilises a speed correction coefficient of

30 for all surface types to avoid introducing step-changes in level at arbitrary thresholds of porosity (which is not precisely known for most sections of road).

Table 10: Speed correction coefficients and surface descriptions from (ISO 11819-2, 2017)

Correction Coefficient B	Surface(s)
25	*"For a porous pavement in relatively new condition, or older but with no severe clogging."*
30	*"For a clogged porous, semi-porous or dense asphalt pavement."*
35	*"For a (non-porous) cement concrete pavement."*
30	*"For all other cases, including cases where the pavement type is unknown."*

Figure 64 shows the change in L_{CPX} relative to 80 km/h as a function of speed for a range of speed exponents following Equation 2. Figure 65 shows a subsection of the same relationship across the typical range of measurement speeds when targeting 80 km/h. Considering speed exponents from 2.5 to 3.5, the difference when correcting for minor speed perturbations is small. However, when extrapolating more than 10 km/h from the measured speed the result is increasingly sensitive to the speed exponent.

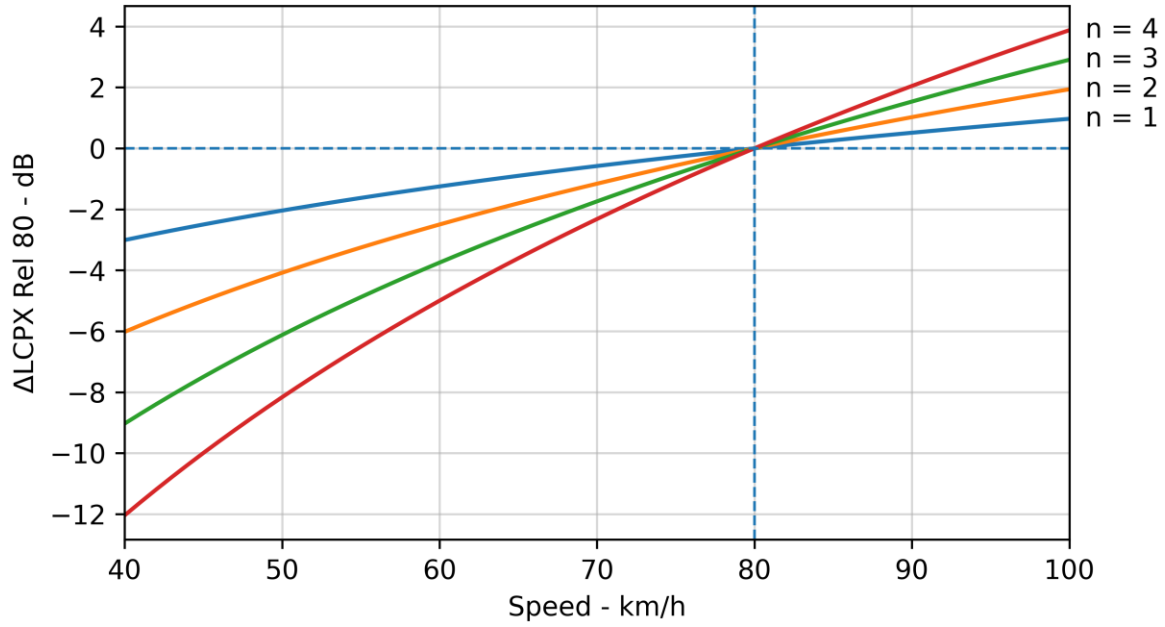

Figure 64: Theoretical change in L_{CPX} relative to 80 km/h for speed exponents from 1 to 4, following ISO 11819-2:2017.

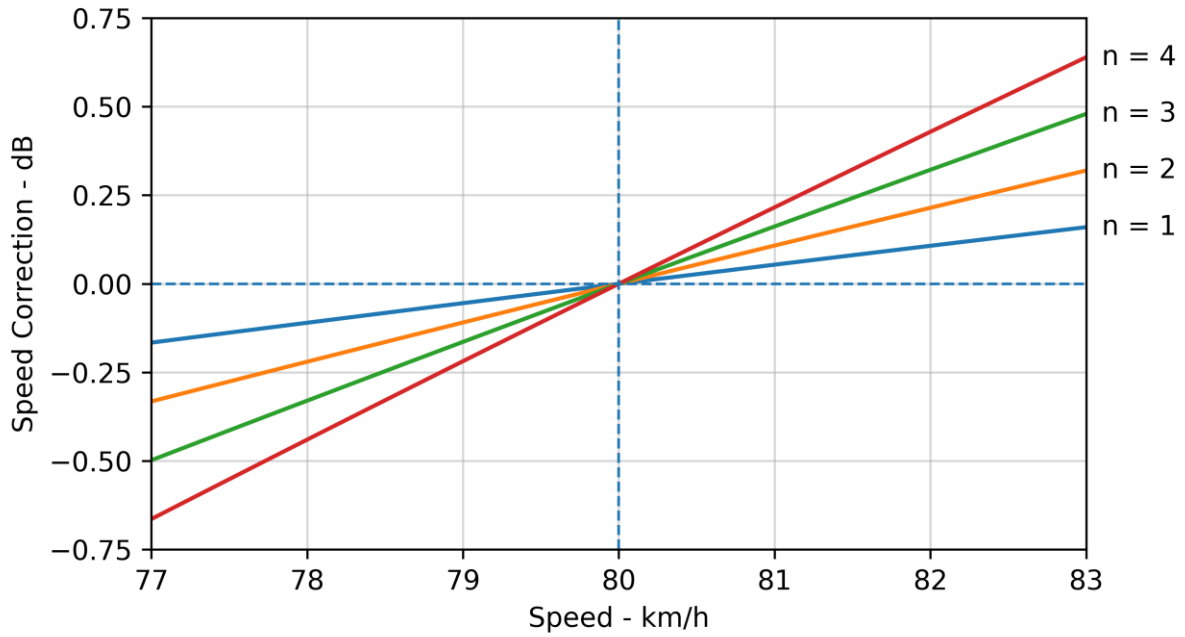

Figure 65: Correction for L_{CPX} to 80 km/h for speed exponents from 1 to 4 for the typical speed variation range during a measurement session.

The speed exponent is known to be a function of frequency, where high frequencies (>800 Hz) have a higher speed exponent (Sandberg & Ejsmont, 2002). The stronger influence at high frequencies is attributed to air resonances and air pumping. Low frequency noise is driven by texture-induced vibration, which is known to have a lower speed exponent (Beckenbauer et al., 2001; Sandberg & Ejsmont, 2002).

Speed has been shown to influence the temperature correlations, where tyre/road noise is less affected by temperature at higher speeds (Bühlmann et al., 2015). Speed was also observed to have a greater effect at higher frequencies.

From the available literature, the speed influence is indicated to be a function of frequency, surface material and age, and temperature.

2.2 Tyre Hardness

It is well understood that tyre/road noise is positively correlated with tyre hardness for the P1 tyre. The method for normalising tyre hardness is described in (*ISO/TS 11819-3*, 2021). A correction is applied to the measurements to normalise the tyre hardness to 66 Shore A using Equation 3.

$$\Delta L_{CPX} = \beta_t \left(H - H_{ref}\right) \qquad \text{Equation 3}$$

Where:

β_t Tyre hardness coefficient – dB/Shore A

H Measured tyre hardness – Shore A

H_{red} Reference hardness - Shore A

The value for the hardness coefficient is specified as 0.12 dB/Shore A in the standard. The correction is subtracted from the measured level to normalise the result to a hardness of 66 Shore A.

The measurements utilised three P1 tyres with hardness values of 67.9, 74.2, and 78.1 Shore A with corresponding labels of "soft", "medium" and "hard", respectively. Figure 66 shows the L_{CPX} correction as a function of tyre hardness; the three tyres are also included in the plot. Note that the displayed correction is subtracted from the measured level. Waka Kotahi has typically measured with tyres having a hardness of up to 74 Shore A, which results in a correction of up to 1 dB.

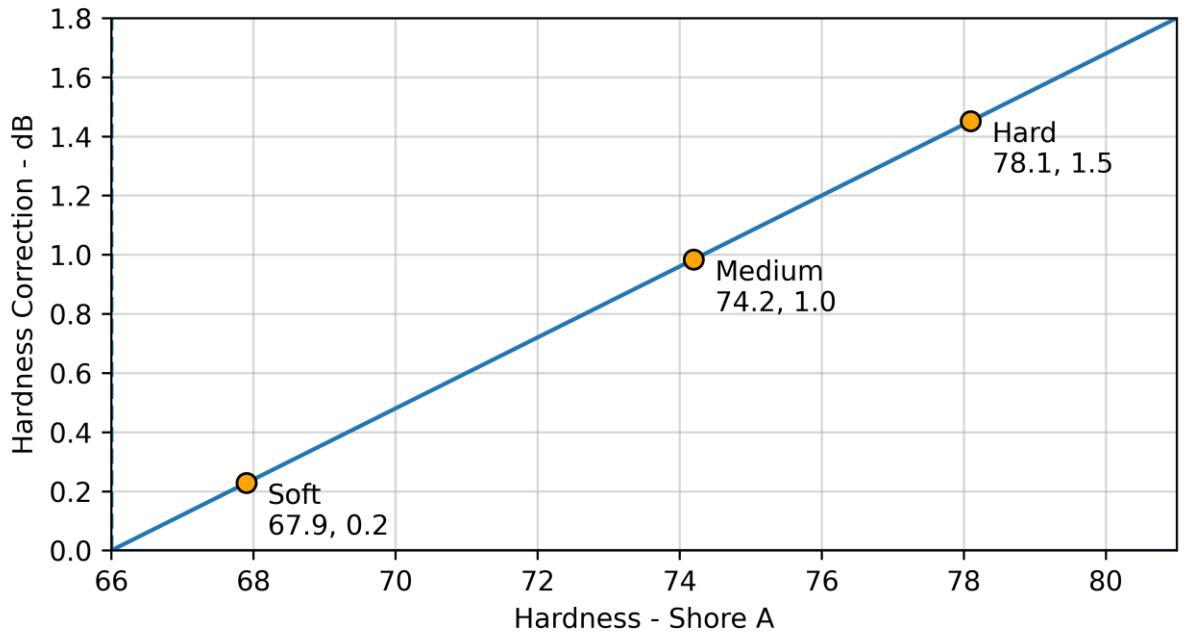

Figure 66: Correction to L_{CPX} due to tyre hardness including the three tyres used for the present study.

Tyre hardness increases over time, with the rate being a function of environmental conditions and usage. It was demonstrated that the hardness of the P1 tyre increased by 3 Shore A over one measurement season, which corresponded to an increase of 0.05 Shore A per measurement day (Bühlmann et al., 2013).

While the corrections are applied uniformly across the reported sound spectra, it is stated that the actual relationships vary by frequency with the 1,000 to 3,000 Hz range being most influenced (Sandberg & Ejsmont, 2002). Conversely, it was described as not significantly affecting the spectral shape by a different study (Oddershede & Kragh, 2014).

Tyre hardness was observed to have no effect for very smooth surfaces, with increasing influence on surfaces with greater texture (Sandberg & Ejsmont, 2007).

From the available literature, the influence of tyre hardness on L_{CPX} is indicated to be a function of frequency, surface material and texture, and the specific tyre.

3 Measurements

All CPX measurements for the speed and tyre hardness study were completed between the 17th of Nov and 5th Dec 2023. The unique locations, surfaces, speeds, and tyres are shown in Table 11. 28 measurement sessions were conducted (e.g., one session was all surfaces within S2G with the soft tyre at 80 km/h), a list of each session is shown in the appendix in Table 14. All asphalt measurements were completed in an air temperature range from 15.3 to 18.4 °C. All chipseal measurements (i.e., Kirwee) were completed in a temperature range from 11.8 to 15.7 °C. It was assumed that the influence of temperature across the range experienced during the measurements was negligible.

Table 11: Measurement parameters.

Locations	Surfaces	Speeds – km/h	Tyres
S2G	EPA7 (30 mm)	40	Soft - 67.9
Groynes Ramps	EPA 7 (40 mm)	50	Medium – 74.2
WBB	EPA7 (50 mm)	60	Hard - 78.1
CNC	EPA10 (30 mm)	70	
Kirwee	EPA10 HV (30 mm)	80	
	EPA14 (30 mm)	90	
	Grade 2 Single-Coat		
	Grade 2/4 Two-Coat		
	Grade 2/4 Racked-In		
	Grade 2/4/6 Multi-Coat		
	Grade 3 Single-Coat		
	Grade 3/4 Two-Coat		
	PA7 (30 mm)		
	PA7 HS (30 mm)		
	PA7 LV (30 mm)		
	PA10 (30 mm)		
	SMA7 (30 mm)		
	SMA10 (40 mm)		

Tyre hardness can be explored by either hardening of a single tyre or using tyres of different hardness. Both approaches have benefits and limitations. The only viable option for the present study was to use multiple tyres having different hardness values. Using multiple tyres with different hardness values enables measurements to be undertaken in close temporal proximity, therefore eliminating any influence by physical changes to the surface. However, parameterising a tyre with a single hardness value does not allow for the exclusion of other physical differences (e.g., balance, wear, etc.).

4 Results and Discussion

The following points are applicable within the proceeding section:

- Where appropriate, the presently used speed exponent and hardness coefficient are displayed within the figures as dashed red lines.
- Where a thickness is stated on CNC, the laser survey data was used to limit the samples to being within 10% of the specified value (e.g., the EPA7 HS (30 mm) was limited to segments where the mean thickness was 30 mm ±3 mm).
- The six chipseal samples at Kirwee exhibited very similar results and therefore only the Grade 2 and 3 Single-Coat sections have been included in the report.
- Prior to analysing the relationships between hardness and L_{CPX}, the observed frequency-dependent speed exponents were used to correct the nominally 80 km/h measurements.

4.1 Speed

4.1.1 Example – Groynes Off-Ramp

This section contains an example of the method used for calculating the speed exponent for a surface. The surface used in this example is the SMA10 (40 mm) on the Groynes northbound off-ramp.

Two measurement runs were completed at each speed from 40 to 80 km/h in 10 km/h increments. The longitudinal L_{CPX} and speed for each run are shown in Figure 67. There are 14 adjacent 20 m segments in the section.

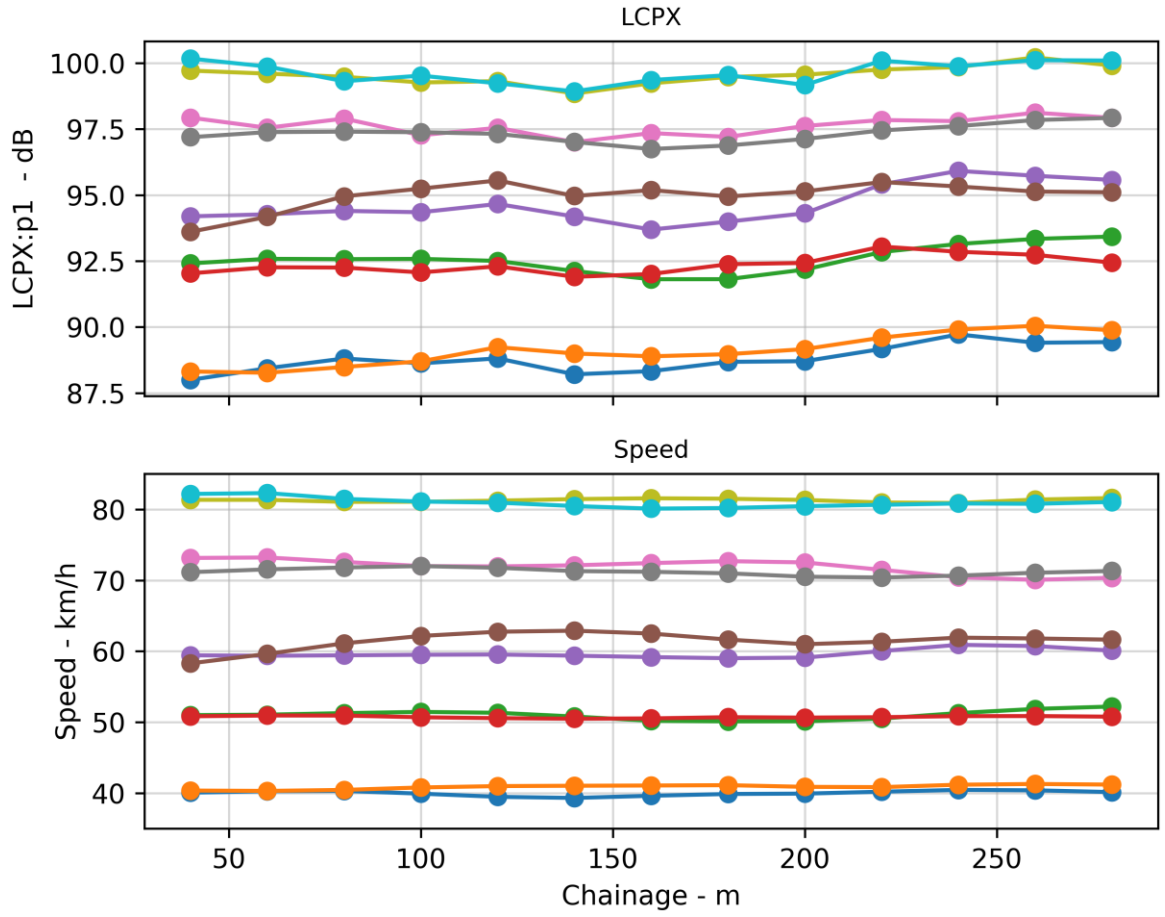

Figure 67: Longitudinal L_{CPX} and speed for the SMA10 (40 mm) on the Groynes off-ramp for all measurement runs.

The speed exponent was calculated by fitting the speed function (Equation 2) to the measured data for each of the 14 segments. Figure 68 contains a plot of L_{CPX} as a function of speed and the associated distribution of speed exponents for all segments. The mean speed exponent of 3.6 is in close agreement with the value prescribed by the standard for an impervious surface (3.5). The standard deviation for the measured speed exponent was low (at 0.12), which indicates minimal inner-surface variation in the speed exponent for the analysed section.

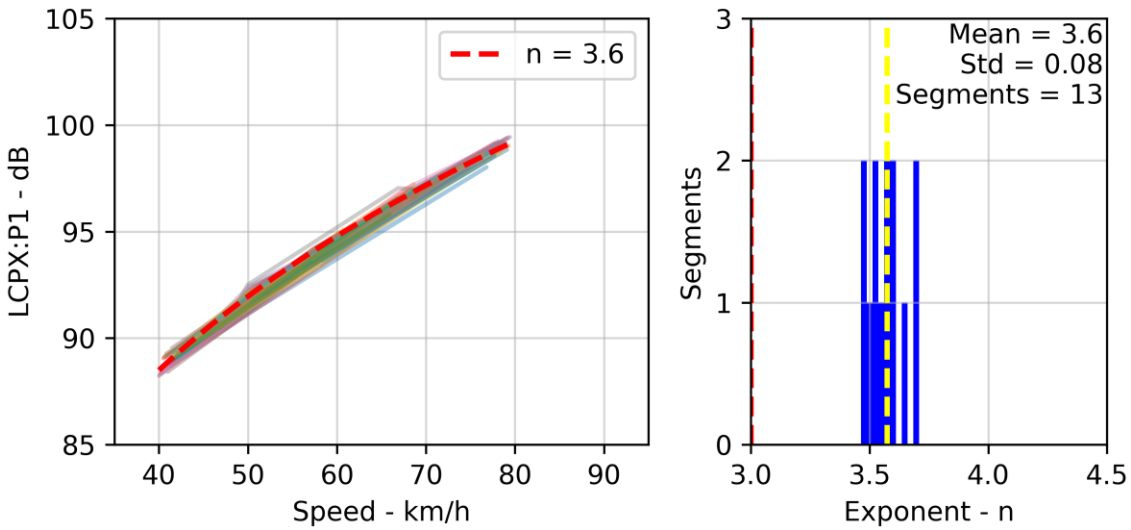

Figure 68: L_{CPX} versus speed and the fitted speed coefficient distribution for each 20 m segment for the SMA10 (40 mm) on the Groynes off-ramp.

The same methodology was applied to each one-third octave band. Figure 69 contains L_{CPX} as a function of speed for each 20 m segment and one-third octave band. Figure 70 contains boxplots of the speed exponents and coefficient of determinations (R^2) for each one-third octave band. From 800 to 5,000 Hz, the fitted models offered excellent agreement with the measured data having an R^2 approaching one for all bands and segments. The L_{CPX} in the 315 and 630 Hz bands were correlated with speed, however the fitted model had lower agreement with the measured data. The L_{CPX} in the 400 and 500 Hz bands were not correlated with speed. The 800 and 1,000 Hz bands possessed the highest speed exponents and are therefore most affected by variations in speed.

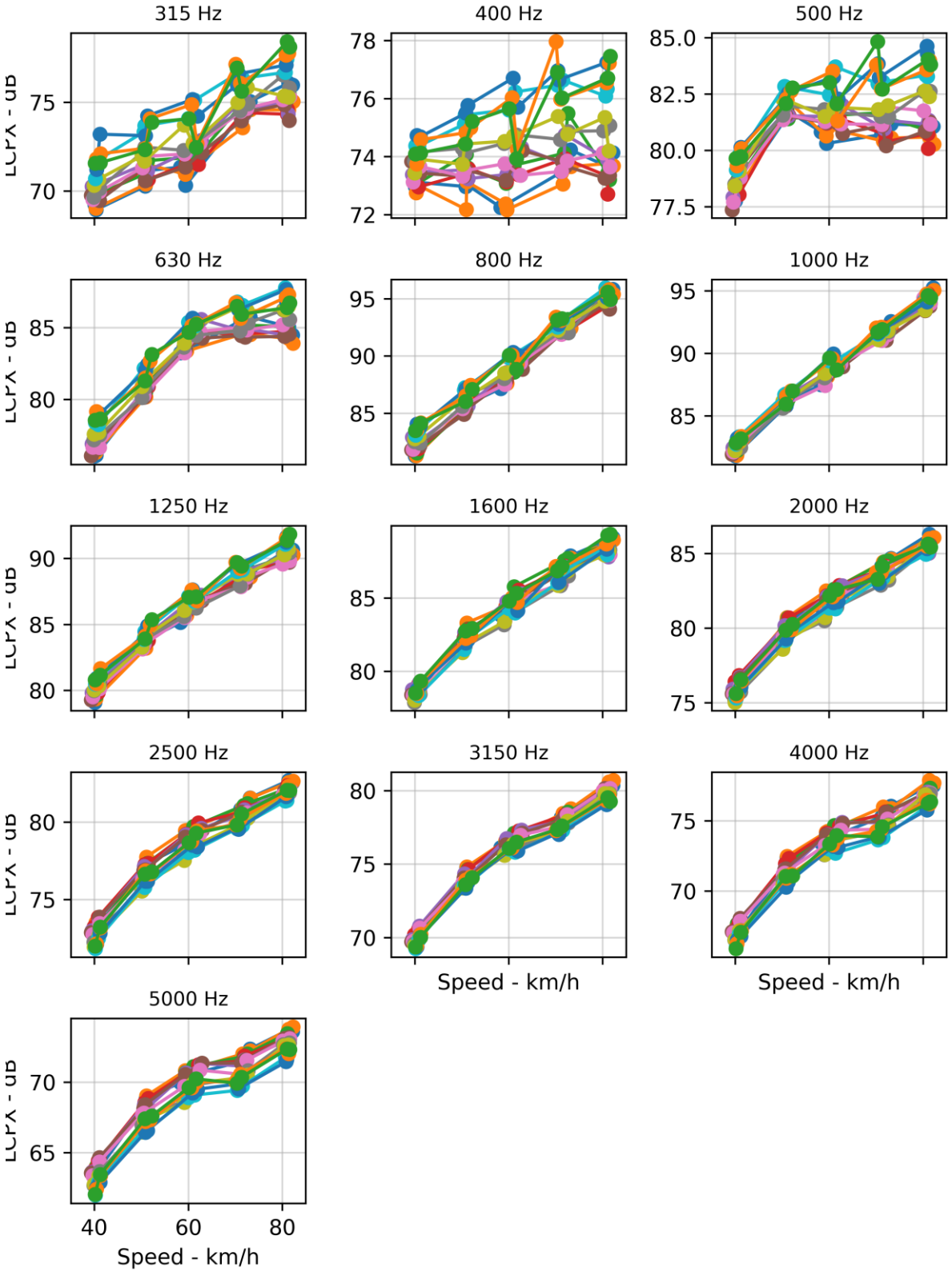

Figure 69: One-third octave band L_{CPX} versus speed for each 20 m segment for the SMA10 (40 mm) on the Groynes off-ramp.

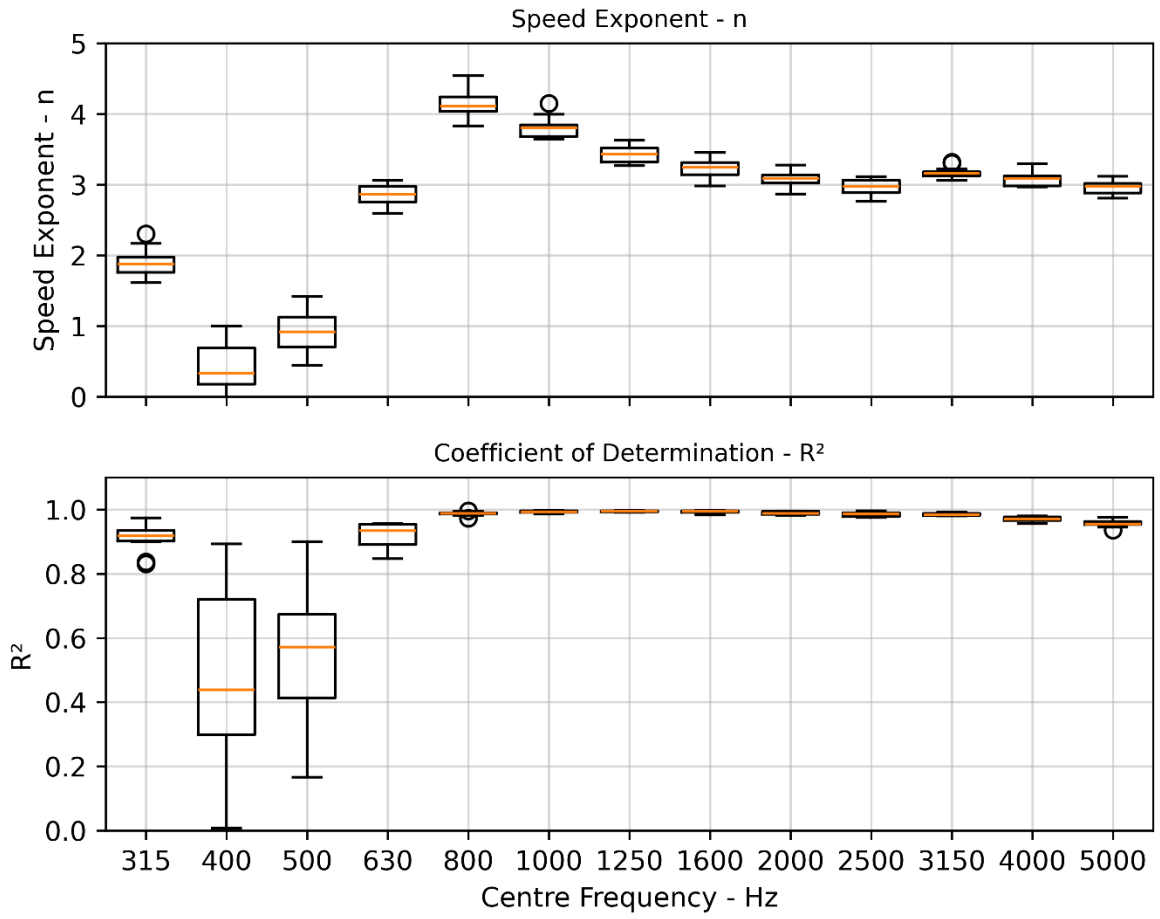

Figure 70: Boxplots of the speed exponent and coefficient of determination for each one-third octave band for the SMA10 (40 mm) on the Groynes off-ramp.

4.1.2 Overall Speed Exponent by Surface

The speed exponent was calculated for each location where speed was varied (Groynes Ramps, CNC, and Kirwee) using the method described above. Figure 71 shows L_{CPX} as a function of speed by surface type. The corresponding speed exponents by surface are shown in Figure 72.

The impervious chipseals and SMA10 (40 mm) had speed exponents of ~3.5, which matches the CPX standard (*ISO 11819-2*, 2017). Excluding the EPA7 (50 mm) on CNC, the speed exponents for the porous asphalt surfaces ranged from 2.4 to 2.9, which aligns well with the 2.5 to 3.0 given in the standard for new to clogged porous surfaces, respectively.

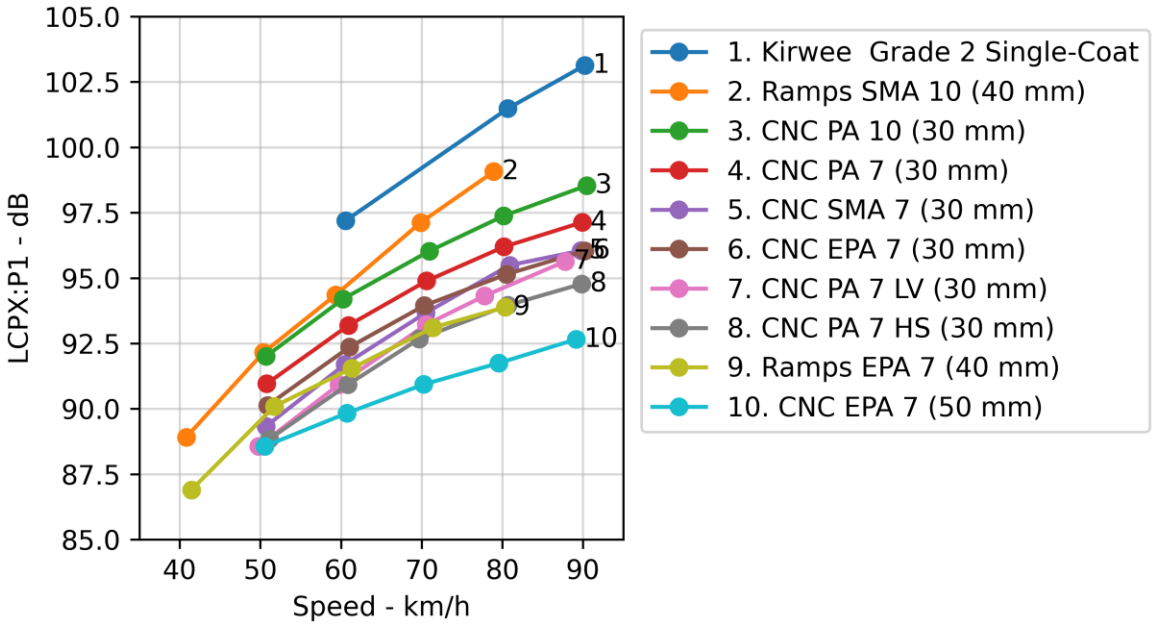

Figure 71: Speed versus L_{CPX} for various surfaces.

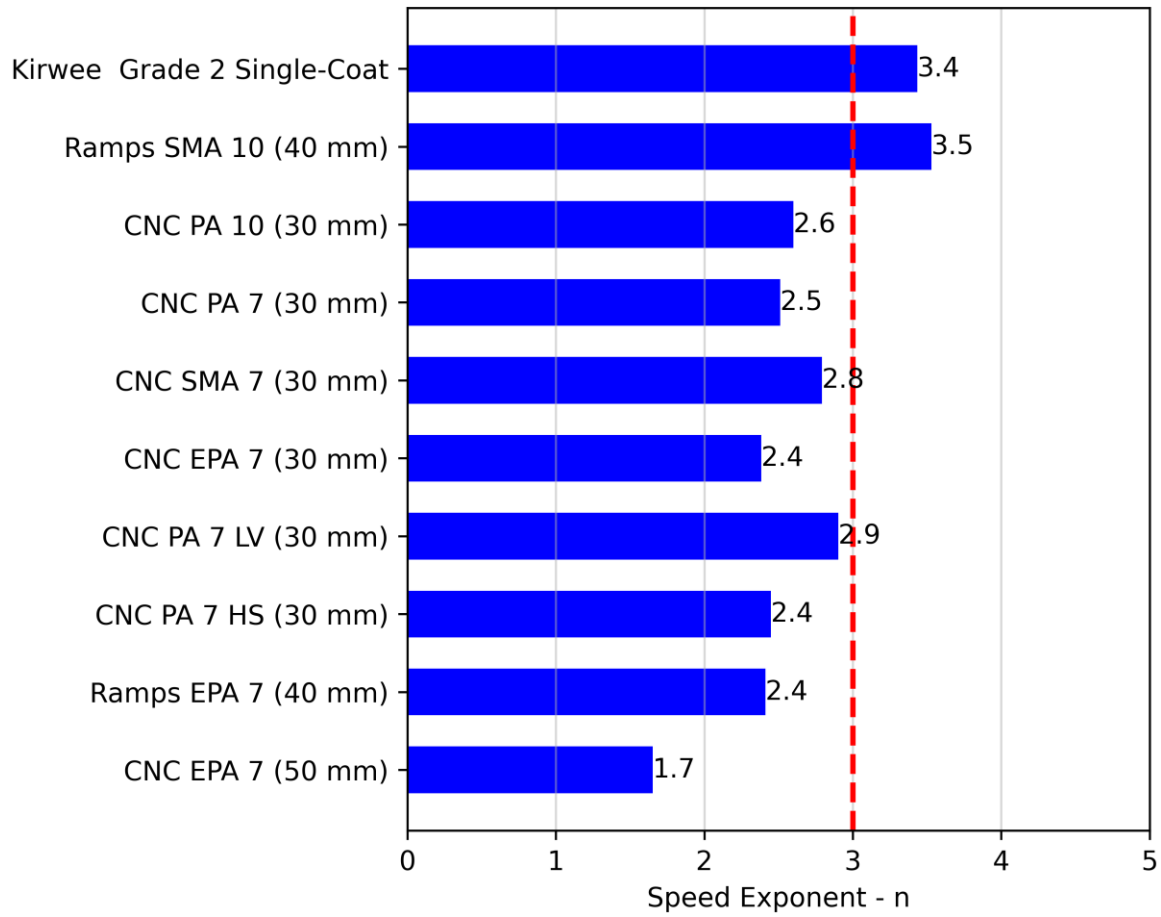

Figure 72: Speed exponent for overall L_{CPX} for various surfaces.

An alternative presentation of the L_{CPX} and speed relationship by surface is shown in Figure 73. The L_{CPX} is shown relative to the SMA10 (40 mm) surface. As the chipseal and SMA10 (40 mm) have the same overall speed exponent, the chipseal also has a near-horizontal line. Surfaces with a lower speed exponent diverge from the SMA10 (40 mm) and chipseal surfaces with increasing speed (i.e., the noise reduction increases with increasing speed). The only surface that changed its ranking was the PA7 LV (30 mm), which has a greater speed exponent than the other porous surfaces; this may be due to the lower void fraction leading to a greater rate of increase of aero-acoustic noise at higher speeds.

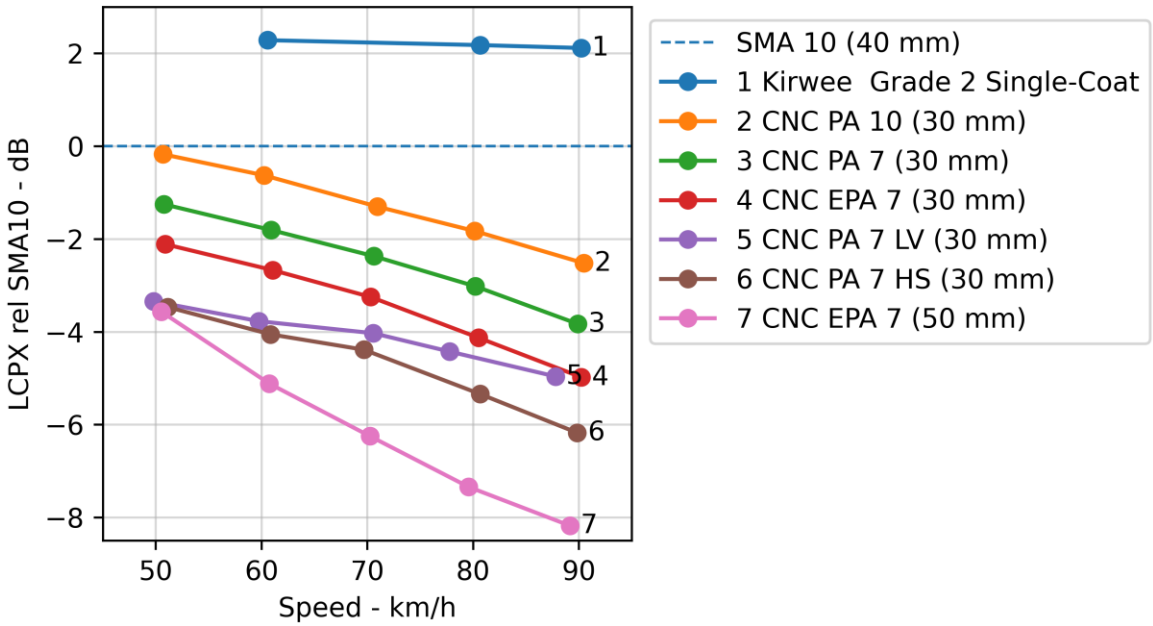

Figure 73: Change in L_{CPX} relative to the Groynes Ramps SMA10 (40 mm) surfaces versus speed.

4.1.3 Spectral Speed Exponent by Surface

Figure 74 shows the mean speed exponent by one-third octave band for each surface. The speed exponent is similar between surfaces from 1,000 to 5,000 Hz. Chipseals demonstrated non-zero speed exponents from 400 to 630 Hz. The SMA10 (40 mm) surface had a low-speed exponent in the 630 Hz band and was the only asphaltic mix surface to have a significant speed exponent in the 800 Hz band.

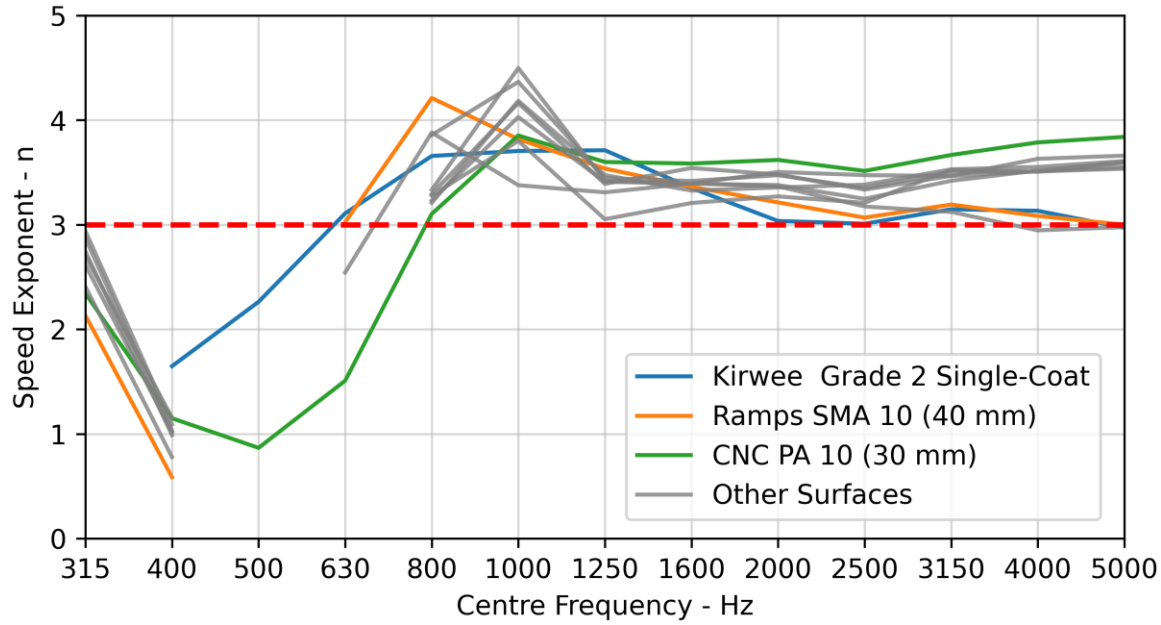

Figure 74: Speed exponent by one-third octave band for various surfaces.

The speed exponents were grouped into chipseals and porous asphaltic mixes (excluding SMA) surfaces, the resulting mean values are shown in Figure 75. The reason for the absence of a correlation between L_{CPX} and speed for porous asphaltic mixes from 400 to 800 Hz is unknown; it may be due to different dominant noise generation mechanisms, attenuation from surface absorption, differences in texture (MPD: chipseals 2.0-2.5 mm, asphaltic mixes 0.7-1.2 mm), or another mechanism.

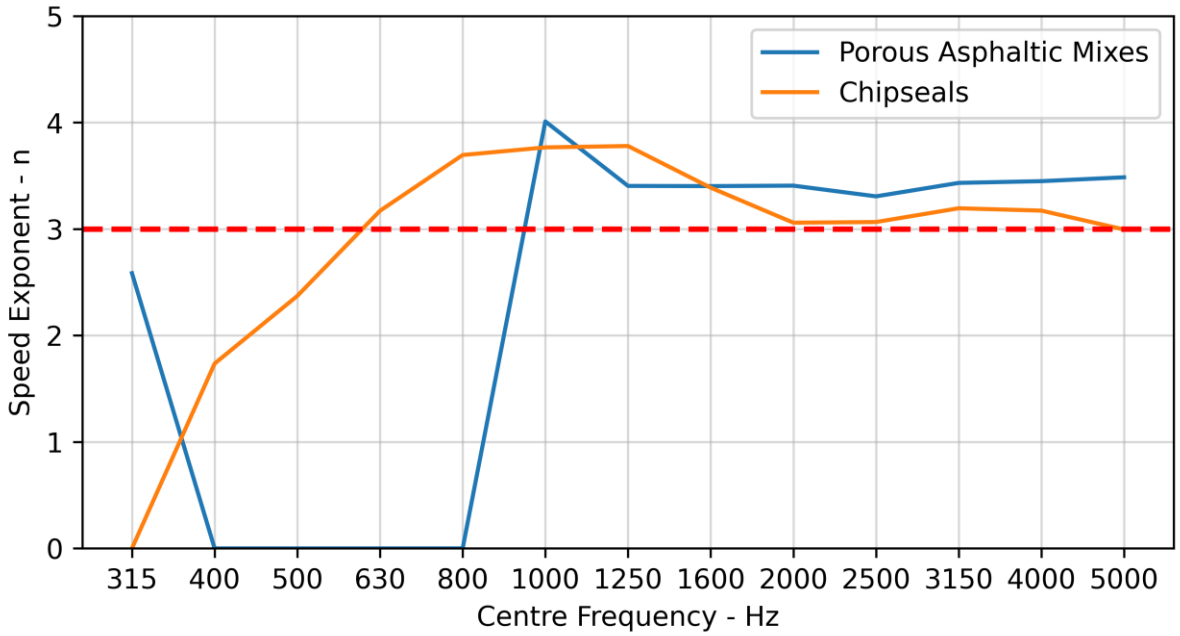

Figure 75: Mean speed exponent by one-third octave band for asphaltic mix and chipseal surfaces.

4.1.4 Speed Exponent and Tyre Hardness

To explore whether the relationship between L_{CPX} and speed is influenced by tyre hardness the analysis was repeated for the hard tyre. The speed exponents for the soft and hard tyres for the measured surfaces are shown in Figure 76. The small differences in the speed exponents indicate that tyre hardness does not significantly affect the relationship between L_{CPX} and speed.

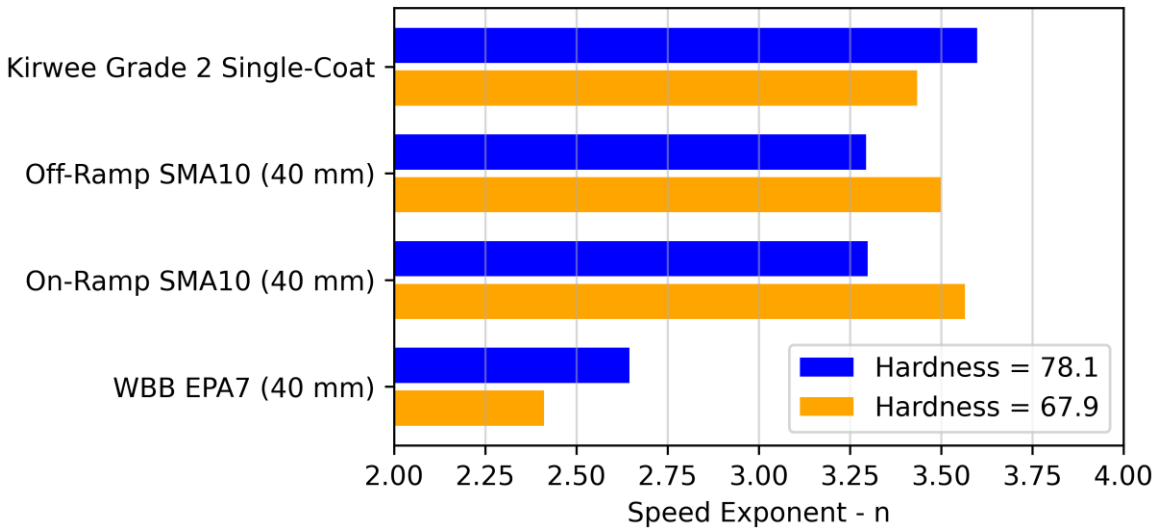

Figure 76: Speed exponent for the overall L_{CPX} for four surfaces for the soft and hard tyres.

4.2 Hardness

4.2.1 Overall Hardness Coefficient by Surface

The hardness coefficient was calculated by applying a linear fit between L_{CPX} and hardness for each surface type. Figure 77 shows L_{CPX} as a function of hardness by surface. Note that several surfaces were only measured with the soft and hard tyres.

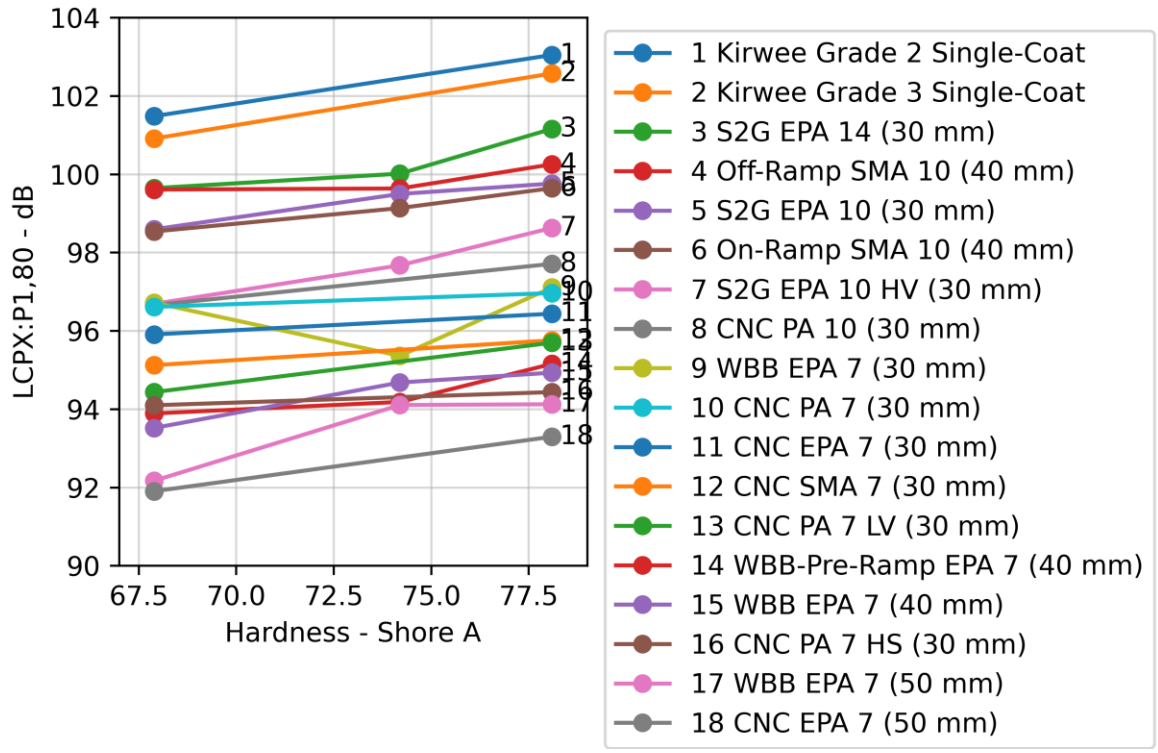

Figure 77: L_{CPX} versus tyre hardness for the measured surfaces.

The hardness coefficients by surface type are shown in Figure 78. The unweighted mean value for all surfaces was 0.13 dB/Shore A, which is similar to the 0.12 dB/Shore A specified in ISO/TS 11819-3:2021.

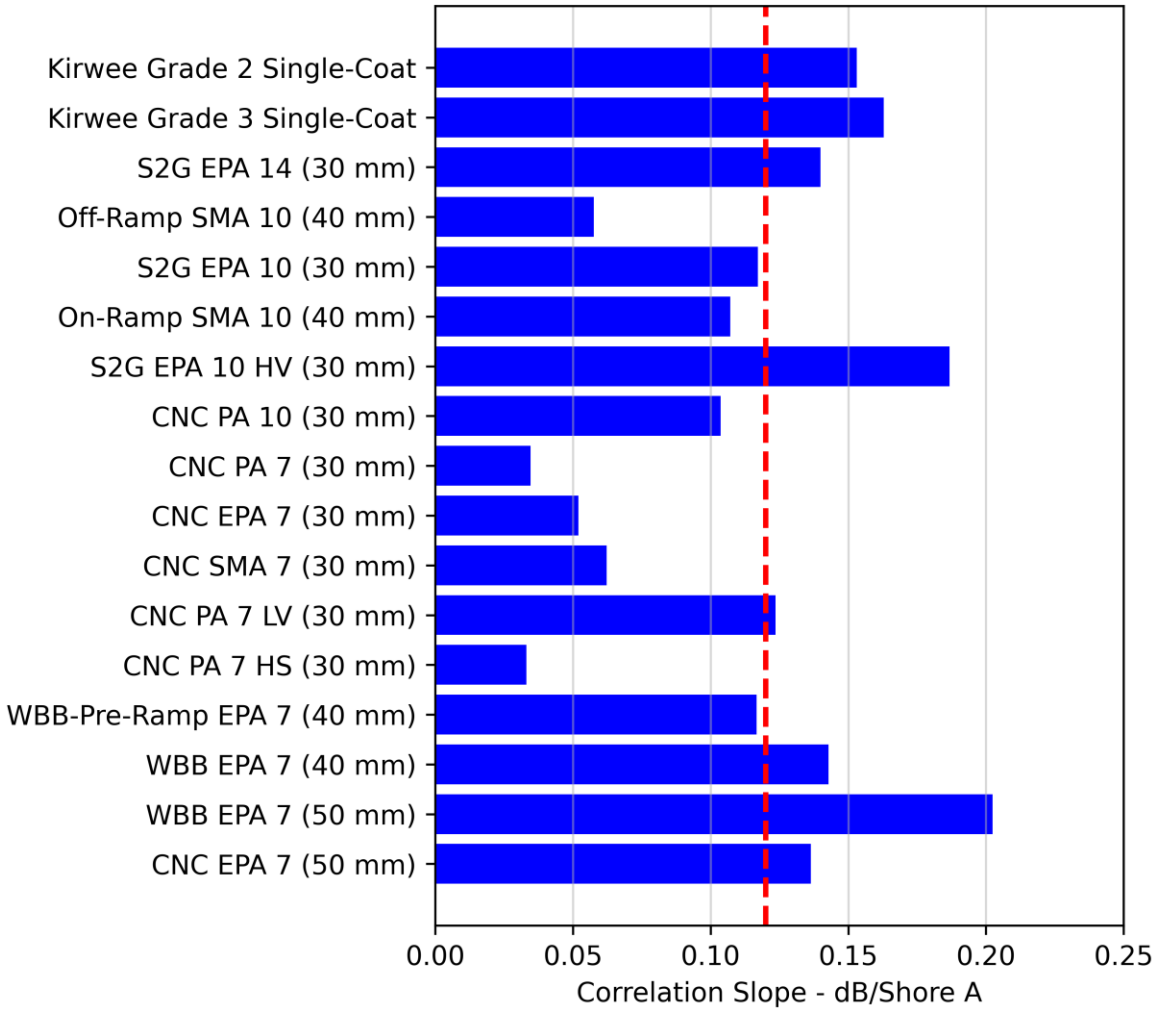

Figure 78: Hardness coefficient by surface type.

It was indicated by Sandberg and Ejsmont (2007) that the hardness coefficient is positively correlated with texture; to verify this the same relationship was analysed for the collected data. Figure 79 shows the hardness coefficient as a function of mean MPD for the measured surfaces. A linear fit between hardness coefficient and mean MPD had a positive slope that was not statistically significant ($p>0.05$, $n=17$) and offered a very weak ($R^2 = 0.21$) prediction of the measured data.

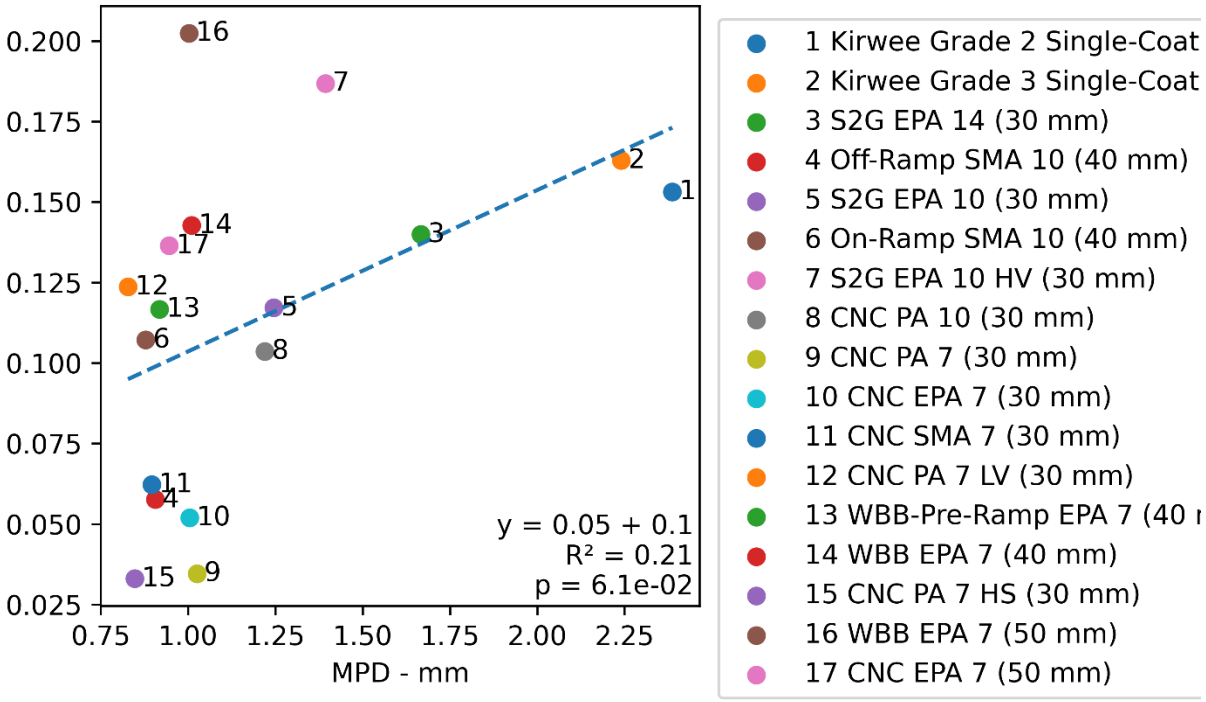

Figure 79: Hardness coefficient as a function of mean MPD for each surface.

Figure 80 shows the hardness coefficient by one-third octave band and surface type. Figure 81 shows the values grouped by asphaltic mixes (excluding SMAs) and chipseals. The relationship between L_{CPX} and hardness varied significantly by frequency. The L_{CPX} for asphaltic mixes was most influenced by tyre hardness (i.e., had the highest hardness coefficient) in the 1,600 and 2,000 Hz bands. The L_{CPX} for chipseals was most influenced by tyre hardness in the 1,250 and 1,600 Hz bands. The L_{CPX} for asphaltic mixes was not influenced by tyre hardness in the 630 and 800 Hz bands.

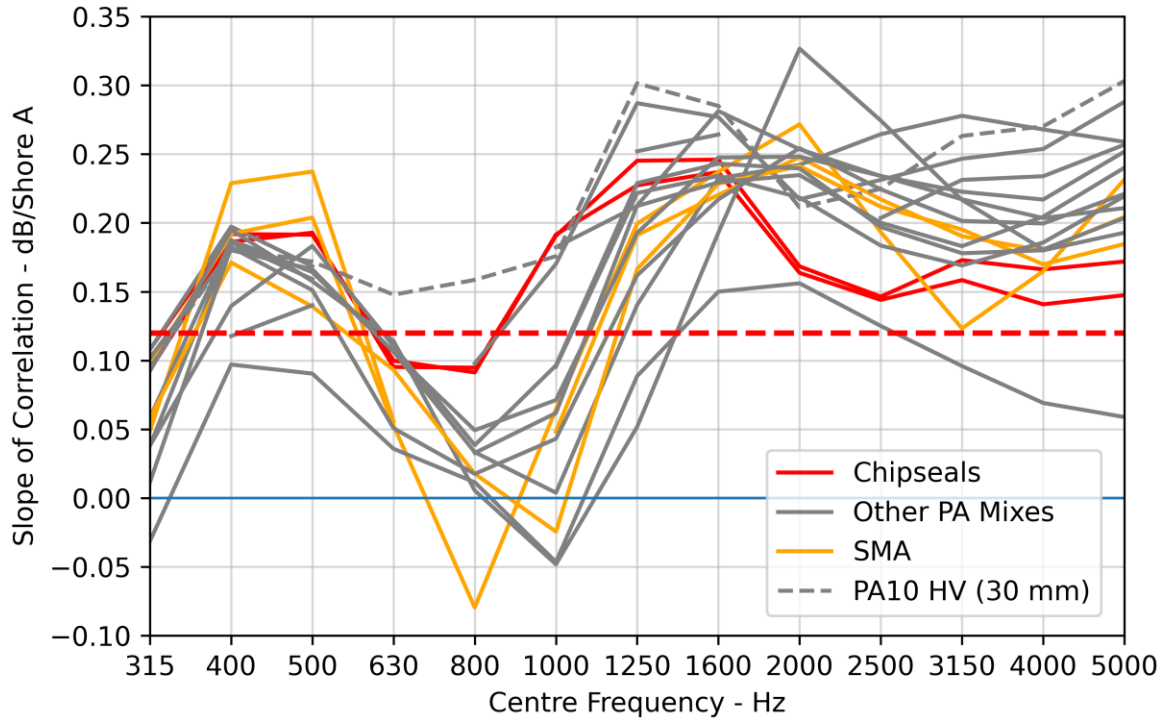

Figure 80: Hardness coefficient by one third octave band by surface type.

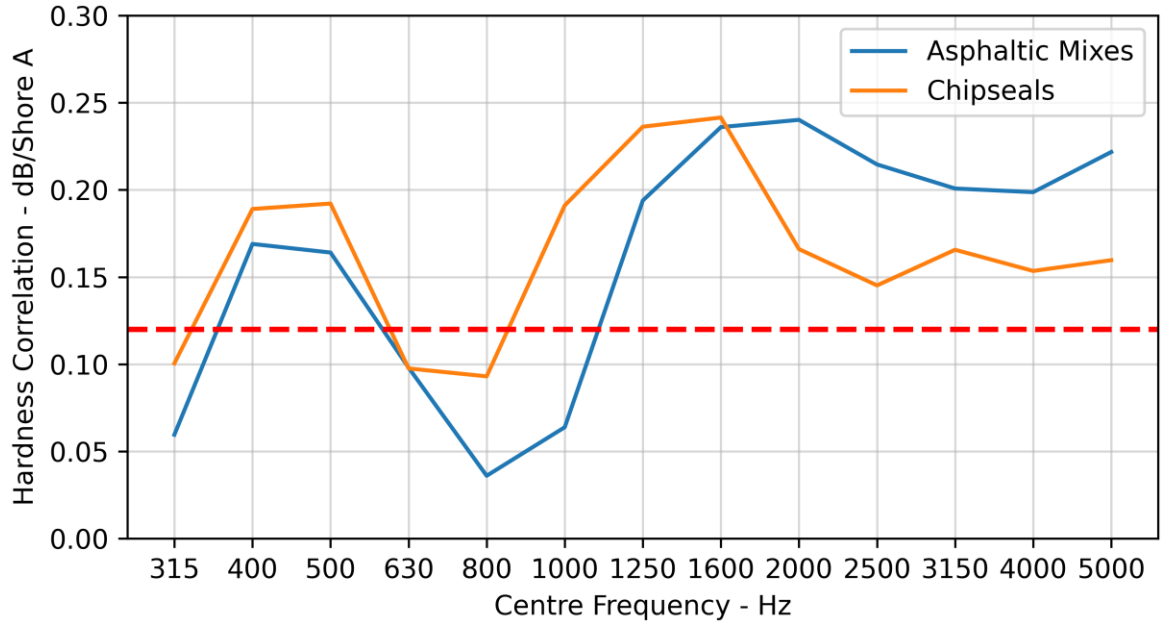

Figure 81: Hardness coefficient by one third octave bands for asphaltic mixes and chipseals.

Due to the limited quantity of tyres, these results should be considered as indicative only. There is also a risk that the observed correlations are an artefact of another unknown attribute of the tested tyres. A larger sample of tyres would be required to gain higher confidence in the fitted hardness coefficients.

4.3 Parameter Influence by Thickness

Between the 30 and 50 mm EPA7 surfaces on CNC, the speed exponent decreased (2.4 to 1.7) while the hardness coefficient increased (0.05 to 0.13). The relationships between L_{CPX}, and speed and hardness were explored in more detail for the 25-60 mm range of thickness in the EPA7 surface on CNC.

Figure 82 shows the fourth-order polynomial fits between L_{CPX} and thickness for each of the measured speeds. For all speeds, the lowest L_{CPX} level was achieved at the highest thickness. Thickness had less effect on the overall L_{CPX} at lower speeds (i.e., 50 and 60 km/h).

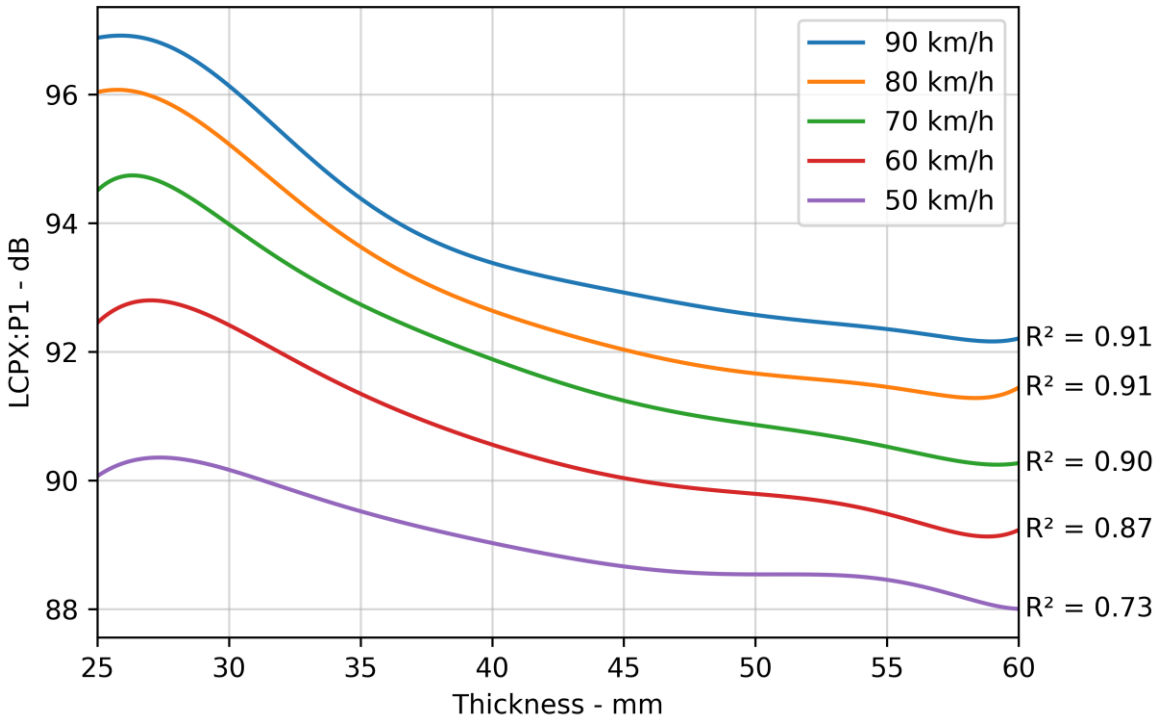

Figure 82: L_{CPX} versus thickness and speed for the EPA7 surfaces on CNC.

The speed exponent and hardness coefficient are shown as a function of thickness in Figure 83. Speed was observed to have a decreasing influence on the overall L_{CPX} as thickness increased (i.e., the speed exponent was negatively correlated with thickness). Tyre hardness was observed to have an increasing influence on the overall L_{CPX} as thickness increased (i.e., the hardness coefficient was positively correlated with thickness).

It is likely that these relationships are a function of the surface-specific noise spectra rather than the thickness causing a physical noise generation/attenuation effect. For example, the noise spectrum for EPA7 (30 mm) surface is dominated by the 800 Hz band, which has almost no influence by tyre hardness. Whereas the noise spectra for EPA7 (50 mm) is flat between 500 and 1,250 Hz, of which the 500, 630, 1,000, and 1,250 Hz bands are strongly affected by hardness.

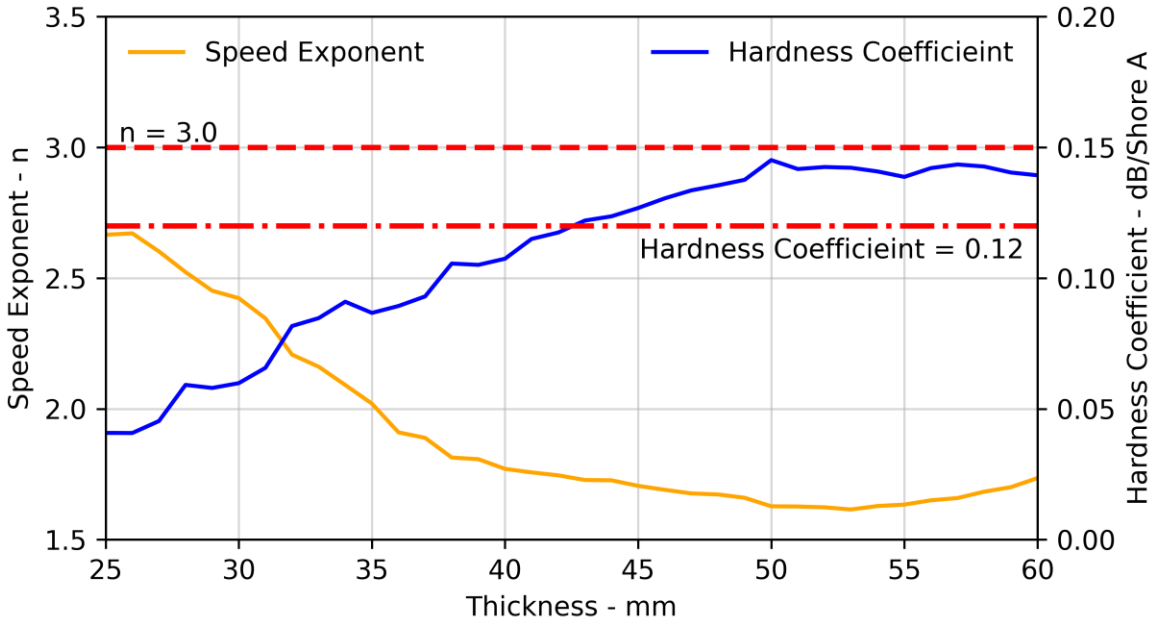

Figure 83: Speed exponent and hardness coefficient versus surface thickness for the EPA7 surfaces on CNC.

4.4 Effect on CPX Results

The correction of CPX results for speed and hardness on the overall L_{CPX} are adequate for routine measurements. However, both corrections are strongly frequency dependent and can make a small difference to the overall level.

To demonstrate the impact of using surface-specific corrections, the two most recent measurements for the Groynes off-ramp were recalculated using the corrections specifically measured on that surface. This location was chosen as it was assumed that the surface did not undergo any changes that would affect the measured tyre/road noise. The two most recent measurements were in March and November 2023. The P1 tyre was replaced between these measurements resulting in a large change in the tyre hardness (-6 Shore A). Table 12 and Figure 84 show the results with the current broadband and surface-specific frequency-dependent methods. The delta between the two measurements decreased from 0.4 to 0.1 dB. The first measurement was over-corrected for speed and hardness. The updated corrections reduced the deltas of the one-third octave band levels to less than 1 dB across all bands.

Table 12: Overall L_{CPX} for the previous two measurements of the SMA10 (40 mm) on the Groynes off-ramp.

Corrections	**Overall L_{CPX} - dB**	
	Mar 2023	Nov 2023
Broadband	98.4	98.8 (+0.4)
Frequency-dependent and surface specific	99.0	98.9 (-0.1)

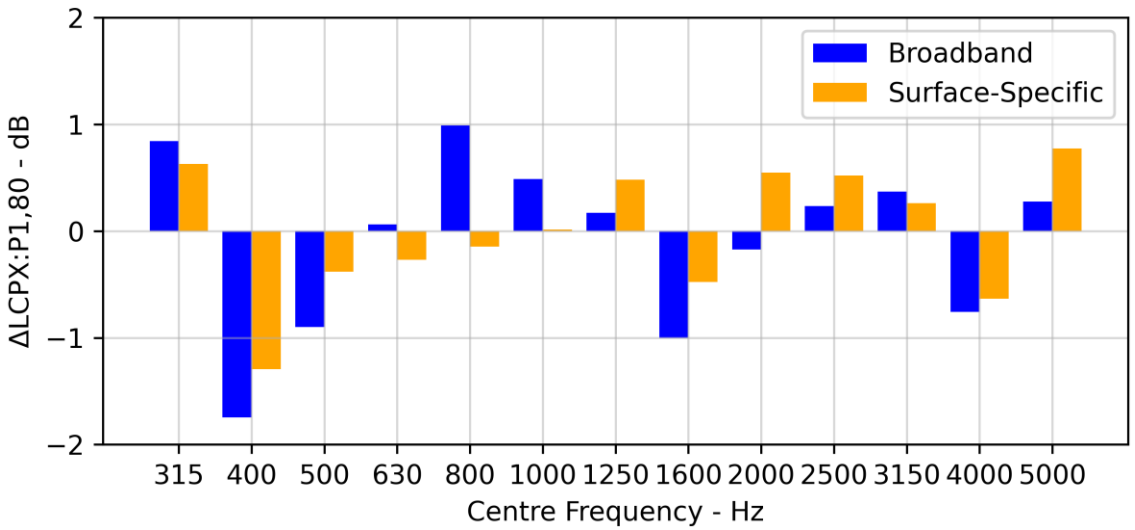

Figure 84: Change from previous measurement (Nov – Mar 2023) for SMA10 (40 mm) on the Groynes Off-Ramp with and without surface specific frequency-dependent corrections.

5 Future Work

The following areas are suggested for future investigations based on the findings in this report.

- **Tyre Hardness**
  Description: Expand the hardness investigation to use more P1 tyres.
  Purpose: Develop more robust hardness coefficients that are specific to the measurement system and measured surfaces.
- **Temperature**
  Description: Evaluate the temperature corrections that are specific to the Waka Kotahi CPX trailer and measured surfaces.
  Purpose: Reduce measurement-to-measurement differences due to temperature changes enabling higher confidence in chronological analyses, and site-to-site comparisons.
- **Enclosure Corrections**
  Description: Explore the relationships between the static enclosure corrections (following the CPX standard) and CPX measurements.
  Purpose: Gain confidence in the enclosure corrections and/or understand how to adjust them to achieve satisfactory results.
- **Reference Surface**
  Description: Update the reference surface analysis method to include surface-specific corrections.
  Purpose: Increase the accuracy and usefulness of the reference surface analysis.
- **Microphone Positions**
  Description: Analyse the hardness and speed relationships for each microphone position.
  Purpose: The microphone positions are affected differently by the noise generation and propagation mechanisms. These mechanisms can be better characterised and understood through a lower-level analysis.

6 Conclusions

A targeted measurement program was undertaken to establish the influence of speed and tyre hardness on the overall L_{CPX} and frequency spectra. 28 measurement sessions were completed covering speeds from 40 to 90 km/h and hardness values from 67.9 to 78.1 Shore A across multiple asphaltic mix and chipseal surfaces.

The measured speed exponents for the overall level were found to have good agreement with the values included in the CPX standard. Impervious surfaces, including SMA10 (40 mm) and Grade 2 Single-Coat chipseal, had speed exponents of ~3.5, while the porous asphalt surfaces had speed exponents from 2.4 to 2.9, with the EPA7 (50 mm) being the only surface outside of this range having the lowest speed exponent of 1.7. For all surfaces, the speed exponent was found to be strongly frequency-dependent with some bands having no consistent or significant relationship.

The range of speed exponents has minimal impact on the correction to the overall L_{CPX} as the actual measurement speed typically only varies by up to ±3 km/h about the target speed. However, the frequency dependence of the speed exponent can have a significant difference on the correction of the one-third octave band levels.

If extrapolating across a wider speed range (e.g., from measurements at 50 km/h to 80 km/h), it would be critical to understand the speed exponent for the specific surface material as the relative levels and rankings of surfaces can change.

The hardness coefficient was found to vary significantly by surface type with the overall mean value of 0.13 dB/Shore A being well aligned with that in the CPX tyre standard (0.12 dB/Shore A). The relationship between L_{CPX} and tyre hardness was found to be strongly frequency-dependent with the 1,000 to 1,600 Hz bands being most influenced.

It was observed that both the speed exponent and hardness coefficient were a function of surface thickness for EPA7. The speed exponent was observed to decrease with increasing thickness while the hardness coefficient increased. These relationships are likely due to the spectral shape rather than a physical interaction with the surface; however, the consequences of these relationships are still present.

The relationship between speed and hardness, and tyre/road noise is frequency-dependent and specific to the surface. The current correction methods employed are adequate for most typical applications. However, for more detailed investigations, such as those examining surface ageing or conducting advanced parameter studies, it is advisable to utilise surface-specific, frequency-dependent corrections.

References

Acoustics—Measurement of the influence of road surfaces on traffic noise—Part 2: The close-proximity method (ISO 11819-2; Version 2017). (2017). https://www.iso.org/standard/39675.html

Ahmed, F. (2015). *Porous Asphalt Clogging Performance Under Swedish Conditions*.

Beckenbauer, T., Kuijpers, A., & GmbH, M.-B. (2001). *Prediction of pass-by levels depending on road surface parameters by means of a hybrid model*.

Bell, G. R. A. (2022). *Analysis of asphaltic mix surfaces*.

Bell, G. R. A. (2023). *Analysis of low-noise asphaltic mix surfaces: Texture, construction, and porosity effects*.

Bühlmann, E., Egger, S., & Ziegler, T. (2013, September 1). *Ageing of the new CPX reference tyres during a measurement season*.

Bühlmann, E., Sandberg, U., & Mioduszewski, P. (2015, August 1). *Speed dependency of temperature effects on road traffic noise*.

Bull, J. (2019). *Porous asphalt thickness and variability study*.

Bull, J., Wareing, R., Chiles, S., & Jackett, R. (2021). Investigating the effect of layer thickness on the variability of porous asphalt tyre/road noise. *Romanian Journal of Transport Infrastructure*, *11*(1), 1–15. https://doi.org/10.2478/rjti-2022-0001

Edmondson, V., Martin, J. E., Ardill, O., Lim, M., Kane, M., & Woodward, J. (2021). Seasonal Signals Observed in Non-Contact Long-Term Road Texture Measurements. *Coatings*, *11*(6), 735–735. https://doi.org/10.3390/coatings11060735

Gardziejczyk, W. (2016). The effect of time on acoustic durability of low noise pavements – The case studies in Poland. *Transportation Research Part D: Transport and Environment*, *44*, 93–104. https://doi.org/10.1016/j.trd.2016.02.006

Herrington, P. (2014). *Epoxy-modified porous asphalt*.

IHARA, T., & INOUE, T. (2003). A STUDY OF TIRE/ROAD NOISE OF ASPHALT PAVEMENTS. *JOURNAL OF PAVEMENT ENGINEERING, JSCE*, *8*, 93–98.

ISO/TS 11819-3:2021 (TS 11819-3). (2021). https://www.iso.org/standard/82067.html

Jackett, R. (2021). *Road Surface Noise Corrections—Part 1: Large CPX Survey of Road Surfaces* (5-27858.01 10CAR). WSP Research.

Lester, T., Dravitzki, V., Carpenter, P., McIver, I., & Jackett, R. (2017). *Research Report 626 The long-term acoustic performance of New Zealand standard porous asphalt*. Opus International Consultants Limited. https://nzta.govt.nz/resources/research/reports/626/

Mobile Laser Scanning | Woods. (2023, October 20). https://www.woods.co.nz/our-work/mobile-laser-scanning

Noise and vibration research | Waka Kotahi NZ Transport Agency. (n.d.). Retrieved January 25, 2024, from https://www.nzta.govt.nz/roads-and-rail/highways-information-portal/technical-disciplines/environment-and-sustainability-in-our-operations/environmental-technical-areas/noise-and-vibration/noise-and-vibration-research/#road-surface-noise-research

Oddershede, J., & Kragh, J. (2014). Changes in noise levels from Standard Reference Test Tyres due to increasing tyre tread hardness. *Proceeding of Forum Acusticum*.

OECD. (2008). *Long-life surfaces for busy roads*. International Transport Forum, Transport Research Centre.

Richard Fanning, G. V. (2021). Guide to Road Design Part 3: Geometric Design. In *978-1-922382-15-3* (Australia and New Zealand). Austroads. https://austroads.com.au/publications/road-design/agrd03

Sandberg, U. (1999). Low noise road surfaces. A state-of-the-art review. *Journal of the Acoustical Society of Japan (E)*, *20*(1), 1–17. https://doi.org/10.1250/ast.20.1

Sandberg, U., & Ejsmont, J. (2007). *Influence of tyre rubber hardness on tyre/road noise emission*. *1*, 394–403.

Sandberg, U., & Ejsmont, J. A. (2002). *TYRE/ROAD NOISE REFERENCE BOOK*. https://trid.trb.org/view/730140

Standard Test Method for Pavement Thickness by Magnetic Pulse Induction (E3209; Version 19). (2020). https://www.astm.org/e3209-19.html

Van Heystraeten, G., & Moraux, C. (1990). Ten Years' Experience of Porous Asphalt in Belgium. *TRANSPORTATION RESEARCH RECORD*.

Vítězslav Křivánek, Alena Pavkova, Marek Tögel, J Jedlicka, & R Cholava. (2015). Cleaning Low-Noise Surfaces as a Basic Condition for Improving Pavement's Acoustic Absorption Capability. *Arabian Journal for Science and Engineering*, *41*(2), 425–431. https://doi.org/10.1007/s13369-015-1713-y

Waka Kotahi NZ Transport Agency. (2024). *Open-graded porous asphalt* (NZTA P11; Version 2023).

Wareing, R. (2022). *Christchurch Northern Corridor—2022 Trial Site Preliminary Investigations*.

Wareing, R., Bull, J., Chiles, S., & Jackett, R. (2021). Optimising New Zealand's State highway low-noise road surface. *Air Pollution*.

Appendix A – Additional Data

This appendix contains supplementary data that is referenced in the body of the report.

Table 13: Configurations of the left enclosure on the CPX trailer.

date	Configuration
1-Mar-18	Sound absorption material: original (UoC). Skirts on the following edges: front, rear, inside (including across wheel arch), outside. No absorption material on the wooden members.
15-Mar-18	Sound absorption material: original (UoC). Skirts on the following edges: front (angled inwards), rear (angled inwards), inside (excluding across wheel arch), outside. Absorption material on the following wooden members: Inner, lower horizontal members (split at wheel arch); Inner, vertical members (either side of the wheel arch).
28-Sep-20	Sound absorption material: original (UoC). Skirts on the following edges: front (angled inwards), rear (angled inwards), inside (excluding across wheel arch), outside. Absorption material on the following wooden members: Inner, lower horizontal members (split at wheel arch); Inner, vertical members (either side of the wheel arch).
7-Oct-20	Sound absorption material: original (UoC). Skirts on the following edges: front (angled inwards), rear (angled inwards), inside (excluding across wheel arch), outside (angled downwards). Absorption material on the following wooden members: Inner, lower horizontal members (split at wheel arch); Inner, vertical members (either side of the wheel arch).
12-Jul-21	Sound absorption material: original (UoC). Skirts on the following edges: front (angled inwards), rear (angled inwards), inside (excluding across wheel arch), outside (angled downwards). Absorption material on the following wooden members: Inner, lower horizontal members (split at wheel arch); Inner, vertical members (either side of the wheel arch).
3-Apr-22	Sound absorption material: original (UoC). Skirts on the following edges: inside (excluding across wheel arch), outside (angled downwards). Front and rear skirt mounting plates remain. Absorption material on the following wooden members: Inner, lower horizontal members (split at wheel arch); Inner, vertical members (either side of the wheel arch).
1-Mar-23	Sound absorption material: original (UoC). All skirts and mounting plates removed. Absorption material on the following wooden members: Inner, lower horizontal members (split at wheel arch); Inner, vertical members (either side of the wheel arch).

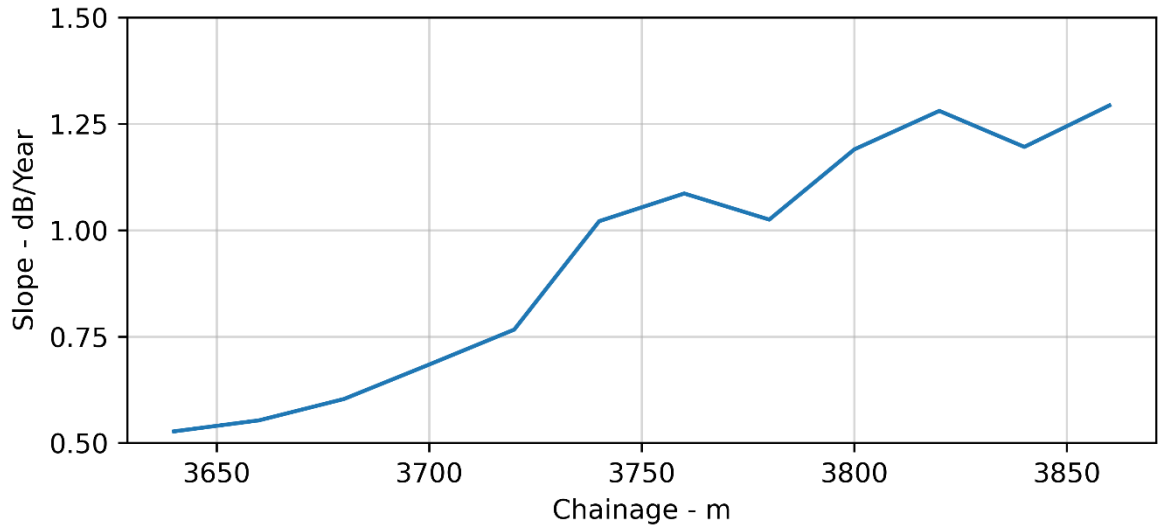

Figure 85. Longitudinal rate of change of L_{CPX} for left lane of EPA10 (30 mm) on S2G.

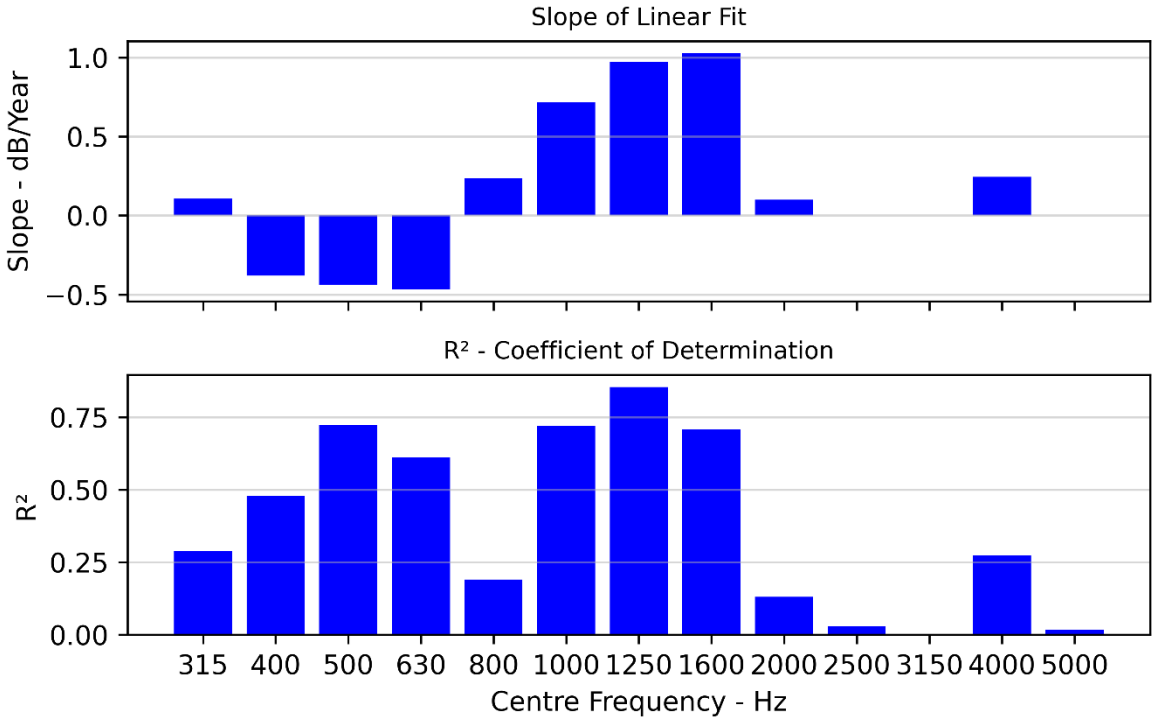

Figure 86. One-third octave band rates of change with time for EPA14 (30 mm) in lane 2 on S2G.

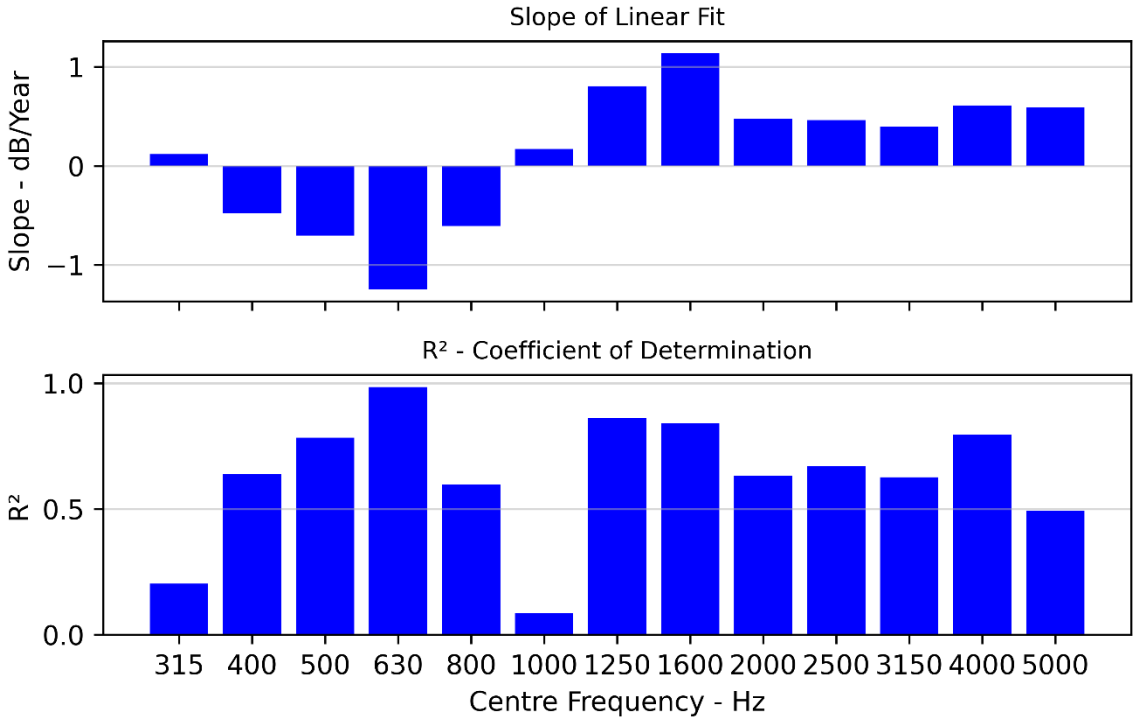

Figure 87. One-third octave band rates of change with time for EPA14 (30 mm) in lane 1 on S2G.

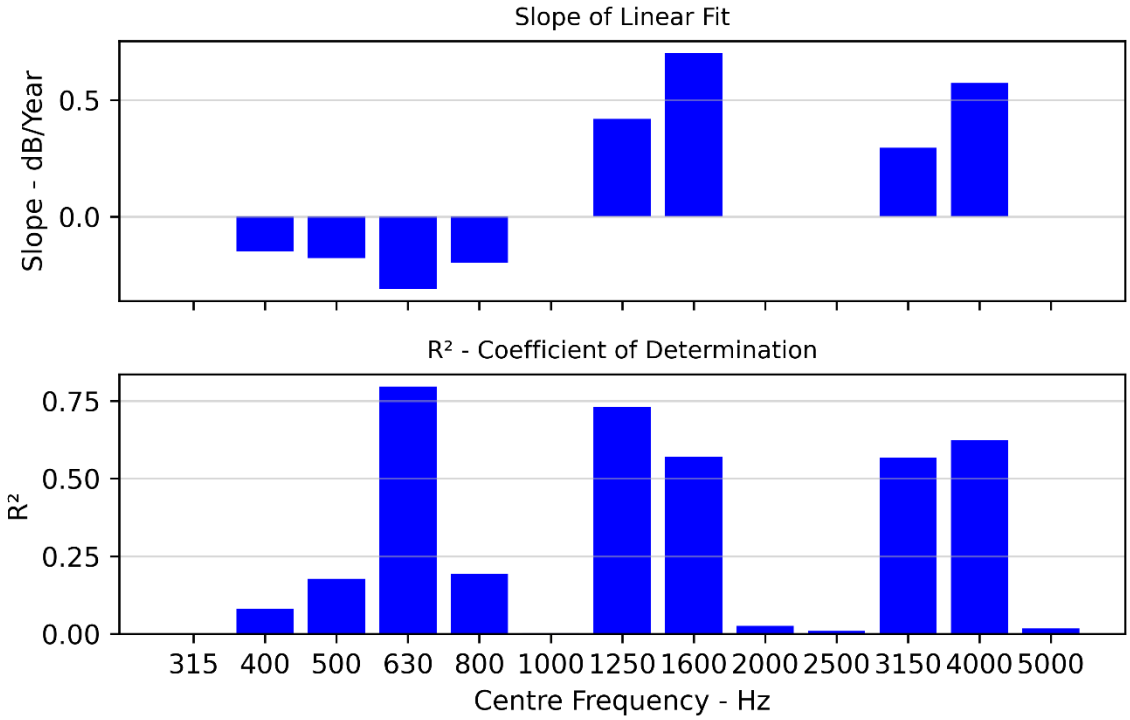

Figure 88. One-third octave band rates of change with time for EPA7 (40 mm) (in lane 1 on WBB ID = 8).

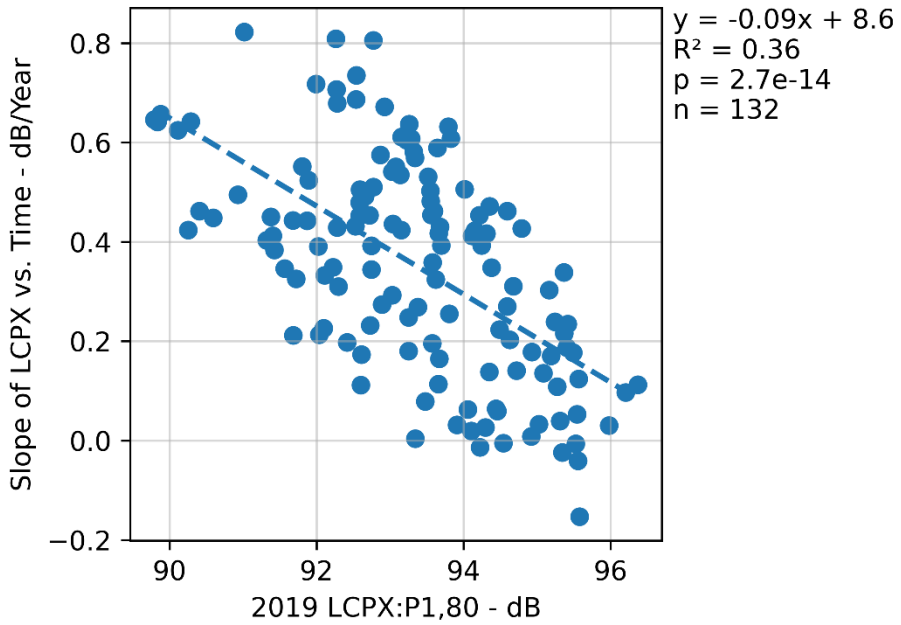

Figure 89. Rate of change of L_{CPX} over time versus initial level for EPA7 (40 mm) (ID = 10).

Table 14: Parameter study measurement sessions.

No.	Location	Speed	Tyre	Surfaces
1	CNC	30	Soft	EPA7 (30 mm), EPA7 (50 mm). PA7 (30 mm), PA7 HS (30 mm), PA7 LV (30 mm), PA10 (30 mm), SMA7 (30 mm)
2		50	Soft	
3		70	Soft	
4		80	Soft	
5		80	Hard	
6		90	Soft	
7	Groynes Ramps	40	Soft	SMA10 (40 mm), EPA7 (40 mm)
8		50	Soft	
9		50	Hard	
10		60	Soft	
11		60	Hard	
12		70	Soft	
13		70	Hard	
14		80	Soft	
15		80	Medium	
16		80	Hard	
17		80	Hard	
18	Kirwee	60	Soft	Grade 2 Single-Coat, Grade 2/4 Two-Coat, Grade 2/4 Racked-In, Grade 2/4/6 Multi-Coat, Grade 3 Single-Coat, Grade 3/4 Two-Coat
19		60	Hard	
20		80	Soft	
21		80	Hard	
22		90	Soft	
23	S2G	80	Soft	EPA10 (30 mm), EPA10 HV (30 mm), EPA14 (30 mm)
24		80	Medium	
25		80	Hard	
26	WBB	80	Soft	EPA7 (30 mm), EPA7 (40 mm), EPA7 (50 mm)
27		80	Medium	
28		80	Hard	

Appendix B – Road IDs and Reference Stations

Table 15: Road ID and Reference Station (RS) mapping.

Road ID	Reference Station
1713	073-0015
1715	01S-0327-D
1716	01S-0327-I
3564	01N-1011-D
3588	01S-0333/04.18-I
3589	01S-0333/04.18-D
3650	01S-0333-I
3653	01S-0333-R1
3663	01S-0333/01.41-I
3664	01S-0333/01.40-D
3736	01S-0333/05.65-D
3816	01N-0995/03.07-I
3843	074-0000-I
3844	074-0000-D

Appendix C – Project and Trial Section Locations

Figure 90. Map of CNC, CSM2, and S2G projects.

Appendix D – Lane Numbering

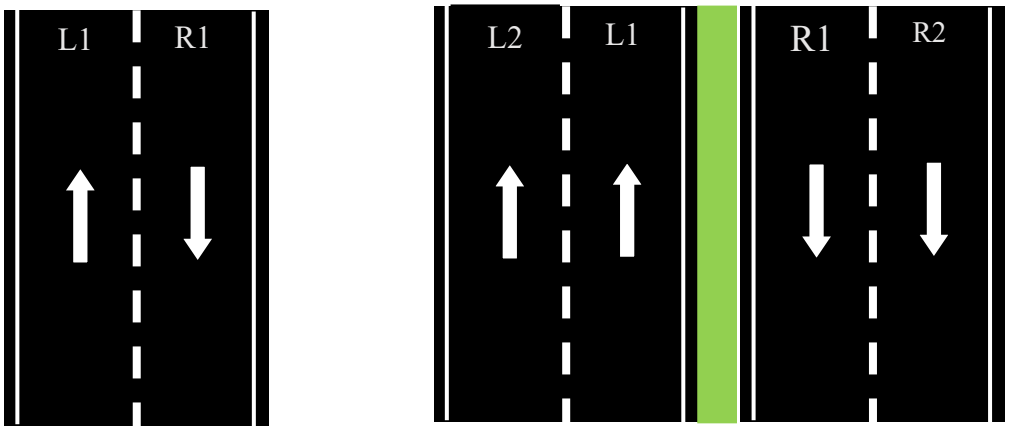

(a) Single carriageway (b) Dual carriageway

Figure 91. Lane numbering convention (assuming increasing direction toward the top of the page).